Fall 2022

Achieving Sustainability in Urban Transit and High-occupancy Vehicle Systems Through Emerging Technologies and Operations

Ruixiao Sun

Achieving Sustainability in Urban Transit and High-occupancy Vehicle Systems through Emerging Technologies and Operations

by

Ruixiao Sun

Bachelor of Engineering
Zhengzhou University, 2015

Master of Science
Central South University, 2018

Submitted in Partial Fulfillment of the Requirements

For the Degree of Doctor of Philosophy in

Civil Engineering

College of Engineering and Computing

University of South Carolina

2022

Accepted by:

Yuche Chen, Major Professor

Yu Qian, Committee Member

Sriram Venkataraman, Committee Member

Qi Luo, Committee Member

Cheryl L. Addy, Interim Vice Provost and Dean of the Graduate School

Dedication

To my baby girl, my love, and my parents.

Acknowledgments

My deepest gratitude is to my advisor, Dr. Yuche Chen. He has created an extraordinary research environment and provided the best platform and resources so that I can devote myself to scientific research. When I had questions and difficulties in my research, he was always available to discuss them with me and helped me with his superb knowledge. In addition to research, his advice on career development is also invaluable. It is my great fortunate to have him as my advisor. My special thanks to Dr. Qi Luo, for his generous guidance and greatly insightful suggestions on my research regarding to transportation cyber security and wireless charging facility deployment. Collaborating with him has been one of my best research experiences. Also, I would like to thank the other members of my dissertation committee, Dr. Yu Qian and Dr. Sriram Venkataraman, for their time and advice on my work. It is such an honor to have them serving in my committee.

I would also like to acknowledge the members in my research group, Xuanke Wu and Yunteng Zhang, thanks for their wonderful collaboration and friendly research environment. I would also like to thank my friends at the University of South Carolina, Jing Wang, Feng Guo, Junlin Ou, Amara Kouyate, etc., and my bestie, Shuo Yan. Thanks to them for the happiness and joy they brought me in the past years. I also want to thank my little cat Kele, playing with him relieved a lot of my stress.

My greatest thanks to my husband and my parents. Thank them for their unconditional love and support. It was their love that accompanied me through the

arduous journey of my doctoral study. Lastly, thanks to my little baby girl, who changed my life and brought me joy and memorable experience of first-time motherhood. Without them, I would have never been able to accomplish what I have.

Abstract

It is critical to reduce road transportation emissions, as it is the major source contributing to greenhouse gas emissions (GHGs) and air pollution. However, the increasing travel demand due to the rise of population and economy makes the task challenging. Mathematically, road transportation emissions can be minimized in the manner of reducing total vehicle miles traveled (VMT) and lowering vehicle emission rate. Many strategies have been proven viable for achieving transportation sustainability. For example, the total VMT can be reduced by switching low-occupancy transportation modes (i.e., driving alone) to high-occupancy transportation modes (i.e., public transit, ridesharing). The development of alternative-fuel vehicles (i.e., hybrid vehicles and electric vehicles) provides the prospect of minimizing vehicle emission rates or achieving net zero emissions. These strategies are active in urban transit and high-occupancy vehicle systems. Many studies focused on the field of urban transit and high-occupancy vehicle systems. However, there are several challenges and scientific gaps related to sustainability in this field. For example, the lack of investigation of energy estimation models for hybrid buses that can support energy-oriented transit operations. The need to develop an environmental impact evaluation framework for assess the energy and environmental impact of ridesharing services with consideration of individual level (i.e., agent) behavior changes. An energy-saving and time efficient charging system for electric buses on complex transit networks is required to developed in order to promote the emerging of electric buses in transit usage.

To fill these gaps, three studies was done in this dissertation: (1) hybrid buses energy prediction, (2) ridesharing operations and assessment, and (3) electric transit system charging infrastructure design. The first study is to estimate the energy consumption of hybrid buses by building machine learning model to help practitioners understand the fuel consumption behavior of hybrid buses and save energy in transit operations. The second study is to conduct ridesharing operations and assessments by developing a simulation platform to assess the energy and environmental benefits of ridesharing services under various scenarios. This study aims to assist policy design and decision-making regarding ridesharing services. The third study is to design an energy-saving and time-efficient charging infrastructure for electric buses with the consideration of tactical bus frequency setting. This study motivated by mitigating the drawback of limited range and charging delay of electric buses.

This dissertation can support transportation planning, decision-making, and policy design of transportation practitioners referring to achieving sustainability in urban transit and high-occupancy vehicle systems, taking efforts on various research technologies, such as artificial intelligent, simulation modeling, and operations.

Table of Contents

List of Tables

List of Figures

Chapter 1

Introduction

1.1 Background and Motivation

Climate change is a global issue. The greenhouse gas emissions (GHGs) continue to rise, and the temperature is getting warmer and warmer. Today, the earth is about 1.1°C warmer than it was in the late 1800s [1]. Many scientists and governments concur that keeping warming below 1.5°C will help humanity escape the worst climatic effects and maintain a habitable climate [2]. The Intergovernmental Panel on Climate Change's sixth assessment report found that it will be impossible to keep global warming at 1.5°C or even 2°C without immediate, rapid, and significant reductions in GHGs [3]. Any human activity that uses energy such as transportation, industry, agriculture, and commerce is responsible for the GHGs. But transportation especially consumes a lot of fossil fuels every day by almost every person. It accounts for 27% of the United State GHGs in 2020 [4]. Transportation is responsible for climate change. In addition to that, it also contributes to air pollution which threatens human health. Every year, transport emissions are linked to almost 400,000 deaths over the death of 7 million people caused by air pollution worldwide [5]. The United Nations Environment Programme reported that the death from exhaust fumes in cities will rise by more than 50% by 2030 if do not cut vehicle emissions immediately [6]. Therefore, reducing transportation emissions to control climate change and protect human health is crucial.

The source of the transportation emissions comes from various transportation modes, from the road to rail to sea. Among all the transportation modes, road transportation is responsible for the majority of transportation emissions, where light-duty vehicles account for almost 60%, and medium and heavy-duty trucks contribute about 30% of the transportation emissions [4]. This motivates the dissertation to focus on

the study of achieving sustainability for road transportation. However, it is not easy to control road transportation emissions. Generally, travel demand is continually increasing as the population and economy rise. Vehicle miles traveled (VMT) is a key indicator of travel demand and behavior, given its effect on both road network performance and the environment [7]. It measures the amount of travel for all vehicles in a region over a given period. A report reveals that VMT in the United State was seven times higher in 2017 than in 1950. The number of vehicles in operation was more than six times higher in that same period, while the resident population doubled [8]. And the number of vehicles and VMTs will continue to rise in the future. Considering this situation, achieving sustainability in transportation, especially in road transportation is challenging.

Mathematically, road vehicle emissions depend on the total VMT and vehicle emissions rates [9]. In this sense, there are mainly two options to reduce road vehicle emissions. The first option is to reduce VMT. Generally, it can be done by switching the transportation mode from driving to green traveling. For example, cycling and walking obviously do not count any vehicle mileage [10]. Many studies examining the role of public transit in reducing VMT and GHGs have focused directly on mode shifts from driving to transit [11]. Ridesharing systems have been promoted as a demand management strategy for reducing VMT [12, 13]. The second option is to reduce vehicle emissions rates. Vehicle technological improvements support the practical and palatable strategy to enhance the energy efficiency of vehicles. Recently, hybrid vehicles, electric vehicles, and other alternative-fuel vehicles have been used to provide energy efficiency [14]. This dissertation focuses on three of these strategies, public transit, ridesharing, and

vehicle technological improvements. They are also active in urban transit and high-occupancy vehicle systems.

This dissertation aims to support transportation planning, decision-making, and policy design of transportation practitioners to achieve sustainability in urban transit and high-occupancy vehicle systems, through intelligent modeling, simulation, and operations.

1.2 Research significance

Urban transit with high occupancy can reduce GHGs relative to low-occupancy transportation modes [15]. Recently, alternative-fuel buses are emerging in urban transit, like hybrid buses and electric buses [16]. But electric buses are not commonly used by transit agencies due to their limited range and long recharging time. Nation Transit Database shows that 1,268 electric buses out of 63,530 total buses are actively operating at transit agencies across the U.S in 2020 [17]. Hybrid buses can significantly increase energy efficiency and reduce emissions [18]. They've been used in many transit agencies in recent years. Hybrid buses have captured as much as 40% of new transit bus purchases in North America [19]. Ridesharing is a typical high-occupancy vehicle system. It is defined as an arrangement where two or more persons from different households share the use of a privately owned car for part of a trip and share the driving costs [20]. The ride-hailing market is estimated to be USD 85.8 billion in 2021 and is projected to reach USD 185.1 billion by 2026 [21]. Right now, more and more people choose to go out using ride-sharing services such as Uber and Lyft. A recent survey shows that more than 9 percent of Americans carpool to work every day [22]. Previous studies have proven that high-occupancy transportation modes (i.e., transit bus and ridesharing services), along with alternative fuel vehicles (i.e., hybrid and electric vehicles) are potential means to

reduce road transport emissions. However, there are several challenges and scientific gaps in the field of sustainable urban transit and high-occupancy vehicle systems. Some of the gaps are addressed in this dissertation.

One of the gaps is the lack of investigation of fuel consumption estimation models for hybrid buses that can enable transit operators to understand the fuel consumption behavior of hybrid buses, so as to improve their planning and bus operations to achieve their fuel savings and sustainability goals. The research found hybrid diesel buses can achieve significant savings in fuel consumption compared with conventional diesel buses [23-25]. However, few studies focus on estimating the energy consumption of hybrid buses. Relevant studies refer to fuel consumption prediction of transit buses mainly depending on the summary model [18, 26] and estimation models [27, 28], which were done about one decade ago and there is a need to assess the energy benefits of the hybrid bus with the incorporation of recent technologies. Advanced prediction methods, such as artificial intelligence algorithms, are used in literature to predict the energy and emissions of diesel buses [29, 30], but few studies have focused on hybrid buses. Machine learning-based models are investigated in Chapter 2 to estimate the energy consumption of hybrid buses.

An evaluation framework of ridesharing systems that can provide adequate information on the effect of various existing and future ridesharing strategies will be useful for policy design and decision-making of transportation agencies. Most of the existing studies are mainly drawing on survey data or small-scale trip data instead of the raw observed order information [31]. Limited studies investigate ridesharing based on empirical ridesharing data. But their conclusions are retrospective and do not offer

insights into future scenarios, which are important for transportation practitioners in evaluating various ridesharing policies. Additionally, any tools developed should have the capability to consider individual-level behavior when evaluating ridesharing impacts [32]. Literature shows that there is a knowledge gap regarding developing an environmental impact evaluation framework for ridesharing services with consideration of individual level (i.e., agent) behavior changes. In addition, to be useful for transportation practitioners, the developed framework needs to have scenario analysis capability that can evaluate various ridesharing strategies for comparison purposes. This gap is addressed in Chapter 3.

In addition to the energy prediction of hybrid buses and assessment of ridesharing systems, another gap exists in the area of charging infrastructure allocation for battery electric buses. The problems of limited range and charging delays restricted the popularity of electric buses. Dynamic wireless charging (DWC) technology can effectively mitigate the drawbacks of electric buses. It can charge buses when they are in motion. Many projects [33, 34] have developed and implemented DWC technologies on transit buses. The planning of the dynamic wireless charging infrastructure for electric buses is still under development and is very challenging. The existing models either for a single route or multiple routes are all based on the concepts and techniques of OLEV [35-38]. They are not applicable to other systems with different architectures, such as the DWC technologies developed by Utah State University [39] and ORNL [40]. The topology of the power transmitter used in OLEV is a continuous inductive track/cable, while the power transmitter developed in the DWC system of ORNL consists of many circuit coils. An experimental study [40] shows that the energy transferred from a DWC

system is a function of vehicle speed, allowing the power level and the number of coils per mile of a DWC system to be sized for the sustained operation of an EV. Therefore, the sizing of the DWC system can be included in the allocation model to answer the question, how many coils per mile are required at specific road segments according to different driving behaviors and traffic conditions? In addition, the existing studies of the allocation of DWC facilities for bus transit systems treat the routes as unidirectional routes. But in reality, bus transit networks generally consist of many bidirectional routes, especially for the downtown area. The bidirectional routes should be considered. As stated in [36] and [38], the neighboring road segments can share the fixed cost of DWC infrastructure. The bidirectional routes also can share the fixed costs of the DWC system as the parallel road segments are close to each other. Since DWC technology will save the long charging time for electric buses, the tactical bus frequency setting should be adjusted for buses operating in the new charging system. Therefore, in order to promote the emerging of electric buses in transit usage, an energy and time-efficient charging system for electric buses in complex transit networks is required to be designed with the consideration of bus frequency setting. This exploratory research was investigated in Chapter 4.

1.3 Research Questions and Objectives

The overarching goal of this dissertation is to achieve sustainability in urban transit and high-occupancy vehicle systems through emerging technologies and operations. Three studies are included in this dissertation to accomplish the primary objective. They are (1) hybrid bus energy estimation, (2) ridesharing operations and assessment, and (3) charging infrastructure design for electric buses. The construction

framework of the energy estimation model for transit buses provided by the first study is adopted in the third study to build the energy consumption model for electric buses. In addition, these three studies are all conducted on the same testbed, Chattanooga, Tennessee. Chattanooga is a good testbed for the studies of achieving sustainability in urban transit and high-occupancy vehicle systems given there is a well-built public transit system named Chattanooga Area Regional Transportation Authority (CARTA), its travelers' openness to rideshare services, and air quality problems need to be addressed due to high vehicle-related vehicle ownership.

Each of the three studies has its own specific set of questions and objectives.

1.3.1 Hybrid buses fuel consumption prediction

Energy saving-oriented operation of the transit bus plays a key role in achieving sustainability in public transportation. This can be achieved by providing accurate energy consumption information to drivers and transit system managers, to help them better plan operations and eco-driving in transit service. In this study, hybrid buses refer to non-plug-in hybrid buses. They use a combination of gasoline-fueled engines and electric motors, where gasoline engines are sued to keep their small batteries charged during driving, the electric motor normally engages to supply a portion of propulsion at low-speed driving with high acceleration or stop-and-go driving conditions. Thus, changes in fuel consumption of a hybrid bus depend on the driving cycle and driving behavior. The diversified operations and driving cycles of the hybrid bus make it difficult to accurately estimate fuel usage. The question for the first research is: how can we build better energy prediction models for the hybrid electric bus to provide accurate information for energy saving oriented operation of the transit bus?

The main goal of this research is to develop ANN-based models for predicting fuel consumption rates for hybrid buses at two levels, microscopic and mesoscopic. The microscopic level model is to predict the energy consumption at a high resolution, second by second. It uses velocity, acceleration, and road grade, as well as other vehicle and road characteristics at 1 Hz frequency as the input variables. The mesoscopic model estimates the energy for different trip durations. The input data is the aggregated traffic pattern information for different trip durations, such as 5, 15, 30, and 60 min. In addition, fuel consumption differences between hybrid and diesel buses and potential influencing factors are assessed.

1.3.2 Ridesharing operations and assessment

As illustrated before, ridesharing recently has had fast growth and commercialization. Ridesharing services can reduce traffic congestion and vehicle emissions. Most study used travel survey data to assess the effects of ridesharing. Their conclusions are mainly about the current situation of ridesharing and do not offer insights into future scenarios. But transportation practitioners need to know the effect of different scenarios when evaluating various ridesharing policies. The research questions are: (1) how to develop an impact evaluation framework for ridesharing services in a bottom-up way that can quantify the effects of ridesharing services at the individual level, and (2) how to implement scenario analysis that can be used by transportation practitioners to evaluate the potential impacts of various ridesharing strategies.

To tackle these questions, this study proposes an integrated framework to analyze the efficiency and environmental benefits of ridesharing under various scenarios on a regional scale. Specifically, the framework utilizes an agent-based traffic simulation

package (i.e., SUMO) to replicate traffic activities for commuting trips on a city scale based on real-world traffic data. Meanwhile, this study develops an effective heuristic matching algorithm for arranging ridesharing trips among travelers that can be applied in the simulator and has the flexibility to represent various ridesharing scenarios. We construct scenarios representing different ridesharing strategies and penetrations. Last, travel efficiency and environmental performance are evaluated and compared among different ridesharing scenarios.

1.3.3 Charging infrastructure design for electric buses

Generally, charging facilities have already been built in many cities for electric bus operation. To best use the source of existing infrastructures, we should consider the collaboration of wireless charging lanes with static charging facilities. Since DWC will save a lot of charging time for electric buses, the bus frequency should be rescheduled for buses operating in the new charging system. Therefore, we should consider the trade-off between bus frequency and the deployment of DWC facilities. A real-world electric bus system always contains bidirectional multiple bus lines. To be realistic, serving such complex multiple routes should be considered when designing a new charging system for electric buses. So, the question for this research is: how to deploy wireless charging lanes and set the bus frequency to minimize the overall social costs in large-scale complex transit systems?

The primary goal of this study is to provide a practical engineering tool to support system-level decisions for the wireless charging-based transit system. In this study, we develop a MIP optimization model to address the allocation problem of DWC lanes on bidirectional multiple routes, considering the bus frequency setting for the new charging

system. Our goal is to find an optimal DWC system design for electric buses that minimize the social costs relating to the bus operation on the new charging system, including the total construction cost of DWC facilities, electric bus fleet purchase cost, passenger waiting cost, and cost for producing and transmitting electricity for charging facilities. We consider three groups of constraints, including the DWC deployment constraints, bus frequency setting constraints, and energy constraints.

1.4 Structure of Dissertation

The dissertation includes five chapters. The first chapter is a general introduction to the background, research significance, research questions, and objectives. The last chapter includes research conclusions and recommendations for future study. Chapters 2 through 4 are prepared in paper format, including published and submitted papers. Therefore, some essential explanations may be repeated.

Chapter 2 is titled “Hybrid electric buses fuel consumption prediction based on real-world driving data”, where the microscopic and mesoscopic machine learning models are developed for estimating the energy consumption of hybrid buses based on real-world driving data. The model selection and construction framework in this study are also employed in Chapter 5 for modeling the energy consumption of electric buses.

Chapter 3 is entitled “Assessing the impacts of ridesharing services: An agent-based simulation approach”. In this study, a travel efficiency and environmental impact evaluation framework for various ridesharing strategies and penetrations with consideration of individual-level behavior changes was developed.

Chapter 4 is titled “Planning of dynamic wireless charging lanes considering bus frequency setting for battery electric buses”. In this study, the optimization model of

planning DWC facilities for battery electric buses with the integration of tactical bus frequency setting is constructed.

Chapter 2

Hybrid Electric Buses Fuel Consumption Prediction based on Real-world Driving Data[1]

[1] Sun, R., Chen, Y., Dubey, A. and Pugliese, P., 2021. Hybrid electric buses fuel consumption prediction based on real-world driving data. *Transportation Research Part D: Transport and Environment*, 91, p.102637.

Abstract

Estimation of fuel consumption by hybrid diesel buses is challenging due to its diversified operations and driving cycles. In this chapter, a unique long-term transit bus monitoring data is used to empirically compare fuel consumption of diesel and hybrid buses under various driving conditions. The artificial neural network based high-fidelity microscopic (1Hz) and mesoscopic (5-60 min) fuel consumption models for hybrid buses are built. The microscopic model contains 1 Hz driving, grade and environment variables. The mesoscopic model aggregates 1Hz data into 5~60-minute traffic pattern factors and predicts average fuel consumption over the durations. The prediction results show mean absolute percentage error of 1-2% for microscopic models and 5-8% for mesoscopic models in predicting fuel consumption rate. The data are partitioned by different driving speed, vehicle engine demand and road grade to investigate their impacts on prediction performance.

2.1 Introduction

Globally, the transportation sector consumes 79 quadrillion BTU of energy, produces 5.7 gigatons of greenhouse gas (GHG) emission and other criteria pollutants that contribute to 200,000 annual premature deaths [41]. Public transportation has potential in reducing energy consumption due to its benefits in conveying larger passenger volume in less space than private automobiles [42]. Emerging technologies, including automation, internet of things, and the sharing economy enable innovations in transit operations, which provide greater potential in achieving sustainability goals in the transportation sector [43]. However, public transportation service has high operational and capital costs due to its low occupancy rate. For example, in United States, the

average operating and capital costs of the nation's 10 largest bus systems are $0.85 and $0.16 per passenger mile, which are substantially higher than those of private automobiles, which are $0.11 and $0.14 per passenger mile[2]. According to United States Bureau of Transportation Statistics, fuel cost is approximately 20 percent of total transit operating costs [44]. The non-plug-in electric hybrid bus has attracted attention from transit authorities, and its market share has been steadily increasing over the past decade. For brevity, the non-plug-in electric hybrid bus is referred to as the hybrid electric bus in this paper. A hybrid bus has a small battery and an electric motor on board, which can provide supplemental propulsion, particularly at low speeds with heavy traffic and frequent stop-and-go driving. Thus, changes in fuel consumption of a hybrid bus, as compared with conventional diesel buses, depend on the driving cycle, driving behavior, and energy management of the hybrid bus. [45] showed improvements to fuel economy ranging from 16% to 48% for hybrid buses, when compared to diesel buses, based on different driving cycles. Therefore, to implement energy-saving operation of transit buses, accurate prediction models are needed to understand the fuel consumption behavior of hybrid buses. However, there is currently a knowledge gap regarding this understanding in the literature.

In literature, methodologies to estimate the energy consumption and savings of transit buses can be divided into summary or estimation models. Summary models focus on comparing trip or daily average energy consumption of transit bus based on in-use or

[2] The data is obtained from the website http://www.portlandfacts.com/cost_of_transit_&_cars.html , accessed on September 28th, 2020

simulated data. [23] tested several types of buses including conventional diesel, natural gas and diesel hybrid, in Beijing and Macao, using portable emission measurement systems (PEMS). They found hybrid diesel buses can achieve 18-29% savings in fuel consumption. Though not studying hybrid bus, [26] is one of the limited studies to compare fuel consumption of a hybrid electric passenger car to a car with internal combustion car with the same chassis under real-world driving and defined "benefit" factor of the hybrid car for each vehicle specific power bin. In addition to laboratory tests, some research summarized energy benefits of hybrid electric buses with the simulation-based method [18, 46]. [24] developed a methodology that provided comparisons of high-resolution fuel use and emission characterization of a hybrid diesel school bus as compared with a conventional diesel bus. They summarized energy use and benefits of hybrid bus under five driving cycles. They found that the hybrid bus provides large energy benefits on arterial routes and less benefits on highway or local routes. This is a relevant study but was done about one decade ago and there is a need to assess energy benefits of hybrid bus with the incorporation of recent technologies. Additionally, these summary models do not explore statistical relationships between fuel consumption and influencing variables but rather depend on a large number of measurements to ensure statistically robust results.

Estimation models refer to energy consumption prediction of transit bus using different types of statistical models and on different granularity. Linear or nonlinear regression-based prediction methodologies are most popular in literature, particularly for diesel bus energy estimation. [27, 28] adopted a regression model with categorical independent variables on time of day, time of week, and road type to predict fuel rate of

buses in different countries. [47] developed quadratic format fuel consumption models for diesel and hybrid buses. They found fuel consumption rate achieve the lowest level when buses are cruising at speed between 39 to 47 km/h within grades 0%-8% and will decrease with higher grade and load. Some studies developed advanced and machine learning-based models. Advanced prediction methods, such as neural network or support vector machine, are used in literature to predict energy and emissions of diesel buses [29, 30], but few studies have focused on hybrid buses.

The literature review demonstrates a need to develop fuel consumption estimation models for hybrid buses based on long-term, in- use experiment data. A high-resolution fuel prediction model for hybrid diesel buses can enable transit operators to improve their planning and bus operations to achieve their fuel savings and sustainability goals. In this study, we propose artificial neural network (ANN) based fuel consumption estimation models that utilize real-world operation data with 1 Hz granularity to achieve accurate predictions of microscopic and mesoscopic fuel consumption of hybrid diesel buses. Specifically, the microscopic model utilizes second-level vehicle trajectories to predict fuel consumption rate of hybrid diesel buses at 1 Hz frequency. The mesoscopic model estimates average fuel consumption rate at 5, 15, 30, and 60-minute durations based on aggregated traffic pattern factors. In addition, fuel consumption differences between hybrid and diesel buses and potential influencing factors are assessed. We acknowledge that the developed model and estimation coefficients obtained in this study are specific to the studied fleet and region. However, the ANN estimation model framework is applicable to different fleets in other regions if similar transit bus measurement data are available.

2.2 Experiment Setup and Input Data

The data used in this study are 1 Hz driving and fuel consumption measurements recorded by on-board sensors on one diesel transit bus and one hybrid non-plug-in electric transit bus between March 2019 and March 2020. The buses are in the transit operating fleet of the Chattanooga Area Regional Transportation Authority (CARTA). They were manufactured by Gillig Brothers Inc. Table 2.1 summarizes the specifications of the diesel and hybrid buses. The collected data were 1 Hz frequency real-time location coordinates (i.e., latitude, longitude), elevation, ambient temperature, vehicle dynamics (instantaneous speed and acceleration), and fuel consumption rate. Data on vehicle dynamics and fuel consumption were obtained by gathering information with the vehicle's control area network bus (CAN bus) using a data logger called Datahub developed by ViriCiti Inc[3], which complies with the Society of Automotive Engineers J1939 standard. The data logger contained an accelerometer to measure instantaneous speed and transform the location to longitude and latitude coordinates. The temperature was obtained through query Dark Sky API weather data[4]. The elevation data were queried through elevation databases according to instantaneous bus coordinates. The elevation database was provided by the Tennessee elevation LiDAR project, which is a coordinated effort with the United States Geological Survey. The Tennessee Elevation LiDAR database provides elevation data and the majority of GPS locations (with 1–2 foot contour) in State of Tennessee. Based on the elevation data, the road grade of each 1 Hz measurement is calculated by dividing the elevation difference between current and

[3] ViriCiti Inc. DataHub. https://viriciti.com/datahub/

[4] Dark Sky Weather API. https://darksky.net/dev/docs

previous measurements by the driving distance. We have to acknowledge that there are limitations on using geographic information system data to calculate road grade, because road grade normally does not match the general slope of the land. Particularly, major roads are constructed to reduce grade if the terrain is hilly. We use the road grade data based on Tennessee Elevation LiDAR database, but will look for better road grade data if they are available. The driving data are collected from transit buses running on all routes operated by CARTA, as shown in Figure 2.1(a), and typical driving trajectory for each route is presented in Figure 2.1(b). The routes represent typical mountainous terrain patterns in the region, which is surrounded by the Tennessee River and the ridge-and-valley Appalachians. The driving cycles have speeds up to 40–50 kph and an acceleration range of -2 to 2 m per second.

Table 2.1 Chassis and Engine Information for Gillig Model Year 2014 Diesel and Hybrid Buses

Characteristic	Diesel Bus	Hybrid Bus
Seat Capacity	32 seats	32 seats
Model year	2014	2014
Hybrid architecture	N/A	Parallel
Powertrain	Engine: Cummins ISL	Engine: Cummins ISB Motor: Allison H40EP
Powertrain Power	264 kW	261 kW (209 kW for engine)
Curb weight	11,600 kg	12,400 kg
Engine Storage System Weight	N/A	440 kg

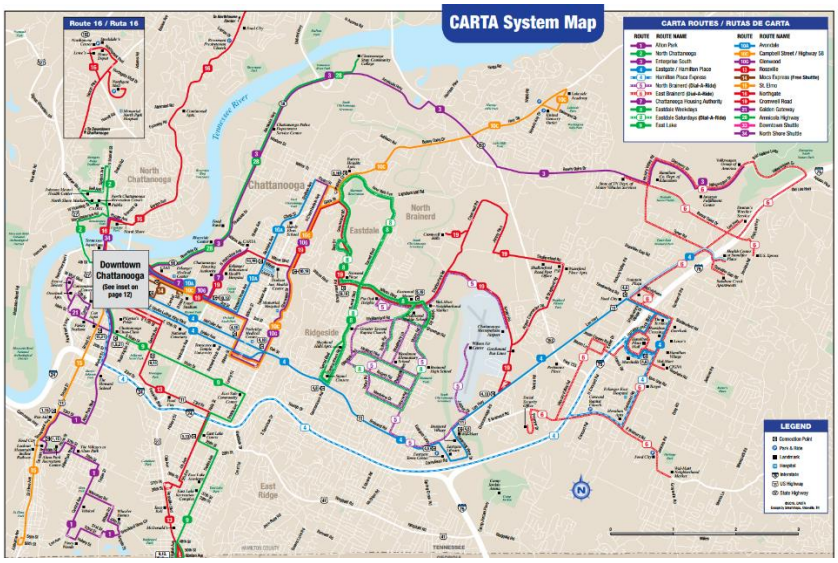

(a)

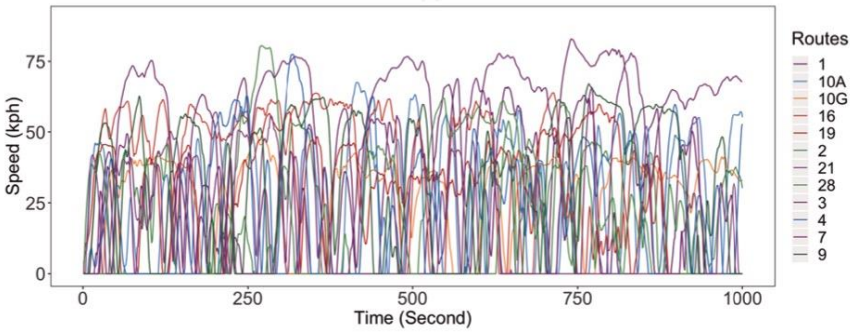

(b)

Figure 2.1 Route map (a) and typical driving trajectories for bus routes (b) of Chattanooga Area Regional Transportation Authority (CARTA)

2.3 Comparison of Hybrid and Conventional Diesel Buses

In Figure 2.2, the distribution of amount of time spent in vehicle specific power (VSP), speed, and road grade bins for diesel and hybrid buses are compared. VSP is an evaluation metric for vehicle energy consumption and emissions. As stated in [48], "it is the sum of loads resulting from aerodynamic drag, acceleration, rolling resistance, and hill climbing, all divided by the mass of the vehicle". VSP is calculated by dividing the instantaneous power for kinetic, potential, rolling, and aerodynamic resistance by vehicle weight,

$$VSP = \frac{\frac{d}{dt}(KE + PE) + F_{rolling} * v + F_{Aerodynamic} * v}{m}$$

$$= \frac{\frac{d}{dt}\left(\frac{1}{2}m * (1 + \epsilon_i) * v^2 + m * g * h\right) + C_g * m * g * v + \frac{1}{2}\rho * C_D A v^3}{m}$$

$$= v * \left(a * (1 + \epsilon_i) + g * garde + g * C_g\right) + \frac{1}{2}\rho * \frac{C_D A}{m} v^3$$

The unit for VSP is kW per ton. VSP is considered to be a surrogate measurement for the instantaneous power demand of a vehicle normalized to its own weight and has been used in recent literature [49, 50]. Figure 2.2 show similarities in driving status and road grade conditions for the diesel and hybrid buses.

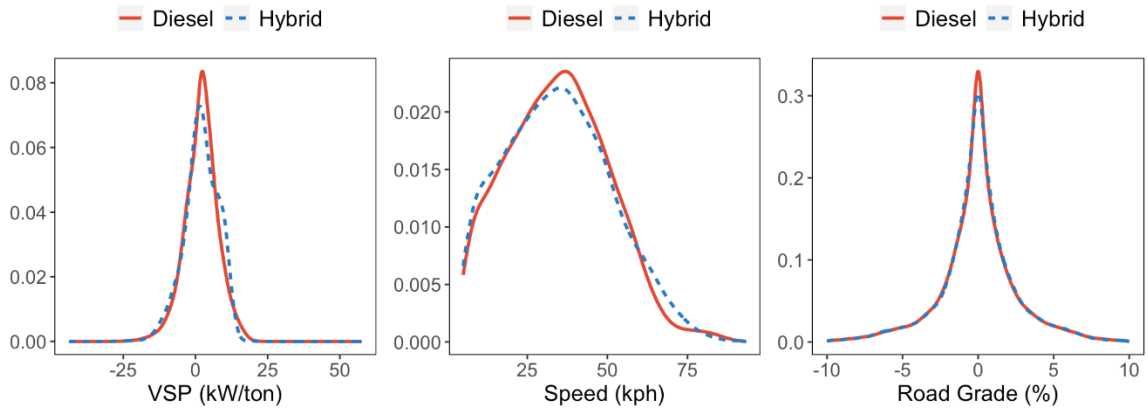

Figure 2.2 Vehicle specific power, speed and road grade distribution comparison of diesel and hybrid driving.

Figure 2.3 shows the average fuel consumption rates of diesel and hybrid buses as a function of instantaneous VSP with 1 kW/ton interval. VSP measures a vehicle's tractive power normalized to its own weight. Thus, the comparison in Figure 2.3 accounts for the difference in the weight of hybrid and diesel buses. Each average fuel consumption rate was averaged over at least 2,000 instantaneous measurements to ensure statistical robustness. The results show a positive relationship between VSP and the bus fuel consumption rate. However, the slope of the curves decreases when VSP is greater

than 15 kW/ton. This observation is expected and is consistent with previous studies [51, 52]. Similar patterns of fuel savings for hybrid buses were observed in other studies [53, 54].

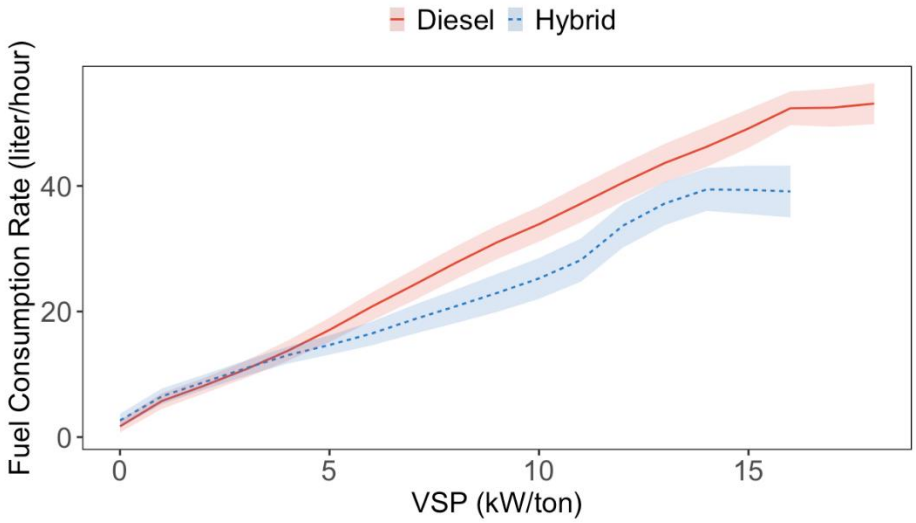

Figure 2.3 Mean fuel rate (liter per hour) and 95% confidence interval (shaded area) for diesel and hybrid bus as a function of instantaneous vehicle specific power bins from 0 to 18 kW/ton with 1 kW/ton interval.

Figure 2.4 reports the percentage of fuel savings for hybrid buses compared with diesel buses, accounting for driving speed and VSP. The results are controlled in three speed categories: (1) 1 to 40 kph (equivalent to 25 miles per hour), (2) 40 to 80 kph (equivalent to 50 miles per hour), and (3) above 80 kph. These three categories correspond to typical local, arterial, and highway driving conditions. This categorization is consistent with that used in MOVES, a widely used model for vehicle energy and emission analysis [55]. Figure 2.4 shows that the fuel benefits of hybrid buses vary, depending on driving conditions. For local driving (speeds up to 40 kph), the fuel savings for hybrid buses increase linearly as the VSP increases. The fuel savings could be as little as 0% at low VSP (5 kW/ton) or as high as 70% at high VSP (17 kW/ton). In local driving, the high VSP typically represents aggressive acceleration from stop or low

speeds during heavy traffic or from bus stops. Under arterial driving conditions (speeds between 40 and 80 kph), hybrid buses have the same fuel efficiency as the diesel buses until the VSP is greater than 15 kW/ton. At a VSP of 18 kW/ton, the fuel savings are approximately 10%. The high VSP in arterial driving typically corresponds to aggressive acceleration to avoid heavy traffic. For highway driving, the fuel efficiency of hybrid buses is worse than diesel buses when VSP is greater than 5 kW/ton. However, steady highway driving does not appear to account for drivers that are "dithering" the pedal, which would result in vibrative power demand and create charging opportunities for hybrid buses. Very high-resolution speed data are needed to perceive the "dithering" effect, which may be a direction for future data collection and research. [26] found that the fuel consumption for a hybrid gasoline passenger car is 5–20% worse than a comparable gasoline car under highway driving conditions with a VSP greater than 10 kW/ton. [24] showed that a parallel hybrid diesel school bus reported 3–9% worse fuel consumption rates than a comparable conventional diesel school bus under highway and arterial driving conditions.

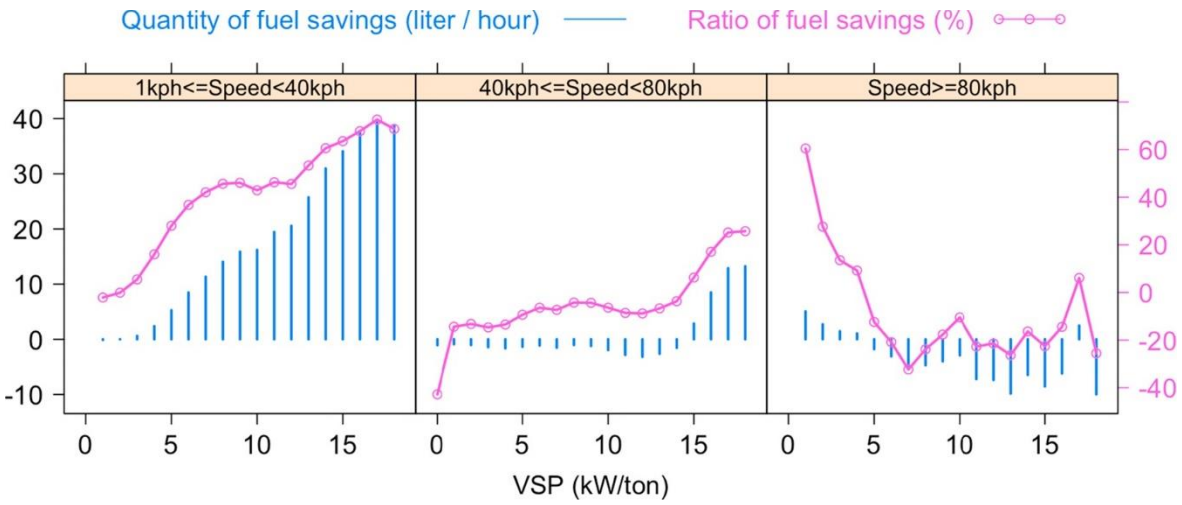

Figure 2.4 Fuel savings percentage of hybrid buses as compared with diesel buses by driving speed and vehicle specific power.

2.4 Development of Fuel Consumption Prediction Model

This study aims to develop ANN-based models for predicting fuel consumption rates for hybrid diesel transit buses at the microscopic and mesoscopic levels. In the microscopic model, the fuel rate (liters per hour) is estimated based on velocity, acceleration, and road grade, as well as other vehicle and road characteristics factors at 1 Hz frequency. In the mesoscopic model, fuel estimates are based on aggregated traffic pattern information for trip durations of 5, 15, 30, and 60 min. As shown in Figure 2.5, the model development and applications are illustrated in three modules. In the 1st module, which is referred to as "data preparation.", vehicle trajectory and fuel consumption data at 1 Hz frequency are collected and processed into 5, 15, 30, or 60-minute trip duration average metrics. In the "model development" module, artificial neural network models are built for 1 Hz data and aggregated data at different trip durations to estimate the fuel rates of hybrid buses. In each model, the dataset was divided into datasets of training, validation, and testing. Training data was used to fit a prediction model. The validation set was used to perform parameter/model selection and to cope with overfitting, which is considered part of the training process. The testing set was used to evaluate model performance. The prediction results were at the same time resolution of the input data, as prepared in "data preparation" module. Finally, in the "model application" module, the developed models can be applied at different time resolutions with various input variables, depending on the specific applications. This approach provided flexibility in model application, particularly given that users have varying degrees of access to the input data.

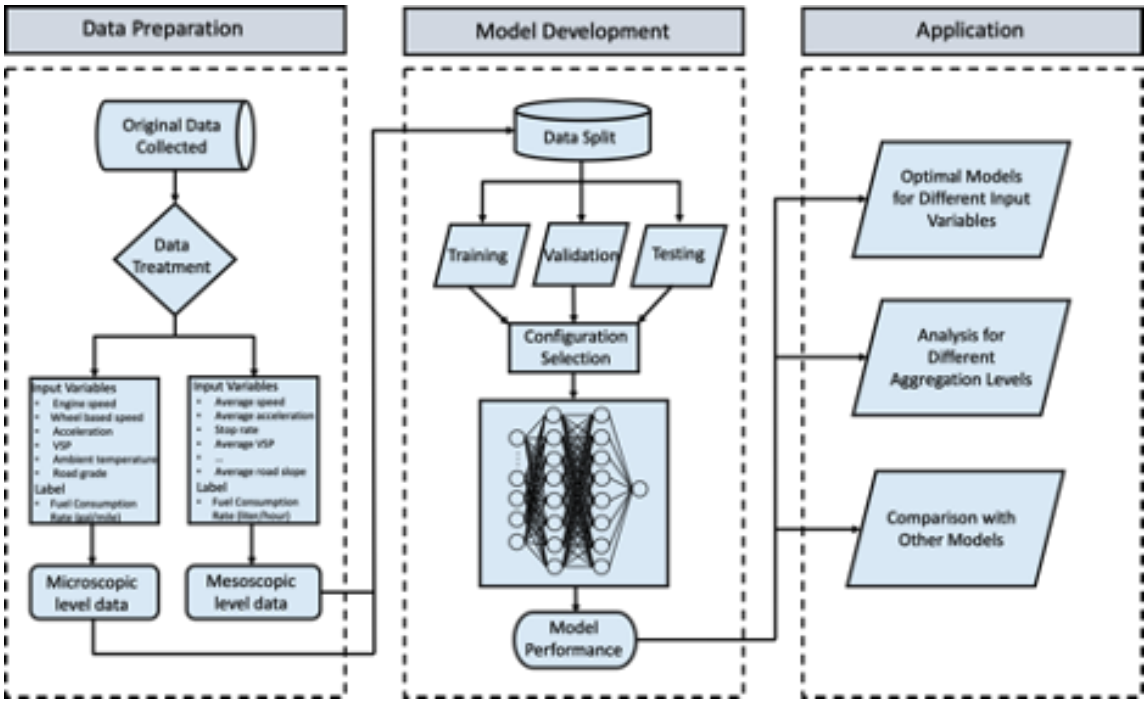

Figure 2.5 Flowchart of the main tasks.

2.4.1 Data preparation

The microscopic model predicts fuel consumption rate (liters per hour) using vehicle speed/velocity, acceleration, road grade, ambient temperature, and VSP at 1 Hz frequency as the input variables. To prepare mesoscopic models, the collected 1 Hz data are processed into 11 independent variables and the predicting variable, i.e., fuel consumption rate (liter per 100 km), as shown in Table 2.2. The ability to capture temperature data was helpful for both microscopic and mesoscopic models to infer fuel consumption used for air conditioning since all the buses in this study were not equipped with a heating burner. Passenger load can influence the fuel consumption of buses, particularly under heavy load conditions [56]. However, passenger load information was not included in the data that was collected for this study. However, obtaining this information may be a future direction for data collection and future research.

Table 2.2. Description of mesoscopic model input data.

Symbols	Descriptions
n	The index of analysis snippet
T	The time span of an analysis snippet (i.e. 5min, 15min, 30min, 60min)
t	The index of second in an analysis snippet, *t={1,2,…, T}*
d_t^n	The cumulative distance at second *t* of snippet *n* (mile)
v_t^n	The instantaneous speed at second *t* of snippet *n* (kilometer/hour)
f^n	The cumulative fuel consumed at the end of snippet *n* (gallon)
$\bar{v}^n$	The average speed of snippet *n* (mile/hour)
$v\sigma^n$	The standard deviation of speed in snippet *n*
$\bar{a}^n$	The average acceleration of snippet *n* (meter / second^2)
a_t^n	The instantaneous acceleration at second *t* of snippet *n* (meter / second^2)
$a\sigma^n$	The standard deviation of acceleration in snippet *n*
VSP_t^n	The vehicle specific power at second *t* of snippet *n* (kW/Metric Ton)
l_t^n	The elevation of vehicle at second *t* of snippet *n* (meter)
g_t^n	The road grade at second *t* of snippet *n* (%)
$g\sigma^n$	Standard deviation of road grade at second level in snippet *n*
g^n	The road grade at snippet *n* (%)
s_t^n	The driving status index of a bus at second *t* of snippet *n*, 1=moving, otherwise 0
q^n	The total number of stop-and-go driving events in snippet *n*
s^n	Percentage of time in stop position during snippet *n*
w_t^n	The ambient temperature at second t of snippet *n* (°F)
r^n	Average fuel consumption rate in snippet *n* (liter per 100 km)

(1) Average speed (kilometer/hour) in snippet *n*: $\bar{v}^n = \frac{d_T^n - d_1^n}{T}, \forall\, n$.

(2) Standard deviation of speed in snippet *n*: $v\sigma^n = \frac{\sqrt{\sum_{t=1}^{T}(v_t^n - \bar{v}^n)^2}}{T-1}$.

(3) Average acceleration (meter/second^2) in snippet *n*: $\bar{a}^n = \frac{\sum_{t=2}^{T}(v_t^n - v_{t-1}^n)}{T-1} = \frac{v_T^n - v_1^n}{T-1}$.

(4) Standard deviation of acceleration in snippet *n*: $a\sigma^n = \frac{\sqrt{\sum_{t=1}^{T}(a_t^n - \bar{a}^n)^2}}{T-1}$.

(5) Stop-and-go times in snippet *n*: $sg^n = \sum_{t=2}^{T}|s_t^n - s_{t-1}^n|$.

(6) Stop rates in snippet *n*: $s^n = \frac{\sum_{t=1}^{T} s_t^n}{T}$.

(7) Average ambient temperature (°F) in snippet *n*: $\bar{w}^n = \frac{\sum_{t=1}^{T} w_t^n}{T}$.

(8) Average road grade at second level in snippet *n*: $\bar{g}^n = \frac{\sum_{t=1}^{T} g_t^n}{T}$.

(9) Standard deviation of road grade at second level in snippet *n*: $g\sigma^n = \frac{\sqrt{\sum_{t=1}^{T}(g_t^n - \bar{g}^n)^2}}{T-1}$.

(10) Road grade in snippet *n*: $g^n = \frac{l_T^n - l_1^n}{d_T^n - d_1^n}$.

(11) Average Vehicle Specific Power (VSP) (kW/Metric Ton) in snippet *n*: $\overline{VSP}^n = \frac{\sum_{t=1}^{T} VSP_t^n}{T}$, where, $VSP_t^n = v_t^n(1.1a_t^n + 9.81g_t^n + 0.132) + 3.02 \times 10^{-4}(v_t^n)^3$, with v_t^n in meter/second and a_t^n in meter/second^2 [48].

(12) Fuel used rate in snippet *n*: $r^n = \frac{f^n - f^{n-1}}{d_T^n - d_1^n}, \forall\, n, f^0 = 0$.

2.4.2 Artificial neural networks development

The artificial neural network (ANN) approach was employed to estimate fuel consumption rates using the prepared data. An ANN model processes information in the same way that the human brain processes information [57]. Specifically, an ANN model contains input, along with hidden and output layers, and each layer contains data processing components called neurons. These neurons or processing components are connected to each other and can form complex nonlinear models through activation functions. The activation function determines the value of the neurons in the next layer or the output, based on the values and coefficients of neurons in the current layer. Thus, the ANN model can identify the relationship between input and output variables by exploring different forms and weight combinations of neurons in the input and hidden layers, which makes the ANN model a perfect candidate model to be used in this study. For example, a previous study showed that air conditioning (AC) loads in buses can consume significant amounts of energy [53]. However, the measurement data did not include AC auxiliary

power. To account for AC loads in fuel consumption, ambient temperature is included as an input variable in the estimation model. The relationship between temperature and fuel consumption of buses is not a linear relationship, but a convex quadratic relationship with higher fuel consumption at high and low ends of the temperature spectrum. Thus, the ANN model is capable of representing complex nonlinear relationships.

The activation function is responsible for transforming the set of neurons in one layer into a given neuron or output in the next layer. There are two major types of activation functions: the nonlinear activation function and the linear activation function. Nonlinear activation functions allow neural network models to represent complex relationships using only a small number of input variables. Therefore, several major types of nonlinear functions were tested to identify the functions that maximize the predictability of the model. These functions are the sigmoid function ($\frac{1}{1+e^{-x}}$), the tanh-sigmoid function ($\frac{2}{1+e^{-x}} - 1$), and the rectified function ($\max\{0, x\}$).

Due to severe computations on the high dimensional data when training the ANN models, it is a common practice to scale input data using normalization, $x_i = \frac{x_i - \min(x)}{\max(x) - \min(x)}$, where x_i is the observation for the parameter and min(x) and max(x) are the minimum and maximum observations respectively. Clearly, the performance of an ANN model depends on its configuration. Selecting more hidden layers may increase the accuracy of the network but can increase training time due to its complexity and may result in overfitting. [58] proved that a neural network with up to two hidden layers is sufficient to represent complex, nonlinear relationships. Moreover, the experimental results in this paper reveal that the first and second hidden layers should contain an equal number of neurons so that the network can be trained easily. The number of neurons in

hidden layers are generally determined by using a trial-and-error method (Maier and Dandy, 2001). A frequently used upper limit for the number of neurons in a hidden layer is $N_h \leq 2N_i + 1$, where N_h is the number of neurons in the hidden layers and N_i is the number of input variables [59-61]. Additionally, [62] recommend $N_h \leq \frac{S_t}{N_i+1}$, where S_t is sample size of training data to avoid overfitting. In this study, the minimum of the two N_h is chosen as the upper limit for the number of hidden layer neurons. To get the best approximation of the hidden layer neurons, the number of neurons can be reduced, and training is done to determine whether the network converges to the same solution.

The measurement data are randomly partitioned into training, validation, and testing datasets as 70%:15%:15% [63]. Specifically, an ANN model is trained using the training set. Then, before testing for prediction performance, training progress is monitored by using independent data, i.e., the validation set, to measure how well the neural network is generalizing outside of the training set. Only models that satisfy our prediction performance threshold on the validation set will be chosen and used for predictions using the test set.

2.5 Results and discussion

2.5.1 Microscopic model selection and prediction performance

Data that are collected at 1 Hz frequency are considered to be independent variables in the microscopic model. These data include engine speed, wheel-based speed, acceleration, road grade, ambient temperature, and VSP. The best model yields a mean absolute percentage error (MAPE) of 36%, R2 of 0.96, and a mean absolute error (MAE) of 1.5 L per hour, although there are several model setups that have similar prediction performance metrics. The prediction metrics are calculated by comparing the predicted

and actual fuel consumption of each 1 Hz record. Then, the results are averaged or aggregated to obtain the metrics. Figure 2.6 compares actual and estimated fuel consumption rates (liters per hour) at every second for one randomly chosen trip. The results show a general alignment between the actual and estimated fuel consumption rates. However, estimation randomness can lead to larger absolute percentage errors at small (i.e., small denominator when calculating the percentage error) fuel consumption rate occurrences. Therefore, the MAPE of 36% for the 1 Hz level prediction is primarily determined by errors at small fuel consumption occurrences.

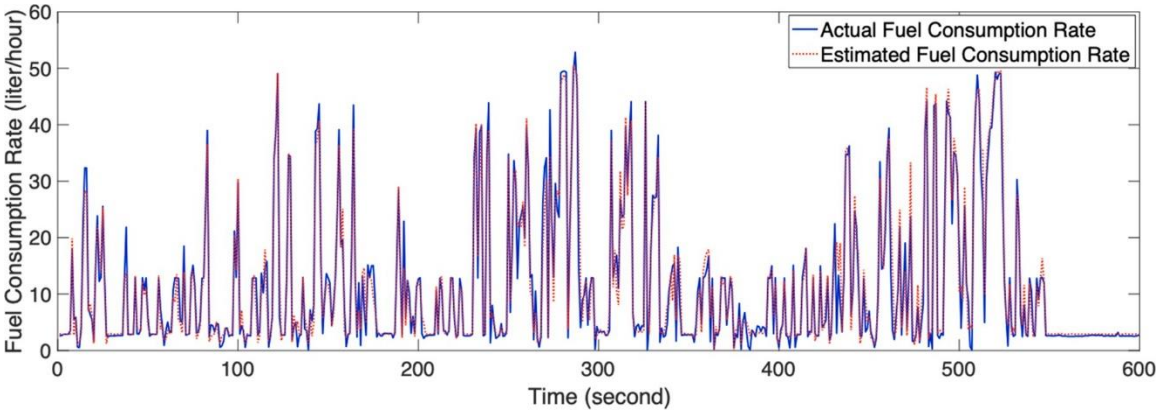

Figure 2.6 Second-by-second actual fuel consumption rate (liter per hour) versus estimated fuel consumption rate for one trip.

The fuel consumption predictions are accumulated into 5, 15, 30, and 60-minute average fuel consumption rates and compared with actual values. We acknowledge that evaluating the microscopic model using cumulative error over a trip could overlook variations in prediction error at the 1 Hz level. Since the targeted user scenario of the proposed models is transit operation planning, the focus was on trip level results, although the prediction was done at 1 Hz level.

Trips are formed by aggregating the continuous 1 Hz data with equal time durations of 5, 15, 30, 60-minute. Each 1 Hz record contained the actual and predicted fuel consumption from our microscopic model. For each trip, the fuel consumption over the 5, 15, 30, and 60-minute durations was aggregated over actual/predicted values and compared to obtain the absolute percentage error of the prediction. Figure 7 presents a boxplot of the absolute percentage error (%) for the microscopic model at aggregated levels. It shows that when fuel predictions are aggregated between 5 and 60 min, the mean absolute percentage error reduces as the trip duration increases. However, the MAPEs were near or below 2%, which demonstrated the capability of the microscopic model to predict 1 Hz fuel consumption rates and achieve high accuracy at 5 to 60-minute trip levels.

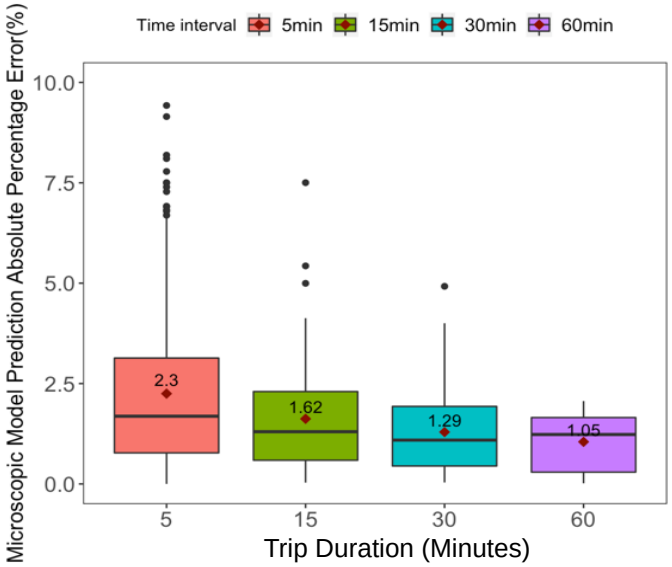

Figure 2.7 Boxplot of absolute percentage error for microscopic model predictions aggregated at 5, 15, 30, 60 minutes. The bar within each box represents the median absolute percentage error and the two sides of box correspond to 1st and 3rd quartiles. The diamond (with number) in a box is the mean value.

Figure 2.8 compares the absolute percentage prediction error for the ANN model and the non-neural network linear regression model as a function of trip duration (left) and instantaneous vehicle specific power (right). For Figure 2.8 (right), the measured and predicted fuel consumption data at 1HZ were averaged based on each VSP bin from 0 to 15 kW/ton to report prediction error. The MAPE and confidence intervals of the ANN model were consistently lower than those of the linear regression model, although the differences seemed to diminish as the trip duration increased. Specifically, the MAPE of the ANN model was consistently near 2%, while it was reduced from 6% to 2% for the linear regression model when the trip duration increased from 5 to 60 min. This reduction was expected, as shorter trip durations typically constitute more dynamic traffic and driving conditions. Thus, the ANN model can capture changes in fuel consumption more effectively using complex model formats. When accounting for VSP, the ANN model outperformed the linear regression model in all of the VSP bins. The improvements in prediction error are significant in low VSP areas (VSP < 3 kW/ton) for the ANN model.

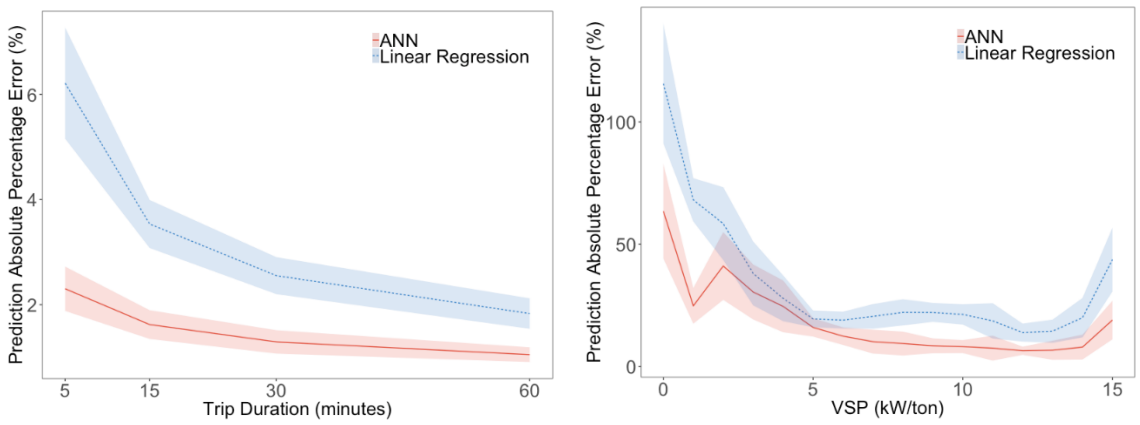

Figure 2.8 Mean absolute percentage error and 95 percentage confidence intervals for predictions of artificial neural network (ANN) model and linear regression model with the same independent variables as a function of trip duration (left) and vehicle specific power (right).

Table 2.3 Description of Microscopic level ANNs Configuration Selection Process.

Hidden layers	Neurons		MAE (liter/hour)	RMSE	MAPE (%)	R^2
	1st layer	2nd layer				
1	13		1.6	2.4	38	0.95
	1		2.4	3.2	72	0.92
2	13	13	1.6	2.3	36	0.95
	11	11	1.5	2.3	36	0.96
	1	1	2.2	3.1	71	0.93

* The results are just for illustration rather than listing all tested microscopic models.

2.5.2 Mesoscopic model selection and prediction performance

The mesoscopic model predicts fuel rates over a time period based on aggregated traffic pattern factors. Different model configurations were compared to determine the best prediction model (Table 2.4). The best model yielded a MAPE of 8.9%, R2 of 0.91, and an MAE of 4.0 L per 100 km. The prediction metrics were calculated by comparing predicted and actual fuel consumption per km of each 5-minute trip. The average fuel consumption rate was 45 L per 100 km, i.e., 5.2 miles per gallon, which is consistent, in terms of magnitude, with the average fuel consumption rate for diesel hybrid buses reported by [45].

Table 2.4 Description of Mesoscopic Level ANNs Configuration Selection Process.

Hidden layers	Neurons		MAE (liter/km)	RMSE	MAPE (%)	R^2
	1st layer	2nd layer				
1	23		0.04	0.025	9.4	0.84
	6		0.03	0.024	9.2	0.91
	1		0.04	0.028	11.4	0.85
2	23	23	0.04	0.025	9.6	0.86
	1	1	0.04	0.028	11.4	0.79

Figure 2.9 (left) presents boxplots of absolute percentage error (%) for the mesoscopic model at 5, 15, 30, and 60-minute trip durations. Similar to the microscopic model, the MAPE of the mesoscopic model generally decreases as the trip time increases;

however, it remains flat when the trip time is greater than 30 min. Figure 2.9 (right) evaluates the prediction error as a function of speed for each trip duration by differentiating trips by speed ranges of 1–40 kph and 40–80 kph for each trip duration. The former trips correspond to typical urban driving, while the latter trips represent a combination of driving under urban, arterial, and highway conditions. There are limited data points to develop robust statistics on travel with an average speed of 40 kph for 30 and 60-minute trips. This lack of data is understandable, given that the average speed of a transit bus in the United States is 22 kph [64]. As a result, a limited number of 30 or 60-minute trips would achieve average speeds above 40 kph. The MAPEs of 40–80 kph trips were higher than those of trips below 40 kph for 5 and 15-minute trips. Thus, higher uncertainty exists when predicting fuel consumption at high-speed driving, which normally consists of a combination of urban, arterial, and highway driving.

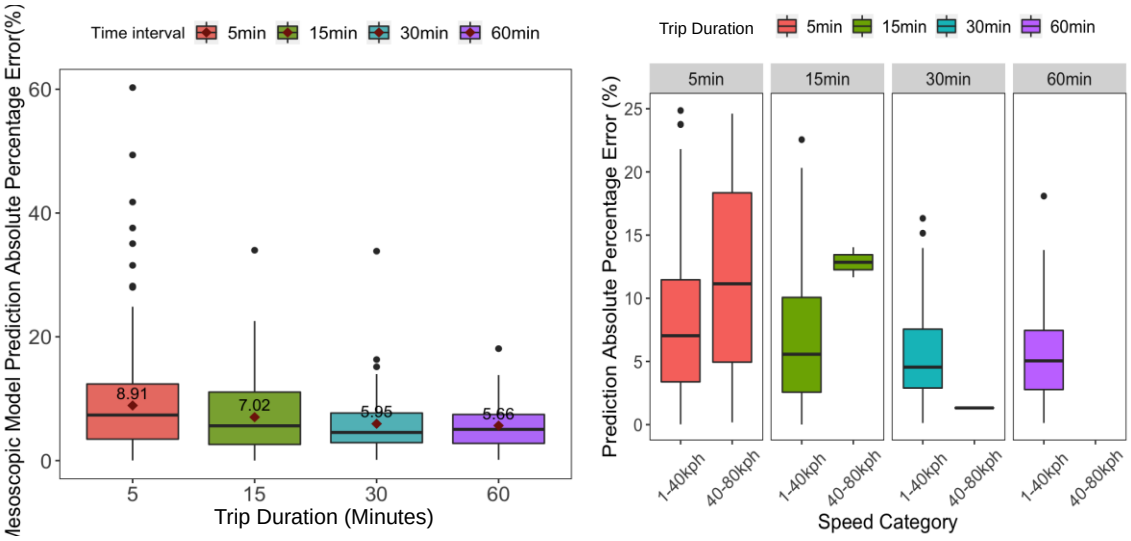

Figure 2.9 Boxplot of absolute percentage error for mesoscopic model predictions at 5, 15, 30, and 60-minute trip duration (left) and discriminating by speed category (right). The bar within each box represents the d absolute percentage error and the two sides of box correspond to 1st and 3rd quartiles. The diamond (with a number) in a box is the mean value.

The mesoscopic model is based on eleven independent variables that are averaged at different trip durations to predict the fuel consumption rate of hybrid buses. Clearly, models with more input variables would result in stronger correlations with output variables and yield better prediction performance. However, due to challenges in data collection, the eleven variables may not be readily available. In this study, we explore the impacts of data availability on the performance of mesoscopic prediction models. First, three scenarios are established, which represented three levels of data availability. “Scenario 1” contained only the average speed variable, which is the minimum data requirement. This scenario is applicable because the average speed of a road network is regularly monitored by transportation authorities. “Scenario 2” contained average speed and road grade variables. This scenario combines traffic data and infrastructure data that are normally available to transportation practitioners. “Scenario 3” contained the eleven independent variables. For each scenario, a model selection procedure is conducted and the optimal model configuration is presented in Table 2.5. A higher MAPE was expected for scenarios with fewer input variables. The single input variable, Scenario 1, had a MAPE of 14%, which was the largest. Studies have used average speed as the sole piece of information to predict the fuel consumption of vehicles, such as the Motor Vehicle Emission Simulator [55, 65] and. However, a few recent studies have adopted single input variable prediction models, due to concerns regarding prediction accuracy [49]. The MAPE of the best model in Scenario 2 is 12%. The speed and road grade variables in Scenario 2 have been used in recent studies [52, 66, 67]. Specifically, speed and road grade can be used to calculate VSP, which is an effective proxy for vehicle power demand [48].

Table 2.5 Comparison of optimal ANN model configurations under different data availability scenarios.

	Neurons		MAE (liter/km)	MAPE (%)	R^2
	1st layer	2nd layer			
Scenario 1	2	--	0.06	14	0.77
Scenario 2	4	--	0.04	12	0.82
Scenario 3	6	--	0.03	9	0.91

Figure 2.10 compares the MAPE of fuel consumption estimates at 5, 15, 30, and 60-minute duration for the three scenarios in the mesoscopic and microscopic models. Within each scenario, it is observed that using data with longer trip durations led to improved prediction performance. This finding was expected because averaging longer time periods can reduce noise in data, which can improve prediction accuracy. However, averaging data into longer periods is not necessarily a better practice. The mean absolute percentage errors of the microscopic model were less than 2%. However, the extra effort to obtain detailed trajectory data must be balanced with improvements in prediction accuracy to justify the use of the microscopic model.

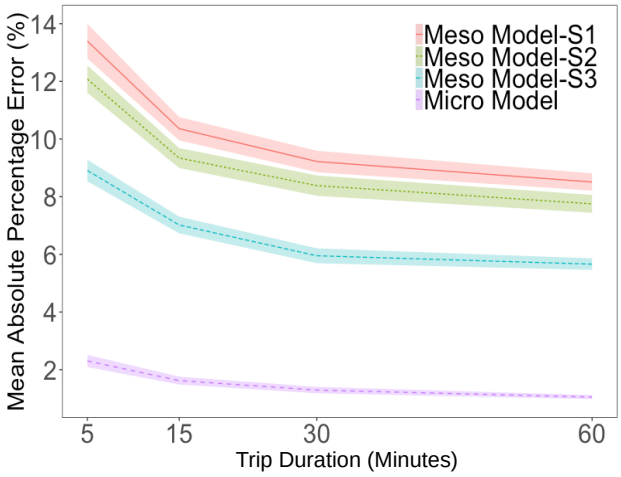

Figure 2.10 Mean and 95 % confidence (shared area) absolute percentage error for microscopic and three scenarios of mesoscopic models as a function of trip duration.

Relevant literature on fuel consumption estimation of transit buses are reviewed and their input variables and model setup are summarized in Table 2.6. Those models used input data at either 1 Hz or trip-average granularity. The prediction outputs were liters per hour for 1 Hz level prediction or trip-average fuel consumption rate (liters per kilometer). The input data (1 Hz and 5-minute average granularity) from this study were applied to models from the literature to compare their prediction performances with our models. Table 2.6 summarizes the comparison results. The MAPEs of trip-level models from the literature ranged from 12% to 22%, which are consistent with the MAPEs reported in the literature using their data. The MAPEs of our models are between 5% and 8%. Three out of the four trip-level models in the literature utilized linear regression-based methods. The other models used the supporting vector machine (SVM) method and reported a MAPE of 12%. The two 1 Hz microscopic models adopted quadratic and exponential regression methods and resulted in MAPEs of 47% and 59%, respectively, which were also aligned with results in their studies. If the 1 Hz prediction results are aggregated into 5 to 60 min, their MAPEs are between 5% and 9%. The comparison shows the potential of the ANN model to accurately predict the fuel consumption of buses under real-world driving conditions.

Table 2.6 Comparison with fuel consumption estimation models in literature.

	Method type	Input variables	Granularity	MAPE
This study	ANN	Speed (average), acceleration, grade, temperature, VSP	Trip	5-8%
Frey et al. [50]	Regression	VSP	Trip	12%
Delgado et al. [68]	Regression	Speed (average), acceleration	Trip	22%
López-Martínez et al. [28]	Regression	Speed (average, max), acceleration,	Trip	18%
Zeng et al. [52]	SVM	Speed (average, variance)	Trip	12%
This study	ANN	Speed, acceleration, grade, temperature	1 Hz	36% (1 Hz) 1-2% (aggr. at 5-60 min)
Wang and Rakha [47, 51]	Regression-quadratic	VSP	1 Hz	47% 1-2% (aggr. at 5-60 min)
Hung et al. [69]	Regression-exponential	Speed	1 Hz	59% 1-2% (aggr. at 5-60 min)

2.6 Conclusions

Hybrid buses have gained popularity in recent years due to their potential savings in transportation fuel. Estimating fuel consumption for hybrid diesel buses is challenging because their operation and driving conditions are diversified. In this paper, we proposed ANN microscopic and mesoscopic models to estimate the fuel consumption of hybrid diesel buses based on long-term transit bus monitoring data collected from CARTA. The microscopic model predicted instantaneous fuel consumption rates based on driving, grade, and environment variables at the same frequency. The ANN-based microscopic model results showed 1–2% of cumulative absolute error when aggregating second-level results to 5 to 60-minute trips. The results showed that ANN models can achieve lower error, compared to linear regression models, using the same input variables. The

mesoscopic model predicted average fuel rates for 5 to 60-minute trip durations based on traffic factors for the same period. Our results show that the absolute prediction error for mesoscopic models ranged between 5 and 9%. This range is higher than that of the microscopic model; however, the independent variables of the mesoscopic model, e.g. average traffic speed, congestion level, etc., are typically monitored by the local transportation authority. The experimental data contained 1 Hz data of hybrid and diesel buses that have similar driving conditions in terms of speed, engine demand, and road grade. Our investigation of fuel rates showed that hybrid buses have the largest fuel savings during low-speed driving with high acceleration and no or increased fuel consumption during highway driving. The electric motor of hybrid buses normally engages to supplement or replace a portion of propulsion provided by the diesel engine at low-speed driving with high acceleration, which can help achieve better fuel efficiency. Similar fuel savings were observed in hybrid passenger car experiments that can be found in the literature. One limitation of this study is that the experiment did not collect operational data for electric motors within the hybrid bus. Therefore, we could not fully understand the energy management system mechanism within the hybrid bus. One future research direction may be to collect and leverage electric motor operation data from hybrid buses to better understand their fuel-saving mechanism. Another future research direction may be to collect passenger load information on buses and assess the impacts of passenger load on the fuel consumption of hybrid buses under real-world driving conditions.

Chapter 3

Assessing the Impacts of Ridesharing Services: An Agent-based Simulation Approach[5]

[5] Sun, R., Wu, X. and Chen, Y., 2022. Assessing the impacts of ridesharing services: An agent-based simulation approach. *Journal of Cleaner Production*, p.133664.

Abstract

A shift from privately owned vehicles to shared mobility services can affect mobility, energy consumption, and vehicle emissions. Existing literature on ridesharing services has focused on evaluating their traffic and economic impacts. In this chapter, an integrated framework is proposed to analyze the efficiency and environmental benefits of ridesharing on a regional scale. The framework utilizes an agent-based traffic simulation package (i.e., SUMO) to replicate traffic activities for commuting trips in a mid-size city, Chattanooga, Tennessee, based on real-world travel-demand data. Scenarios representing different ridesharing strategies and penetrations are constructed. The simulation and results analysis shows that with a ridesharing ratio of 5% to 75% over travel demand on a city scale, many (65%–75%) ridesharing travelers will experience up to a 15-minute delay. About 80% of drive-alone travelers will arrive earlier compared with no ridesharing scenario. The average early arrival time would be 5.6 minutes for all drive-alone travelers. The results also show ridesharing services can achieve a 2%–50% reduction in total city-scale vehicle emissions and energy consumption compared with the no ridesharing scenario. The framework and results of this study can be helpful to transportation practitioners to evaluate environmental benefits when implementing ridesharing services on a city scale.

3.1 Introduction

Road transportation is a major consumer of energy and a contributor to air pollution [70, 71]. Shared mobility is considered an effective way to enhance efficiency in the road transportation system [72]. Shared mobility is an innovative transportation strategy that provides users with short-term access to transportation on demand. The

definition of shared mobility includes various formats, including carsharing, ride-hailing, and ridesharing. These services aim to break traditional car ownership, instead providing users with travel options through a pay-per-use approach. In recent years, there has been rapid development and commercialization of ridesharing services (e.g., Uber, Lyft). Ridesharing is defined as an arrangement where two or more people from different households share the use of a privately owned car for part of a trip and share the driving expenses [20]. Rideshare services have the potential to eliminate traffic congestion and reduce vehicle emissions based on studies in different localities [31, 73, 74].

Despite progress in ridesharing services, knowledge gaps still exist, and this prevents transportation practitioners from fully understanding the potential impacts of ridesharing services. As stated by Yu et al. [31], "most of the existing studies are mainly drawing on the survey data or the small-scale trip data instead of the raw observed order information." In the limited studies based on empirical ridesharing data, their conclusions are retrospective and do not offer insights for future scenarios, which are important for transportation practitioners in evaluating various ridesharing policies. Any tools developed should have the capability to consider individual-level behavior when evaluating ridesharing impacts [32]. Thus, the research questions to address in this study are: (1) how to develop an environmental impact evaluation framework for ridesharing services that consider individual-level (i.e., agent) behavior changes; and (2) how to implement scenario analysis that can be used by transportation practitioners to evaluate the potential impacts of various ridesharing strategies.

In the literature, researchers studied rideshare services in terms of behavior, operation management, and impacts on traffic networks and the environment. Research

related to the behavior of rideshare focused on the motivations and constraints of people using rideshare services. The literature shows that people use rideshare services due to their benefits in cost savings [75, 76] and time savings [77, 78]. People's sociodemographic characteristics have been shown to influence their choice of ridesharing services [20, 79, 80]. Various types of the online and offline driver–passenger matching algorithms have been developed to improve operational efficiency in ridesharing services [81-85].

Recently, studies have focused on the impacts of rideshare on congestion, energy consumption, and the emission of transportation. The impacts of rideshare on congestion have been well studied [86-89]. But the energy and environmental impacts of ridesharing services are less studied. Some studies employed travel survey data to investigate the environmental and energy impacts of rideshare. Caulfield et al. [90] explored the environmental benefits of ridesharing in terms of reductions in emissions and vehicle kilometers traveled based on analyzing the 2006 census of Ireland. Minett et al. [91] estimated the energy savings of ridesharing for leisure trips in San Francisco is about 1.7 million to 3.5 million liters of gasoline per year, or 200 to 400 liters for each participant, based on ridesharing opinion data. Other studies used similar approaches with survey data to analyze the energy and emission benefits of ridesharing services in other countries, like China [31], Canada [73] and globally [92]. Although these surveys were rigorously implemented, the data can only represent survey participants' choices under hypothetical conditions. When investigating the energy and emission benefits of ridesharing services, it is important to consider a bottom-up approach that can quantify the benefits at the

individual level and evaluate how changes in driving trajectories can lead to changes in aggregated vehicle emissions.

Agent-based traffic simulation is a technique that can model the transportation system as a collection of autonomous decision-making agents, i.e., travelers, and simulate their movements in the system [93]. It has the advantage of modeling a complex transportation system by tuning the interactions among independent decision-making agents. It is possible to evaluate various traffic management policies in traffic simulation and gain insights into the system that would not be possible a priori. Recently, limited studies began to utilize agent-based traffic simulation tools to study the impacts of various formats of shared mobility. Becker et al. [94] established a multimodal traffic simulation application in MATSim to evaluate the economic and travel time impacts of car sharing, bike sharing, and ride-hailing. They simulated the road network in Zurich, Switzerland, and implemented scenarios with different shared car or bike fleet sizes. Other studies used similar traffic simulation tools to assess car sharing [95, 96], shared autonomous taxis [97], and transit first- and last-mile connections [98]. Thus, agent-based traffic simulation can be a viable method to study the impacts of ridesharing at the transportation system level.

This review of the literature shows that there is a knowledge gap in the literature regarding developing an environmental impact evaluation framework for ridesharing services with consideration of individual-level (i.e., agent) behavior changes. In addition, to be useful for transportation practitioners, the developed framework needs to have scenario analysis capability that can evaluate various ridesharing strategies for comparison purposes. In this study, we propose an integrated framework to analyze the

efficiency and environmental benefits of ridesharing on a regional scale. Specifically, the framework utilizes an agent-based traffic simulation package (i.e., SUMO) to replicate traffic activities for commuting trips in a mid-size city, Chattanooga, Tennessee. We utilize real-world travel origin and destination demand data for the city and develop a heuristic matching algorithm for arranging ridesharing trips among travelers. We construct scenarios representing different ridesharing strategies and penetrations. Last, efficiency (delay at system and individual levels) and environmental performance are evaluated and compared among different ridesharing scenarios.

The remainder of this chapter is organized as follows. Section 3.2 presents the traffic simulation methodology, data sources, and construction of simulation scenarios. Section 3.3 discusses simulation results and analyzes road network efficiency and environmental impacts due to the implementation of ridesharing services. Section 3.4 discusses our study and points out some policy implications for transportation practitioners Section 3.5 provides the conclusions and future research directions of this study.

3.2 Methodology

To assess the energy and environmental impacts of ridesharing services, we configure an integrated framework to run scenario-based traffic simulations and analyze traffic outputs for environmental impacts (Figure 3.1). The traffic simulation is implemented through Simulation of Urban Mobility (SUMO). SUMO is a highly customizable, open-source microscopic traffic simulator built on an agent-based simulation concept [99]. Additionally, SUMO provides an interface, TraCI, that allows real-time extracting and passing parameters with a simulation [100]. The framework

contains three modules: data preparation, shared mobility simulation, and output analysis. In the “Data Preparation” module, road information is prepared to digitally represent the traffic network in the traffic simulator SUMO. We obtain travel demand origin and destination (OD) matrix data from the metropolitan planning organization of Chattanooga. The travel demand OD matrix is based on the traffic analysis zone (TAZ) and contains hourly vehicle trips between each OD TAZ pair. We assign TAZ-level trips to specific road links according to the land use characteristics of each TAZ. In the “Shared Mobility Simulation” module, a shared mobility toolbox is built using Python. It allows convenient setting of simulation parameters for scenario specifications. In addition, the toolbox enables in-route driver–passenger matching for shared mobility vehicles to maximize matching efficiency. Once scenario-specific simulations are done, the toolbox can process the outputs and generate results at vehicle level (i.e., vehicle trajectory at 1Hz frequency) and road link level (i.e., hourly average speed, density, and volume). The “Output Analysis” module analyzes simulation results and evaluated share mobility impacts on traffic, travelers’ schedules, and the environment under various scenarios. For traffic impact analysis, we aggregate 1Hz vehicle trajectory results into 5- or 15-minute link-level average speed and volume. We evaluate changes in link-level traffic stream characteristics under different rideshare scenarios. For traveler schedule impact analysis, we track and compare the travel time for each individual under base and various rideshare scenarios. For environmental impact analysis, we obtain 1Hz vehicle emissions of CO2, PM, and NOx as provided by SUMO. Vehicle emissions reported by SUMO are based on well-calibrated regulatory vehicle emission model HBEFA and PHEMlight [101] and have been widely used in relevant literature [102-104]. We aggregate the 1Hz vehicle

emission at the trip, link, and network levels to evaluate the environmental impacts of various shared mobility scenarios.

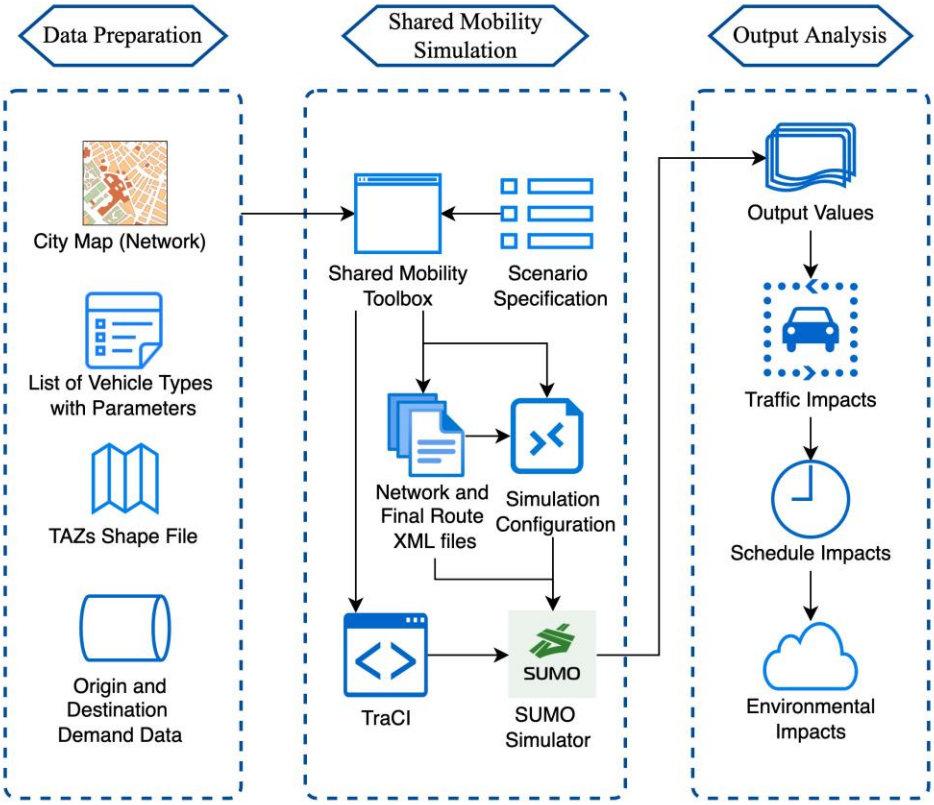

Figure 3.1 Framework of the shared mobility simulation.

For the core part of "Shared Mobility Simulation," the process is as follows:

1. Vehicle trip generation. A vehicle trip contains OD road links for vehicle travel. The OD matrix data provide the number of trips between each TAZ pair. We assign each trip to one road link in the origin TAZ and one link in the destination TAZ, based on land use and other link features (e.g., length, traffic volume, etc.). At this step, we divide all vehicle trips into two travel modes, i.e., driving alone and shared rides. The ratio between the two modes can vary under different share mobility scenarios.

2. Route generation. Given OD links for each drive-alone vehicle trip, we find the route of road links for each trip. We employ SUMO's DUAROUTER algorithm to search

for the route. This algorithm applies a dynamic user equilibrium method to determine the shortest path for each trip based on time-dependent travel time and costs on road links. The time-dependent individual vehicle routes can be used to calculate the arrival time and schedule delay of each traveler. When aggregating individual vehicle routes, we can obtain link-level traffic volume and speed patterns that can be used to evaluate link-level and network-level traffic and environmental impacts from various shared mobility scenarios.

3. Matching passengers with shared vehicles. For rideshare travel demand, we develop a heuristic vehicle–passenger matching algorithm to match passengers with shared vehicles. The pseudocode of the algorithm is shown in Figure 3.2. The main purpose is to ensure every rideshare passenger is served. The algorithm tries to reduce waiting time for riders and minimize routing time for shared vehicles. It first searches for available vehicles that can pick up a rider within 5 minutes of the desired departure time. If a vehicle is identified, the vehicle's route will be modified to pick up the rider and continue to its destination. A shared vehicle is allowed to pick up as many as 3 passengers. When multiple riders are picked up, the shared vehicle drops off passengers in an order that considers both distance to the destination of each rider and the pickup order of riders. If no available vehicles are found in the initial 5-minute window, the algorithm extends the window to 10 minutes and then 20 minutes. At the 20-minute time window, most shared mobility riders can find a matching vehicle.

The experiment scenarios constructed in this paper are based on real-world data for the city of Chattanooga, Tennessee. This city has a population of 182,803 and is set along the Tennessee River in the foothills of the Appalachian Mountains in the Southeast

region of the United States. It has a motorization index of 951 vehicles per 1,000 people [105]. According to Tennessee Department of Transportation data, 82% of commuting trips are fulfilled by driving cars and 10% of commuters regularly or sometimes used ridesharing services. Chattanooga was designated as an air quality nonattainment area mainly due to its high vehicle-related emissions. Chattanooga commuters spend an average of 20 minutes traveling one way [106]. Thus, Chattanooga is an ideal testbed for our ridesharing framework given its high vehicle ownership, travelers' openness to rideshare services, and air quality problems due to vehicle-related emissions. In this study, we quantify the traffic and environmental impacts of various ridesharing scenarios in Chattanooga.

Algorithm 1: Ride matching algorithm

Result: Mapping set of rider to car $\boldsymbol{M} = \{\boldsymbol{r} : \boldsymbol{c}\}$;
Initialization:
Available cars $\boldsymbol{AC}_r = \emptyset$ for rider r and a set of cars fully occupied $\boldsymbol{FC} = \emptyset$;
for $r \in \boldsymbol{R}$ **do**
  Statements of depart time (dt_r), depart position (pos_r) for each rider r, and depart time (dt_c), depart position (pos_c) for each candidate shared car c;
  while $length(\boldsymbol{AC}_p) = 0$ **do**
    Search available cars for each rider r within the time widow $TW_r = [dt_p - 2T, dt_p - T]$;
    for $c \in \boldsymbol{C}$ **do**
      if $dt_c \in TW_r$ & $c \notin \boldsymbol{FC}$ **then**
        $\boldsymbol{AC}_r \leftarrow \boldsymbol{AC}_r \cup \{c\}$;
      end
    end
    Update $length(\boldsymbol{AC}_r)$;
    if $length(\boldsymbol{AC}_r = 0)$ **then**
      repeat
        $TW_r \leftarrow TW_r + T$;
        Extend TW with time interval T and continue to search;
      until $TW_r[upperbound] > TW_r + 2T$;
    end
  end
  for $c \in \boldsymbol{AC}_r$ **do**
    Calculate the path length $L(pos_c, pos_r)$ between available car c and rider r;
    Estimate the traveling time $T(c, r) \leftarrow L(pos_c, pos_r)/speed$;
    Get time difference $t(c, r) = T(pos_c, pos_r) + dt_c - dt_r$
    between the arrival of c at pos_r and departure of r;
  end
  $c^* \leftarrow argmin_c t(c, r)$;
  $\boldsymbol{M} \leftarrow \boldsymbol{M} \cup \{p : c^*\}$;
  if $count(c \in \boldsymbol{M}) = 4$ **then**
    $\boldsymbol{FC} \leftarrow \boldsymbol{FC} \cup \{c\}$;
  end
end

Figure 3.2 Pseudocode for the heuristic matching algorithm.

To make our framework more applicable, we utilize real data from Chattanooga to set up the simulation. We obtain Chattanooga's TAZ-level OD demand for a typical weekday from the Chattanooga transportation planning organization. We use travel demand during morning peak hours (6 to 9 a.m.) as the OD demand in the traffic simulation. The OD demand shows the number of trips between each TAZ, and each trip is considered to be fulfilled by one agent. Figure 3.3 visualizes the travel demand for the 746 TAZs in Chattanooga for the morning peak period. Specifically, we categorize all

TAZs into 10 homogenous TAZ clusters based on socio-demographic information. For each TAZ cluster, we split the travel demand into driving alone and sharing rides with different ratios. Specifically, the "Base" scenario assumes all trips are driven alone, which is comparable to the existing situation in Chattanooga. We define five additional scenarios that have a share ratio of 5%, 10%, 25%, 50%, and 75%, respectively, of travel demand to be fulfilled by shared mobility services. According to the literature, the current ridesharing ratio in Chattanooga is 10% [106] and the national average ridesharing ratio is 9% [107]. Therefore, the 5% and 10% scenarios are realistic scenarios that reflect the current ridesharing status. And our framework can evaluate its environmental impacts. The 25%, 50%, and 75% ridesharing scenarios are built in to explore possible impacts of future ridesharing scenarios that could be seen as high at present time. Overall, we are to quantify the environmental benefits of ridesharing in current and future scenarios.

We randomly choose 5%, 10%, 25%, 50%, and 75% of the trips in drive-alone scenarios to be fulfilled by ridesharing services for the corresponding scenarios. These travelers will make themselves available to be picked up based on their original departure times in the drive-alone scenario. They are picked up based on the availability of drivers and traffic conditions in the road network.

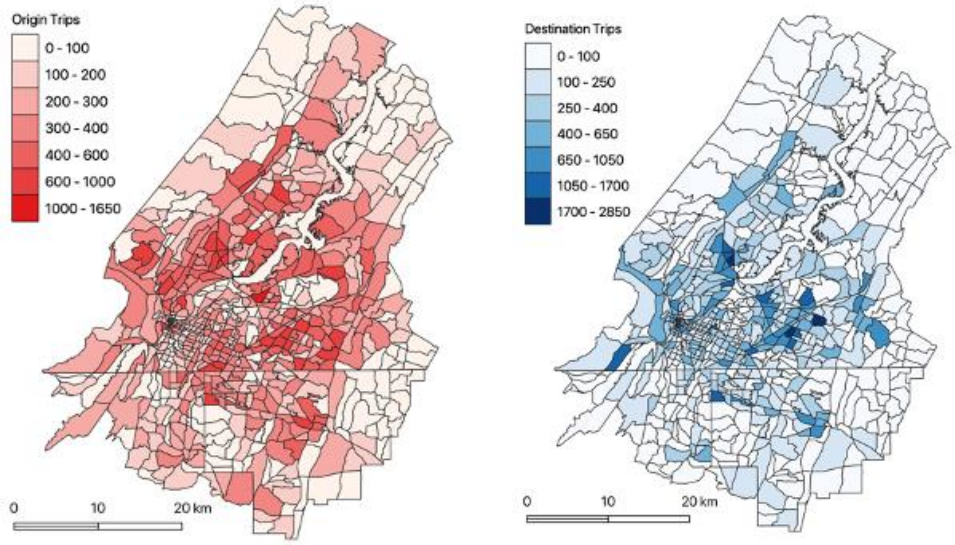

Figure 3.3 Spatial distribution of passenger cars departing (left) and arriving (right) in each TAZ of the Chattanooga model area.

3.3 Results

We construct six scenarios in the shared mobility simulation: (a) no share (all vehicles driving alone); (b) 5% of trips are shared; (c) 10% of trips are shared; (d) 25% of trips are shared; (e) 50% of trips are shared; and (f) 75% of trips are shared. We first split passengers according to the proportions of the scenario based on demand and then assign shared vehicles to each passenger. Table 3.1 summarizes the volumes of passengers, shared vehicles, and drive-alone vehicles, as well as the average vehicle occupancy for shared vehicles under each scenario. Various outputs are generated by simulating these scenarios, including link-level traffic measurements, trajectories of each vehicle, trip-level information, and person-level trip summary. The link-level traffic measurements describe macroscopic values such as the average speed, density, and occupancy of the road link during a specified interval (e.g., 5 or 15 minutes). Trip-level information

contains the departure time, arrival time, and route length of each vehicle and person and the sum of all emissions by the vehicle during its journey.

Table 3.1 Summary of trip volume under different scenarios during peak times.

Trip volume	No rideshare	5% share ratio	10% share ratio	25% share ratio	50% share ratio	75% share ratio
Passengers	0	7250	14501	36,252	72,504	10,8755
Shared vehicles	0	6635	12433	28,421	40,246	33,022
Vehicles driving alone	145,007	131122	118073	80,334	32,257	3,230
Average vehicle occupancy	1	1.09	1.17	1.28	1.80	2.94

3.3.1 Impacts of ridesharing on traffic

Figure 3.4 shows the 5-minute average speed distributions at the link level of the three scenarios compared with the base scenario during morning peak hours. We observe that all scenarios have a similar spread of link-level speed ranging from 0 to 88 km/h and all density lines have two main peak points at a similar segment-level speed; the primary one lies at around 20 km/h, and the secondary peak is located at about 38 km/h. The pattern of the distribution indicates that many vehicles are driving at a low speed (20 km/h), corresponding to local collector roads. In addition, another group of vehicles is driving around 38 km/h, corresponding to arterial or major arterial roads. This implies that the investigated area encounters traffic congestion during the simulated morning peak hours. As shown in Figure 3.4, the densities of shared scenarios (5%, 10%, 25%, 50%, and 75% share ratios) at their primary peak point (20km/h) are lower than that of the base scenario (no share). Differences between the base scenario and the three shared scenarios at the secondary peak point are also observable, although they are not statistically significant. These differences reveal that the volume of vehicles driving at a

relatively low speed is reduced, which means shared mobility significantly contributes to reducing traffic jams. In other words, ridesharing is capable of easing traffic congestion during rush hour. In Figure 3.4, we further observe that the reduction of the density at the primary peak point in the high share ratio scenario is the largest, followed by the medium share ratio scenario and the low share ratio scenario. As mentioned, these three scenarios are designed according to the proportions of passengers who would like to share rides with others. Therefore, the comparison among the three scenarios indicates that the remission of traffic congestion is determined by the proportion of passengers in the shared mobility simulation. The higher the proportion of passengers, the fewer vehicles in the traffic jam.

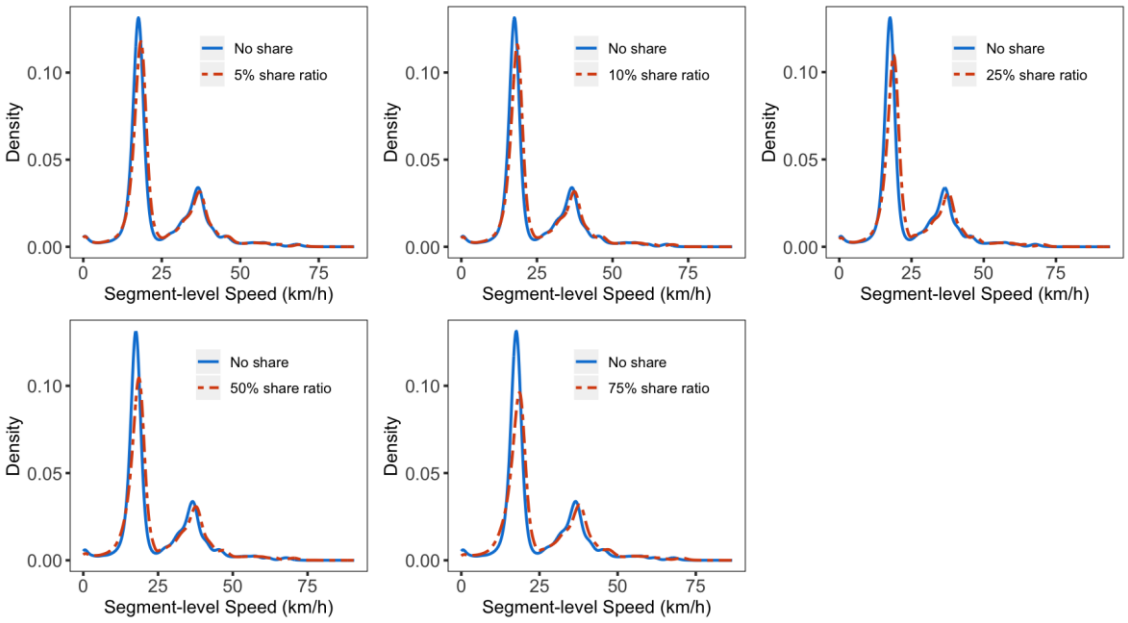

Figure 3.4 Distributions of the segment-level speed of three scenarios compared with the base scenario.

3.3.2 Impacts of ridesharing on schedule

Besides relieving traffic congestion on the road network, ridesharing has the potential to affect the travel schedule of individual travelers. Figure 3.5 reports distributions of changes in arrival time for drive-alone travelers and rideshare travelers. In the simulations, drive-alone travelers will depart at the same time, but arrival times will differ due to different traffic conditions in the road network. Ridesharing travelers' departure (pickup) and arrival (dropoff) times can vary due to driver availability and traffic conditions on roads.

Figure 3.5 (left) presents the distribution of changes in arrival time for drive-alone travelers under the three ridesharing scenarios. It shows that most (70%–82%) drive-alone travelers arrive early compared with their original arrival time in the no-ridesharing scenario. The early arrival of drive-alone travelers is caused by fewer vehicles on the road due to some travelers choosing ridesharing services. In all five ridesharing scenarios, less than 20% of travelers are delayed by more than 5 minutes and the magnitude decreases as the rideshare percentage increases. Some drive-alone travelers experience delays in travel time that are longer than 5 minutes, but the percentages are minimal. Although traffic volume in the whole network is reduced because of ridesharing services, in certain regions, there could be more traffic due to ridesharing vehicles routing to pick up and drop off passengers. This caused a small fraction of drive-alone travelers to spend extra time on the road. Our results also indicate an average time savings of 5.6 minutes per drive-alone traveler, which is a significant benefit in travel time for those travelers. Figure 3.5 (right) presents the distribution of arrival delays for travelers using ridesharing services as compared with travel time if they drive alone. We categorize the arrival

delays into four intervals: 0–5 minutes, 5–15 minutes, 15–30 minutes, and more than 30 minutes. The high share scenario leads to a higher share of travelers with delays of less than 5 minutes. The results also show that 65% to 75% of travelers are expected to experience an arrival delay that is less than 15 minutes under various ridesharing scenarios. The main cause of delay for ridesharing travelers is waiting for vehicle matching and pickup. Particularly, travelers living in remote areas with lower population density are more likely to experience longer delays. The results show that the high share scenario, where more travelers are participating in ridesharing services, has the highest percentage of delays of 30 minutes or more. This is because in the high share scenario, it is more likely that travelers from isolated areas will need rides.

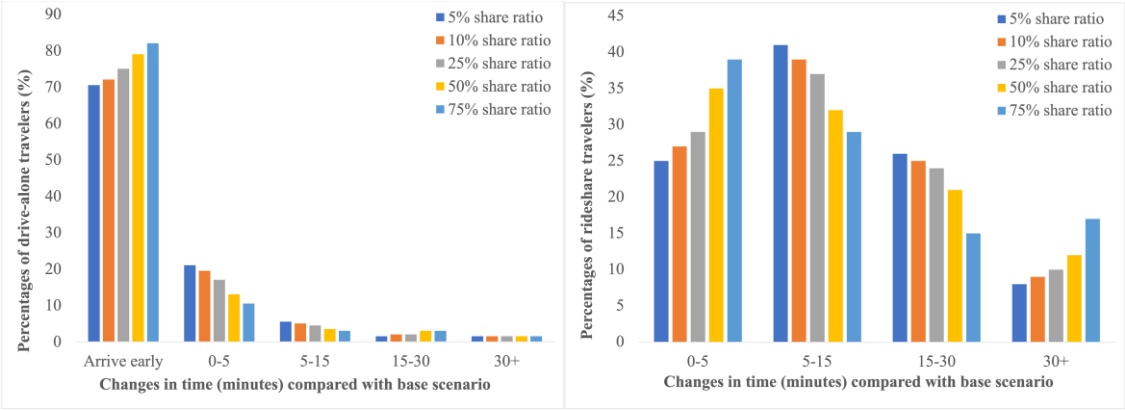

Figure 3.5 Distributions of arrival delays of drive-alone travelers (left) and ridesharing travelers (right) under three ridesharing scenarios as compared with the no-share scenario.

3.3.3 Impacts of ridesharing on energy and emission

We investigate the impacts of ridesharing on trip-level vehicle-related emissions. Specifically, we calculate and compare vehicle emissions caused by each traveler in ridesharing scenarios. For the base (no rideshare) case, each traveler drives one car and has a unique vehicle trajectory at 1Hz frequency. We estimate second-level CO2 emissions based on trajectory-level speed and acceleration and aggregate to trip-level

CO2 emissions of each traveler. For rideshare scenarios, the trip-level CO2 emissions of each drive-alone traveler are calculated the same way as in the base (no share) scenario. For travelers using ridesharing services, we split the CO2 emissions among travelers sharing the same vehicle based on their traveling distance. Figure 3.6 presents the scatterplot comparing trip-level CO2 emissions in the no share scenario and each of the three ridesharing scenarios. If the emissions of each traveler remain the same in the base and ridesharing scenarios, the scatter points should cluster along the red diagonal line. If the emissions of each traveler in ridesharing scenarios are lower than those in the base (no share) scenario, the scatter plots would be expected to appear above the diagonal line, and vice versa. Figure 3.6 shows a larger portion of scatter points above the diagonal line for all three ridesharing scenarios compared with the base (no share) scenario, which means that travelers can generally reduce vehicle emissions with ridesharing options. In addition, the higher the ridesharing ratio, the higher portion of points that appear above the diagonal line. This is expected, because a higher ridesharing ratio can achieve more reductions in vehicle emissions of each traveler. The average trip-level CO2 emissions are 4.3kg, 4.2kg, 4.0kg, 3.8kg, 3.2kg, and 2.9kg for no rideshare, 5%, 10%, 25%, 50%, and 75% share ratio scenarios, respectively. Clearly, higher ridesharing generally leads to lower average trip-level emissions given the same amount of travel demand. Though the exact reduction in CO2 emissions is subject to the specific operation of ridesharing services and travel demand, our results are consistent with existing literature on the environmental impacts of ridesharing services, such as Yu et al. [82] in Beijing, Fagnant and Kockelman et al. [108] in Austin, and Caulfield et al. [90] in Dublin.

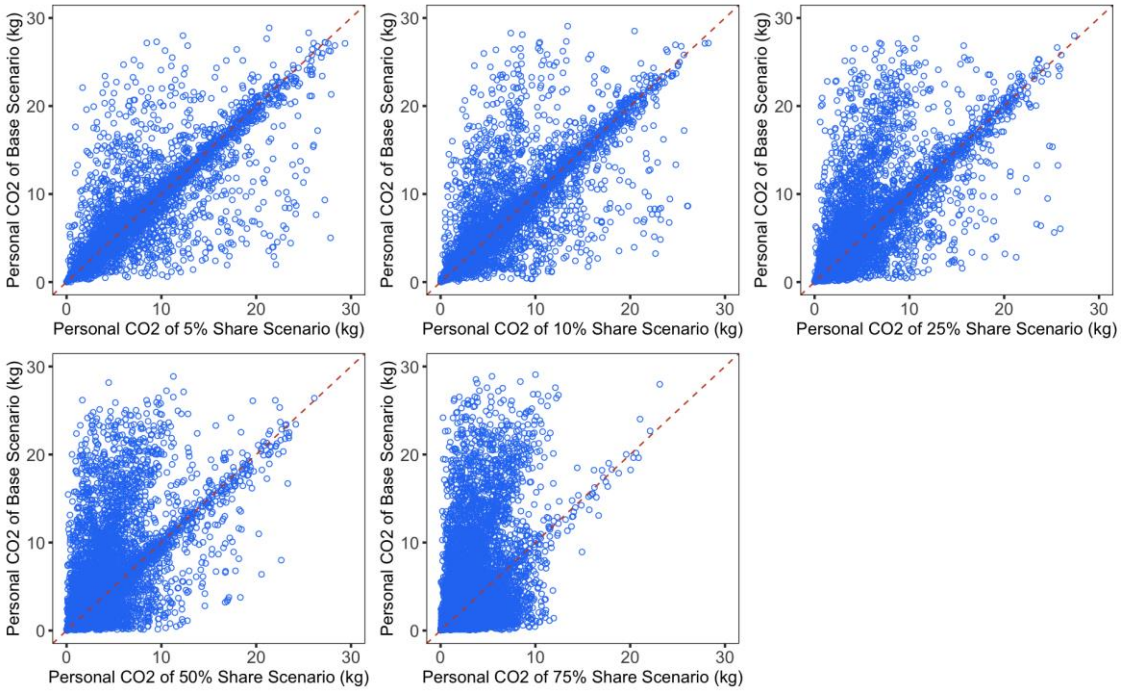

Figure 3.6 Scatter plots of CO_2 emissions under five scenarios versus the CO_2 emissions under the no share scenario for passengers, shared vehicles, and vehicles driving alone.

The system-level impacts of energy consumption, vehicle emissions, and link average speed under different scenarios are presented in Table 3.2. The exhaust emissions including CO2, CO, HC, NOx, and PM are significantly reduced from the no share to high share ratio scenarios during the three morning peak hours. CO2 emissions drop 33% for a 75% share ratio, 21% for a 50% share ratio, 7% for a 25% share ratio, 5% for a 10% share ratio, and 2% for a 5% share ratio, compared with no share. Besides CO2, the CO, HC, NOx, and PM emissions under a 75% share ratio dropped 46%, 46%, 35%, and 36%, respectively, relative to the base scenario. The energy consumption falls from 67,951 gallons under no share to 45,618 gallons under 75% share ratio, a 33% reduction. These reductions in energy consumption and vehicle emissions are expected because the corresponding average link-level travel speed improves across the scenarios. Average travel speed is considered an indicator of vehicle emission and energy consumption [109].

Previous studies showed vehicle emissions decrease as the average speed increases from 5 to 50 mph.

Table 3.2 System-level analysis for different scenarios.

Scenarios	CO_2 (ton)	CO (ton)	HC (kg)	NO_x (kg)	PM (kg)	Fuel (gallon)	Average travel speed (kph)
No rideshare	598	24	124	259	14	67,951	22
5% share ratio	585	23	122	257	13	66,024	22
10% share ratio	570	22	118	250	13	64.865	23
25% share ratio	555	21	110	239	12	63,018	24
50% share ratio	475	16	85	202	10	53,994	29
75% share ratio	402	13	67	169	9	45,618	32

3.4 Discussion and Policy Implications

Our analysis demonstrates the potential of ridesharing services in mitigating traffic congestion and reducing vehicle-related emissions. In this section, we discuss our results in the context of previous studies and point out several policy implications for transportation practitioners in implementing or managing ridesharing services. In Table 3.3, we compare our results on ridesharing services' impacts on traffic and vehicle-related emissions with the relevant literature. It is worth noting that the relevant studies have different scopes and methods; thus, the focus of the comparison is on the general trend of impacts rather than specific numbers. The comparison shows that our results are consistent with existing literature in terms of the magnitude and trend of rideshare impacts on travelers' schedules and CO2 emissions. Most existing studies were based on survey data, and they estimated up to 6% CO2 emission reductions for up to a 10% ridesharing ratio on a city or national scale. For a study that used simulation data [108],

the assessed schedule impacts are comparable to our study. Our study simulates scenarios with ridesharing ratios ranging from 5% to 75%, which provides insights into the potential impacts of ridesharing on high-sharing cases. We found that our studies achieve comparable results to existing studies in assessing the environmental impacts of ridesharing services. Most of the existing literature studied ridesharing services with up to 10% ratio and found benefits in CO2 emission reduction up to 6%. We also find 5% reduction in CO2 emission for 10% rideshare ratio.

Table 3.3 Comparison of rideshare impacts in the literature.

	Granularity and data source	Ridesharing percentage	Changes in schedule	Changes in CO_2
This study	City scale (Chattanooga) empirical and simulation	5%–75%	25%–35% with a 20-minute delay or more	2%–35%
Jacobson et al. [110]	U.S. national survey data	1~10%		-1%–5%
Fagnant et al. [108]	City scale (Austin) simulation data	10%	20% with a 20-minute delay or more	-4%–6%
Caulfield et al [90]	City scale (Dublin) survey data	4%		-2%–4%
Yu et al. [31]	City scale (Beijing) survey data	1,938 sampled travelers		Up to -35% with various levels of electrical vehicle adoption

Our results and the comparison with relevant studies have several policy implications. First, the literature has consistently demonstrated the environmental benefits of implementing rideshare services at various geographical scales. As indicated by Shaheen et al. [72], transportation practitioners in the United States and other

countries have started recognizing the environmental and social benefits of ridesharing services. Thus, transportation practitioners should be encouraged to promote transportation ridesharing projects, though it is always recommended to estimate the benefits in a systematic way through either survey or simulation processes as described in this study. Second, vehicle types used in ridesharing services play an important role in estimating the environmental benefits of ridesharing. Many studies, including our study, estimate environmental benefits assuming ridesharing vehicles are regular gasoline-powered cars. Limited studies, e.g., Yu et al. [31], have investigated potential impacts when electric vehicles are used in ridesharing, and their results show significant environmental benefits. Ridesharing is easier to implement in a centralized operation model [111], and there are studies advocating for the use of electric vehicles in ridesharing services [112-114]. Our study shows a 35% reduction in CO2 emissions if up to 75% of trips are shared, and we expect even larger reductions if some or all vehicles are electric cars.

Our results demonstrate the benefits of ridesharing in reducing transportation emissions and energy consumption, particularly when the ridesharing service ratio is at a high range, e.g., 25% to 75%. Apparently, it takes effort to increase the ridesharing ratio from the current ~10% in Chattanooga to such a high ratio. Literature shows several transportation policies that can help improve the ridesharing ratio. One type of policy is to establish a high-occupancy vehicle (HOV) exclusive lane [115]. Studies have shown that the reduction in both travel time (due to traveling on the faster HOV lane) and fuel cost can further encourage riders to adopt ridesharing services. This type of policy works well in regions with high population density and vehicle ownership, such as the

California Bay area [72]. However, Chattanooga is a city with a relative smaller population size and the road network is not congested for a large portion of the day. Thus, adopting the HOV lane policy might not be as effective in Chattanooga as in other regions. Another type of policy is to provide a monetary incentive to drivers to choose ridesharing services [116]. Studies have shown by appropriately choosing incentives, this policy can significantly improve the ridesharing ratio among drivers [117]. This policy can be considered for implementation in Chattanooga. There are various government transportation emission reduction programs, such as the federal's Congestion Mitigation and Air Quality (CMAQ), which provides funding to local transportation authorities to implement policies for emission reduction. As long as the air quality benefits can be quantified, it is justifiable to use government funding to incentivize drivers to choose ridesharing services to achieve lower transportation emissions.

3.5 Conclusions

A shift from privately owned vehicles to shared mobility services can affect mobility, energy consumption, and vehicle emissions. In this study, we investigate the efficiency and environmental benefits of ridesharing in a mid-size city (Chattanooga, Tennessee) using an agent-based simulation framework. The purpose of the framework is to help transportation practitioners evaluate the environmental benefits of ridesharing services with a systematic and comprehensive perspective.

The simulation and result analysis demonstrate that ridesharing services have the potential to reduce traffic volume and relieve congestion without significant impacts on travelers' schedules. Specifically, when ridesharing ratios are 5% to 75% (trips fulfilled by ridesharing services) in Chattanooga, many (65%–75%) of ridesharing travelers will

experience a delay of up to 15 minutes. Longer delays, 30 minutes or more, are mainly due to ridesharing travelers in isolated areas because it takes time to match vehicles to pick them up. Ridesharing services can result in external outcomes that can be beneficial to other travelers and society. This analysis shows 60%–80% of drive-alone travelers will arrive earlier compared with the baseline no-ridesharing scenario. The average early arrival time is 5.6 minutes for all drive-alone travelers. The results show ridesharing services can achieve a 2%–35% reduction in vehicle-related emissions and energy consumption with various ridesharing ratios. This is significant considering most vehicle emissions are generated in urban regions with high population density. The reduction in vehicle emissions has the potential to improve air quality and mitigate adverse impacts on the health of local residents.

We acknowledge there are limitations of the current research that could motivate future research directions. First, the vehicles applied in our simulation model were internal combustion vehicles. Electric vehicles are emerging fast and play an important role in reducing energy consumption and cutting emissions. It would be interesting for future research to consider a diversified vehicle fleet for ridesharing services and associated infrastructure planning. Second, researchers can include other travel modes, such as public transit, shared bike, or micro-mobility, with ridesharing to model multimodal travel implementation and estimate associated impacts. This requires more complex planning algorithms to search for optimal mode combinations to reach minimum monetary, time, or environmental impacts. Third, the scenario constructed in our study is for one mid-size city, Chattanooga, where most trips are fulfilled by passenger cars. It would be interesting to look at mega-cities, which normally have diversified travel modes

and trip purposes, to identify the most suitable scenarios and locations for implementing ridesharing services.

Chapter 4

Planning of Dynamic Wireless Charging Lanes Considering Bus Frequency Setting for Battery Electric Buses[6]

[6] Sun, R., Luo, Q. and Chen, Y. Planning of Dynamic Wireless Charging Lanes Considering Bus Frequency Setting for Battery Electric Buses (ready to submit).

Abstract

Dynamic wireless charging (DWC) technology enables the charging of electric vehicles while they are in motion, therefore reducing battery size, increasing driving range, and enhancing convenience. The planning of DWC infrastructure has gained significant attention with the advancement of wireless power transfer technology. This work provides an integrated optimization framework for planning DWC networks for public transit systems. The objective is to minimize the total costs related to electric bus operations, including the annualized DWC construction costs and electric bus fleet purchase costs, costs for transmitting electricity for charging facilities, and penalties for passenger waiting times. To solve the problem of planning DWC lanes for electric buses, we develop a nonconvex mixed integer model that considers 1) the frequency setting of buses that balance between being charged en-route and at the depot, 2) the planning of transmitter coils, 3) the modeling of bidirectional multiple routes. The problem is converted to Mixed Integer Linear Programming (MILP) by applying linearization techniques. Through a case study of Chattanooga, TN, we show the potential reduction of total social cost with optimal DWC lanes design for a large-scale bus transit system. Our sensitivity analysis with parameter changes also provides insights into the conditions for deploying DWC systems for battery electric buses.

4.1 Introduction

The transportation sector accounts for 27% of the greenhouse gas (GHG) emissions in the United States in 2020 [118]. Electrification of transportation is one of the important pathways for reducing GHG emissions. Although we witnessed increased adoption of electric passenger vehicles, there is limited progress on transit electrification

due to their limited range and long recharging time [119]. Nation Transit Database shows that only 1,268 electric buses out of 63,530 total buses are actively operating across the U.S in 2020 [17]. Dynamic wireless charging (DWC) technology enables energy transfer from power transmitters to electric vehicles while vehicles are driving on roads. Since vehicles can be charged wirelessly while driving, it can reduce the demand of a large battery size, which further boost driving ranges. We view wireless charging technology as a promising technology to be applied in transit electrification.

DWC technology has been created and implemented in numerous projects on transit buses all over the world. On-Line Electric Vehicle (OLEV) is the first DWC system to be used for commercial purposes in South Korea [35]. Other programs have tested and deployed wireless charging technology for fleet operations of buses in many cities in Europe, such as the PRIMOVE program [33, 34], the FABRIC project [120], and the VICTORIA project [121]. In the United States, Utah State University is actively conducting research on DWC solutions for electric buses [39]. Oak Ridge National Laboratory (ORNL) proposed the concept and prototype of DWC technology and explained the purpose of mass transit [122]. Researches have investigated the competitiveness of DWC technology with other charging technologies such as stationary charging, quasi-dynamic wireless charging, and battery swapping for electric buses. Van Driessche, et al. [123] indicated that wireless charging could require 0.3% less energy and emit 0.5% less greenhouse gas emissions compared with plug-in charging in the total life cycle. Besides energy and environmental comparison, a few studies compare the cost of various charging technologies. For example, Mpalaskas, et al. [124] compared stationary wireless charging, quasi-dynamic wireless charging, and DWC in a single bus

line and found that DWC lanes have cost-benefit when the frequency of electric buses is large. Chen, et al. [125] established mathematical models to investigate the cost competitiveness of battery swapping, stationary charging, and DWC on a transit line. The results showed that stationary charging is cost competitive only for transit systems with very low service frequency and short lengths of bus lines while DWC is more cost competitive for the bus line with high service frequency and very short or very long line lengths. Route length and bus frequency are important factors that determines cost-effectiveness of DWC infrastructure. To improve the competitive of DWC technology for transport systems, a system optimization of DWC infrastructure planning on transit network that can reduce the related costs with an optimal planning of bus service frequency is needed.

Many researchers have paid attention to the system optimization of DWC infrastructure planning. Ko and Jang [126] first proposed an optimization model to allocate the DWC infrastructure and determine the exact battery size for a single-route bus transit system. Based on the work of Ko and Jang [126], some studies conducted the planning of DWC for single-route bus transit situations [Jeong, et al. [35], 127, 128]. However, transit bus system always contains multiple bus lines. It is advantageous to assign DWC facilities to segments where many bus lines intersect, especially for downtown areas where major bus lines overlay. Hwang, et al. [129] extended the optimization of DWC infrastructure location and bus battery sizes into in a multi-route transit network. Liu and Song [36] developed a robust optimization model for a multi-route transit network considering uncertainty of bus travel time. Considering that stationary charging at terminals could cause a delay in normal bus operation, Alwesabi, et

al. [37] and Alwesabi, et al. [38] incorporated the charging time at bus terminals to simultaneously determine the optimal deployment of the DWC facility and the optimal bus fleet. However, limited studies incorporated bus service frequency decisions into DWC infrastructure design, and we are not aware of any studies that balance the planning of wireless charging and stationary charging infrastructure. As pointed out by existing studies, bus frequency impacts the cost competitiveness of DWC infrastructure for transit system [125]. Higher service frequency can increase utilization of DWC lanes and generate more electricity for bus operations. Whereas low service frequency means more time at bus depots and thus it is beneficial for buses to take stationary charge at depot between trips. In this paper, we are to incorporate the frequency setting of buses that balance between being charged enroute and at the depot in our model.

Based on the topology of the transmitter, DWC systems can be categorized into single transmitter track based and segmented transmitter array based DWC systems [130]. Single transmitter is a long transmitter coil or cable buried in the track while segment transmitter is formed by a series of transmitter coils. Single transmitter has the drawbacks that the electromagnetic fields radiated outside the coupling area are harmful to health and the low efficiency of energy transfer due to the low coupling factor. Segmented transmitter has been widely developed in many programs thanks to its ability to minimize the harmful radiated field and improve the energy transfer efficiency. Existing models of DWC infrastructure planning are all based on the concepts and techniques of OLEV [35] which uses single long cable as the transmitter side. Since these models are to decide the location and length of the single transmitter, they cannot be directly applied to the planning of segmented transmitter array based DWC systems. Foote, et al. [40] pointed

out that the number of coils per mile of a segmented transmitter array based DWC facility should be sized properly to maintain the sustained operation of electric vehicles. This study further discusses the effect of various driving cycles on the coils planning and guides the different layouts of coils for several standard driving cycles. This study attempts to design a segmented transmitter array base DWC system that not only determines the location and length of the transmitter tracks, but also the coil layout of each transmitter segment according to different traffic conditions.

Furthermore, existing transit DWC facility location studies are modeled on unidirectional routes. But it is more realistic to consider bidirectional routes. Liu and Song [36] and Alwesabi, et al. [38] both mentioned that the neighboring road segments can share the fixed cost of DWC infrastructure to make the technology more cost-effective. In addition, the electric bus energy demand estimation plays a key role in planning the new DWC system. We employ an electric bus energy consumption model that was developed in a previous study [131] while we are determining DWC infrastructure and bus frequency setting. The energy consumption model can accurately calculate energy consumption and battery state of charge at different time interval based on bus driving patterns. Additionally, the model included energy recovery through regenerative braking as well as auxiliary load such as lights, heating, and air conditioners.

To summarize, the overarching goal of this study is to provide an integrated planning framework for designing dynamic wireless charging infrastructure for electric bus service operations. We are to contribute the existing literature on following aspects:

(a) This study develops a more realistic optimization model to address the allocation problem of DWC lanes (the exact location of DWC lanes and their layout of coils) in a complex transit system with bidirectional multiple bus lines.

(b) Coordinate planning optimization of wireless and stationary charging infrastructure with various bus passenger demand.

(c) Expand the wireless charging roads from unidirectional (most common in existing studies) to bidirectional feature and utilize a machine-learning based energy model to improve accuracy of electric bus energy consumption.

(d) Provide a MILP reformulation of the original optimization with the minimization of social costs, such as the construction cost of DWC lanes, the wireless charging buses purchase cost, the passenger cost, and the use-phase electricity cost.

The remainder of this paper is organized as follows. Section 2 presents the problem statement and assumptions, groups of constraints, system model, and linearization of the proposed model. In Section 3, we discuss the basic results of the case study and conduct a sensitivity analysis of the model and implement a comparative analysis with previous studies. Section 4 provides the conclusions and future research directions of this study.

4.2 Optimization Model

4.2.1 Problem statement and assumptions

This study considers the following components of the DWC lane for planning, 1) a power inverter on the roadside, 2) wireless power transmitter coils beneath the road, and 3) a power receiver equipped on the bottom of the bus (see Fig. 1). The transmitter coil beneath the road would generate a magnetic field that the power receiver would pick

up and convert into electric power. Our study tries to support the government authorities to make decisions on the planning of DWC facilities for the in-operation transit system, with a minimal social cost. Specifically, the decisions are made on where the DWC lanes are to be located for battery electric buses and what the layout of transmitter coils is for each wireless charging lane. Additionally, bus frequency setting balancing passenger demand coverage and the related cost is considered in this DWC system planning. The system planning considers multiple bus lines as described in Fig. 2. It consists of one base station and several bus routes with shared route parts. Each bus line is for a predesigned route with a fixed loop line. The buses can have the opportunity to charge at the base station between service loops and charge in motion during each service loop. This study develops a nonconvex integer model to tackle this problem. The key assumptions used in the model are given as follows:

(1) Bus fleets bought for operating on different bus lines with DWC are homogeneous with fixed battery size and seat capacity.

(2) Each bus is fully charged overnight.

(3) Buses can always be charged at the base station between services.

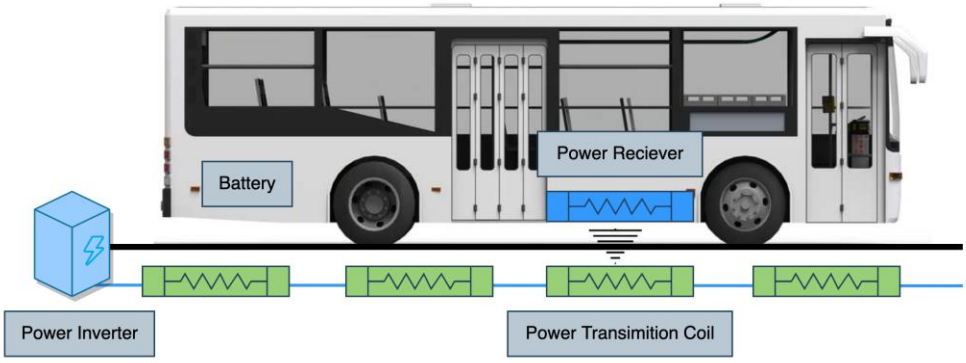

Figure 4.1 Configuration of the DWC lane.

It is noted that the above assumptions are presumed for system modeling purposes and most of them are not restrictive. Relaxing these assumptions may complicate the models, but it does not alter the major findings of this paper. Assumptions (1) through (3) are commonly adopted by DWC deployment literature [36-38, 129, 132].

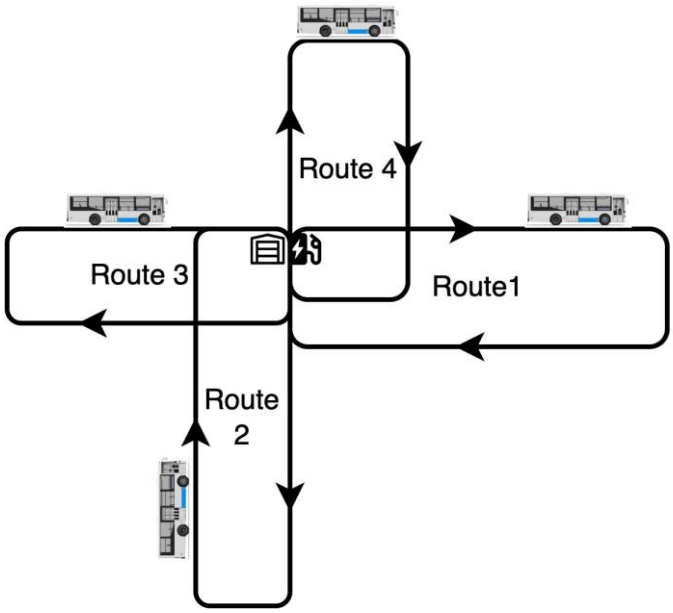

Figure 4.2 The example of multiple bus lines.

4.2.2 Model formulation

We consider a road network of multiple bus lines, where each bus line consists of many small links. Let N represent the set of nodes and L denotes the set of links in the multiple bus lines system. Previous studies [36-38] treat the bidirectional route as two different directed routes. However, the fact that neighbor roads (i.e., adjacent roads and bidirectional roads) can share the fixed cost of installing DWC facilities (i.e., inverter) will influence the placement of DWC lanes. With this consideration, we treat the bidirectional route as it is in our model. Before introducing the model formulation, the notations of sets, parameters, and variables adopted in the formulation are summarized in

Table 1. Our model has five integer decision variables, four continuous decision variables, and several auxiliary variables for linearization as shown in Table 4. 1, and three groups of constraints, including the DWC deployment constraints, bus frequency setting constraints, and energy constraints.

Table 4.1 Notations of sets, parameters, and variables adopted in the model.

Symbol	Description
Sets	
$\boldsymbol{L}$	Set of links in the system, indexed by (i, j)
$\boldsymbol{N}$	Set of nodes in the system, indexed by i
$\boldsymbol{R}$	Set of bus routes, indexed by r
$\boldsymbol{W}$	Directions of the bus line, indexed by $w \in \{+, -\}$, $+$ is outbound, and $-$ is inbound
$\boldsymbol{N_w}$	Set of nodes on direction w, indexed by i
$\boldsymbol{L_{iw}^{in}}$	Set of incoming links of node i on direction w, indexed by (i, j)
$\boldsymbol{L_{iw}^{out}}$	Set of outgoing links of node i on direction w, indexed by (i, j)
$\boldsymbol{T}$	Set of time slots, indexed by t
$\boldsymbol{O_{rw}}$	Set of origin node of two directions for all bus routes, indexed by i
$\boldsymbol{D_{rw}}$	Set of destination node of two directions for all bus routes, indexed by i
Parameters	
$q_{r,t}$	Number of passengers taking bus route r at time slot t
d_{ij}	Length of link (i, j)
c^{fix}	Fix the cost of one consecutive DWC lane
c^{coil}	Coil cost per unit
c^{wait}	The hourly monetary cost of the passenger waiting time ($/hour)
c^{bus}	Cost of the electric bus per unit

c^{elec}	Electricity cost per unit
φ^s	Charging efficiency of static charging
φ^l	Charging efficiency of dynamic charging
p^s	Charging power rate of static charging (kW)
$v_{ij,t}$	Average velocity (mph) of the bus on the link (i,j) at time slot t
$a_{ij,t}$	Average acceleration (mile/hour^2) of the bus on the link (i,j) at time slot t
g_{ij}	Road grade of link (i,j) (%)
$VSP_{ij,t}$	The vehicle-specific power (kW/Metric Ton) on the link (i,j) at time slot t
$c_{ij,t}$	Energy consumption (kWh) on the link (i,j) at time slot t
$load_{r,t}^{max}$	The maximum number of loaded passengers of stops on bus route r at time slot t
Q	Bus capacity
ρ	Bus occupancy rate
E	Battery capacity (kWh)
s	Duration of time slots (hour)
α	Lower battery level rate
β	Upper battery level rate
η	Coefficient of energy supply function of transmitter coils.
n^c	Number of chargers at the base station
f_{up}	The upper limit of bus frequency
τ_{up}	The upper limit of charging time at the base station
π_{low}	The lower limit of coils per mile
π_{up}	The upper limit of coils per mile
M	Large enough positive number
Integer variables	
x_{ij}	$x_{ij} = 1$ if the link (i,j) is covered by power transmitter coils
y_{iw}	$y_{iw} = 1$ if node i on direction w is the starting node of a link that covered by power transmitter coils

z_{iw}	$z_{iw} = 1$ if node i on direction w is the last node of a consecutive DWC lane
θ_i	$\theta_i = 1$ if node i in one direction (i.e., outbound) is covered by DWC lanes of both directions
n_r^{bus}	Number of buses for bus line r
$\gamma_{r,t,u}$	Auxiliary variable for the linearization of the objective function and constraint function
θ_{iw}^z	Auxiliary variable for the linearization of the constraint function
θ_{iw}^y	Auxiliary variable for the linearization of the constraint function
θ_{ij}^x	Auxiliary variable for the linearization of the constraint function
Continuous variables	
$f_{r,t}$	Bus frequency on route r at time slot t
$\tau_{r,t}$	Bus charging time at the base station for bus route r at time slot t
π_{ij}	Number of coils per mile embedded on the link (i, j)
$e_{riw,t,m}$	Bus battery level for direction w on route r traveling through node i at time slot t for the first service ($m = 1$) or not the first service ($m = 0$) of a day
ξ_{ij}	Auxiliary variable for the linearization of the objective function
$\mu_{r,t}$	Auxiliary variable for the linearization of the objective function
$\omega_{rij,t}$	Auxiliary variable for the linearization of the objective function
$\delta_{r,t,h}$	Auxiliary variables for the linearization of the objective function and constraint function

4.2.2.1 The DWC deployment constraints

The cost of the DWC facilities consists of the fixed cost of the inverter for the power track and the variable cost of the power transmitter. The total cost of the power

track depends on the layout of the transmitter coils on the DWC lanes. Specifically, how long is the DWC lane, and how many coils per mile are used in each DWC-covered lane. The total number of coils is $\sum_{ij} \pi_{ij} d_{ij} x_{ij}$, where x_{ij} is the decision variable to identify whether the link $(i, j) \in \boldsymbol{L}$ is covered by the DWC facility or not, π_{ij} is the number of coils per mile (coil density) for each link that is covered by DWC, and d_{ij} is the length of the covered link. The fixed cost of the inverter is the cost for all inverters installed in the system. The main challenge for the DWC deployment is to determine the number of inverters that is necessary for the wireless charging system. Since multiple electric vehicles can pick up power from the transmitter on the same power track simultaneously [36, 126], neighbor links (i.e., adjacent links and bidirectional parallel links) can share the fixed cost of one inverter to reduce the cost. The DWC deployment constraints are to make sure that neighbor links will share one inverter. The primary idea is that we first count the number of inverters for each direction of the bus route and then cancel out the redundant inverters that counted for both directions.

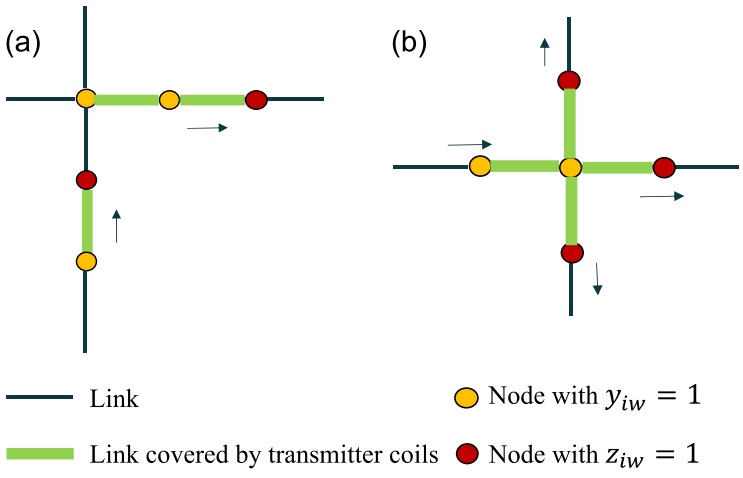

Figure 4.3 Examples of DWC lanes.

As for counting the number of inverters for each direction of the bus route, we introduce two binary variables, y_{iw} and z_{iw}. Fig. 3 shows two examples of DWC lanes in one direction. The yellow node with $y_{iw} = 1$ denotes node i in direction w is the starting node of a link covered by power transmitter coils and the red node with $z_{iw} = 1$ represents node i in direction w is the last node of a consecutive DWC lane. Constraints (1)-(5) are considered the DWC deployment constraints for each direction of the bus route, which are for determining the number of inverters in each direction in the charging system.

$$y_{iw} \leq \sum_{(i,j)\in \boldsymbol{L}_{iw}^{out}} x_{ij}, \forall i \in \boldsymbol{N}, w \in \boldsymbol{W} \quad (1)$$

$$y_{iw} = x_{ij}, \forall i \in \boldsymbol{N}, (i,j) \in \boldsymbol{L}_{iw}^{out}, w \in \boldsymbol{W} \quad (2)$$

$$z_{iw} \leq \sum_{(k,i)\in \boldsymbol{L}_{iw}^{in}} x_{ki}, \forall i \in \boldsymbol{N}, w \in \boldsymbol{W} \quad (3)$$

$$z_{iw} \leq 1 - x_{ij}, \forall i \in \boldsymbol{N}, (i,j) \in \boldsymbol{L}_{iw}^{out}, w \in \boldsymbol{W} \quad (4)$$

$$z_{iw} \geq x_{ki} - \sum_{(i,j)\in \boldsymbol{L}_{iw}^{out}} x_{ij}, \forall i \in \boldsymbol{N}, w \in \boldsymbol{W}, (k,i) \in \boldsymbol{L}_{iw}^{in} \quad (5)$$

Constraint (1) ensures that if all outgoing links of node i in direction w are not covered by DWC, it cannot be the origin node of the link that is covered by a DWC lane. Constraint (2) requires that if a node i in direction w has any outgoing link covered by DWC, it must be the origin node of the link covered by DWC lanes. Constraint (3) ensures that if node i in direction w has no income links, or all income links are not covered by DWC lanes, it cannot be the last node of a consecutive DWC lane. Constraint (4) is to make sure that if a node i in direction w has an outgoing link covered by DWC facilities, it cannot be the last node of a consecutive DWC lane. Constraint (5) ensures that if a node i in direction w has no outgoing links, or all its outgoing links are not covered by the DWC lane, and it has one or more incoming links covered by a DWC, this

node must be the last node of a consecutive DWC lane. The total number of inverters in each direction of the route is $\sum_i z_{iw} - (\sum_{(i,j)\in \boldsymbol{L}_{iw}} x_{ij} - \sum_i y_{iw})$. With the above constraints, we can get the nonredundant inverters in each direction of the bus line. For example, there will be two inverters for case (a) and one inverter for case (b) as shown in Fig. 3.

To cognitive the redundant inverters that counted for both directions, we introduce a binary variable θ_i, $\theta_i = 1$ denotes the node i of one direction (i.e., outbound) is covered by DWC facilities in both directions. Constraints (6)-(8) are the constraints to define the overlay nodes that are covered by DWC lanes in both directions, to determine the redundant inverters that counted for both directions.

$$\theta_i \le x_{ij} + x_{ki}, \forall i \in \boldsymbol{N}_+, w \in \boldsymbol{W}, (i,j) \in \boldsymbol{L}_{i-}^{out}, (k,i) \in \boldsymbol{L}_{i-}^{in} \quad (6)$$

$$\theta_i \ge x_{ij}, \forall i \in \boldsymbol{N}_+, w \in \boldsymbol{W}, (i,j) \in \boldsymbol{L}_{i-}^{out} \quad (7)$$

$$\theta_i \ge x_{ki}, \forall i \in \boldsymbol{N}_+, w \in \boldsymbol{W}, (k,i) \in \boldsymbol{L}_{i-}^{in} \quad (8)$$

Constraint (6) ensures that for node i in the outbound direction if neither the outgoing link nor income link of node i is covered by DWC lanes in the inbound direction, it cannot be the overlay node of links covered by DWC lanes on both directions. Constraint (7) ensures that for node i in the outbound direction if one outgoing link of node i is covered by DWC lanes in the inbound direction, it must be the overlay node of links covered by DWC lanes in both directions. Constraint (8) requires that for node i in the outbound direction if one outgoing link of node i is covered by DWC lanes in the inbound direction, it must be the overlay node of links covered by DWC lanes in both directions. After recognizing the overlay node of links covered by DWC lanes in both directions, the number of inverters that counted twice for the two directions can be

denoted as $(\sum_{i\in \boldsymbol{N}_+}\theta_i z_{iw}-(\sum_{(i,j)\in \boldsymbol{L}_{i+}}\theta_i x_{ij}-\sum_{i\in \boldsymbol{N}_+}\theta_i y_{iw}))$. Therefore, the total number of inverters in the system is represented by $\sum_w\big(\sum_i z_{iw}-(\sum_{(i,j)\in \boldsymbol{L}_{iw}}x_{ij}-\sum_i y_{iw})\big)-(\sum_{i\in \boldsymbol{N}_+}\theta_i z_{iw}-(\sum_{(i,j)\in \boldsymbol{L}_{i+}}\theta_i x_{ij}-\sum_{i\in \boldsymbol{N}_+}\theta_i y_{iw}))$. With this equation, the number of inverters needed for the example shown in Fig. 4 is one.

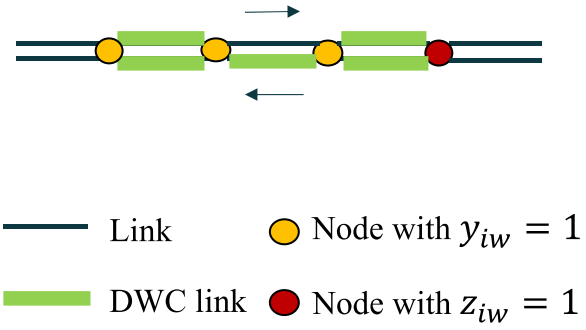

Figure 4.4 An example of bidirectional DWC lanes.

4.2.2.2 Bus frequency setting constraints

In our study, the problem of setting bus frequency is formulated with the explicit consideration of the dynamic passenger demand of each route and the charging capability at the base station, as well as the number of buses assigned for each route.

The maximum hourly loading point method [133] has been widely applied as one of the two primary ways for determining the best line frequency to achieve the required level of occupancy at the busiest stop. According to the maximum hourly loading point method, the bus frequency of route r at time slot t is represented as the below constraint to meet the requirement of the highest loaded stop on route r at time slot t.

$$load_{r,t}^{max}\leq Q*\rho*f_{r,t},\forall r\in \boldsymbol{R},t\in \boldsymbol{T} \quad (9)$$

The conservation of bus service time allows us to create an explicit connection between fleet size and bus frequency. In particular, for each route r, the total number of buses assigned to every bus line n_r^{bus} should at least guarantee the longest service time of

the loops for all the time slots on this line. The service time of one loop is the time a bus charging at the base station $\tau_{r,t}$ plus the time a bus finishes a trip $\sum_{(i,j)\in L_r}\frac{d_{ij}}{v_{ij,t}}$. Therefore, the relationship between bus fleet size and bus frequency can be formulated as below:

$$\max_t \frac{f_{r,t}}{S}\left(\sum_{(i,j)\in L_r}\frac{d_{ij}}{v_{ij,t}}+\tau_{r,t}\right)\le n_r^{bus},\ \forall r\in \boldsymbol{R}. \quad (10)$$

We assume buses either dwell at the base station in charging or serving on the bus line. They will not wait for charging at the base station between services. The charging time of buses charge at the base station is limited by the number of stationary chargers that are available at the base station. Therefore, the relationship between the charging time at the base station and bus frequency for buses on route r at time slot t can be denoted as:

$$\tau_{r,t}\le\frac{sn^c}{f_{r,t}},\forall r\in \boldsymbol{R}, t\in \boldsymbol{T}. \quad (11)$$

The upper limitations for setting the bus frequency and the maximal allowed charging time at the base station are given as below:

$$0\le f_{r,t}\le f_{up},\forall r\in \boldsymbol{R}, t\in \boldsymbol{T} \quad (12)$$

$$0\le \tau_{r,t}\le \tau_{up},\forall r\in \boldsymbol{R}, t\in \boldsymbol{T} \quad (13)$$

4.2.2.3 Energy constraints

The energy constraints are to make sure that the deployment of the DWC charging system is able to satisfy the energy requirement for normal operations of electric buses on all bus lines. As aforementioned, we assume the bus is fully charged overnight, and in day services it can always have partial charging at the base station between services as well as charging during driving. The battery level of each bus is changing

during the daily operation due to the energy supply of the battery charging and the energy consumption of the battery discharging.

For the bus on a bus line $r \in \boldsymbol{R}$, let $e_{riw,t,m}$ be the battery level of the bus at the node i in direction w at time slot t for the first service of the day as $m = 1$ or not for the first service as $m = 0$. We neglect the minor self-discharge of the battery. To preserve the life span of the battery, we set the lower and upper limit rates of the battery level for electric buses as α and β, respectively. The below constraints require the battery level of the bus on each node to be within the upper and lower limits:

$$e_{riw,t,m} \leq \beta E, \forall r \in \boldsymbol{R}, i \in \boldsymbol{N}, w \in \boldsymbol{W}, t \in \boldsymbol{T}, m \in \{0,1\} \quad (14)$$

$$e_{riw,t,m} \geq \alpha E, \forall r \in \boldsymbol{R}, i \in \boldsymbol{N}, w \in \boldsymbol{W}, t \in \boldsymbol{T}, m \in \{0,1\} \quad (15)$$

Let $c_{ij,t}$ denotes the energy consumption of the bus on the link (i, j) at time slot t. The energy supply sources are the energy charged at the base station and charged in motion from DWC. For buses charging at the base station, let p^s be the constant charging rate. The energy supplied by the chargers at the base station for the bus on route r at time slot t depends on the charging time $\tau_{r,t}$, the charged energy is $p^s \tau_{r,t}$. Let $e(v_{ij,t})$ denote the function of energy supply from each coil on speed $v_{ij,t}$ of link (i, j) at time slot t. The energy gained from the link covered by the transmitter coil is the summation of the energy transferred from all the coils embedded in the link, $\pi_{ij} d_{ij} x_{ij} e(v_{ij,t})$. To represent the battery level of the bus on the sequential nodes over time, we have the below constraints:

$$e_{ri+,t,m} = \begin{cases} \beta E & \forall r \in \boldsymbol{R}, i \in \boldsymbol{O_{r+}}, mt = 1 \\ e_{rj-tm} + p^s \tau_{r,t} & \forall r \in \boldsymbol{R}, j \in \boldsymbol{D_{r-}}, mt \neq 1 \end{cases} \quad (16)$$

$$e_{rjw,t,m} = e_{riw,t,m} - c_{ij,t} + \pi_{ij} x_{ij} d_{ij} e(v_{ij,t}), \forall r \in \boldsymbol{R}, (i,j) \in \boldsymbol{L_r}, w \in \boldsymbol{W}, t \in \boldsymbol{T}, m \in \{0,1\} \quad (17)$$

$$e_{ri-,t,m} = e_{rj+,t,m}, \forall i \in \boldsymbol{O_{r-}}, j \in \boldsymbol{D_{r+}}, t \in \boldsymbol{T}, m \in \{0,1\} \quad (18)$$

Constraint (16) is to define the initial battery level of the bus at the first node of each service. We assume buses start their first service of the day at the first time slot. The initial battery level of a bus will be the upper limit battery level when it is the first service of the day, while the initial battery level will be the remaining energy after one service loop plus the energy charged at the base station when it is not the first service of the day. Constraint (17) is to update the battery level of buses that serve on their lines. Constraint (18) ensures the energy conservation between the outbound and inbound of the bus line.

To ensure the total energy level of the bus fleet in route r is within the limitation of the summation battery levels of all buses in the fleet, we have the below two constraints.

$$\beta En_r^{bus} + \sum_t p^s \tau_{r,t} f_{r,t} - \sum_t \left(f_{r,t} \sum_{(i,j)\in L_r} c_{ij,t}\right) + \sum_{t,(i,j)\in L_r} \pi_{ij} x_{ij} f_{r,t} d_{ij} e(v_{ij,t}) \geq \alpha En_r^{bus}, \forall r \in \boldsymbol{R} \quad (19)$$

$$\beta En_r^{bus} + \sum_t p^s \tau_{r,t} f_{r,t} - \sum_t \left(f_{r,t} \sum_{(i,j)\in L_r} c_{ij,t}\right) + \sum_{t,(i,j)\in L_r} \pi_{ij} x_{ij} f_{r,t} d_{ij} e(v_{ij,t}) \leq \beta En_r^{bus}, \forall r \in \boldsymbol{R} \quad (20)$$

The limitation for the coil density embedded on each link is denoted as:

$$\pi_{low} \leq \pi_{ij} \leq \pi_{up}, \forall (i,j) \in \boldsymbol{L} \quad (21)$$

(1) Energy supply function

As illustrated before, the coil density on the DWC lane can be adjusted to accommodate the sustained use of energy by electric vehicles. The experiments in [40] and [134] show that the expected energy transmitted from a DWC transmitter coil is a

function of speed. According to the experiment result in [40], the function of energy transferred per coil on speed can be expressed as the below equation:

$$e\left(v_{ij,t}\right) = \frac{\eta}{v_{ij,t}}, \forall (i,j) \in \boldsymbol{L}, t \in \boldsymbol{T} \quad (22)$$

where η is a constant coefficient depending on the power level. A higher value of η means a higher requirement of power level.

With the above equation, the energy transferred from the link that covered by the transmitter coil $\pi_{ij} d_{ij} x_{ij} e\left(v_{ij,t}\right)$ can be converted to $\pi_{ij} d_{ij} x_{ij} \frac{\eta}{v_{ij,t}} = \eta \pi_{ij} \kappa_{ij,t} x_{ij}$, where $\kappa_{ij,t}$ is the average travel time of buses on the link (i,j) at time slot t. The energy gained on the link embedded with transmitter coils is $\eta \pi_{ij} \kappa_{ij,t}$. Therefore, the term $\eta \pi_{ij}$ can be treated as the charging power rate. Imagine a bus traveling on two links with the same length, to get an equal level of energy on the two links, the link with short traveling time (high driving speed) should be embedded with more coils.

(2) Energy consumption model

The energy As illustrated before, the energy consumption models employed in previous studies ignore the factors of regenerative braking and auxiliary electric devices that will significantly impact the energy consumption of transit buses. Machine learning is able to capture the effect of these factors on energy consumption estimation thanks to the fitness of nonlinear relationships, and the accuracy can be iteratively improved based on the ability of empirical learning and iterative optimization using tremendous historical actual driving data under complicated real-world driving conditions [135]. With this consideration, we build an artificial neural network (ANN) model to estimate the energy consumption of electric buses based on real-world driving data. The real-world driving data are obtained from battery electric buses operated by Chattanooga Area Regional

Transportation Authority (CARTA) in Chattanooga, Tennessee. The experimented electric buses have onboard measurement equipment installed to gather driving, monitoring, and maintenance information about the buses. This information is then sent to a data logger made by [136] in real-time. The temperature and humidity were obtained through query Dark Sky API weather data[7].

The collected data is processed into link-level information, including vehicle dynamics, road conditions, and environmental-related factors for each link. The input variables are average speed $v_{ij,t}$, average acceleration $a_{ij,t}$, road segment length d_{ij} and grade g_{ij}, the temperature $\varrho_{ij,t}$ and humidity $\varsigma_{ij,t}$, and average vehicle specific power (VSP) $VSP_{ij,t}$ of the link (i,j) at time slot t. The output value is the energy consumption of electric buses on the link (i,j) at time slot t which can be defined as:

$$c_{ij,t} = ANN(v_{ij,t}, a_{ij,t}, d_{ij}, g_{ij}, \varrho_{ij,t}, \varsigma_{ij,t}, VSP_{ij,t}), \forall (i,j) \in \boldsymbol{L}, t \in \boldsymbol{T}. \quad (24)$$

VSP is a widely used measurement tool for measuring the energy consumption of vehicles [130]. It is calculated by dividing the instantaneous power for kinetic, potential, rolling, and aerodynamic resistance by vehicle weight,

$$VSP = \frac{\frac{d}{dt}(KE + PE) + F_{rolling} * v + F_{Aerodynamic} * v}{m}$$

$$= \frac{\frac{d}{dt}\left(\frac{1}{2} m * (1 + \epsilon_i) * v^2 + m * g * h\right) + C_g * m * g * v + \frac{1}{2}\rho * C_D A v^3}{m}$$

$$= v * \left(a * (1 + \epsilon_i) + g * grade + g * C_g\right) + \frac{1}{2}\rho * \frac{C_D A}{m} v^3.$$ The average VSP can be expressed as:

[7] Dark Sky Weather API. https://darksky.net/dev/docs

$$VSP_{ij,t} = v_{ij,t}\left(2 \times 10^4 a_{ij,t} + 21.97 g_{ij} + 0.3\right) + 3.39 \times 10^{-3}\left(v_{ij,t}\right)^3, \forall (i,j) \in \boldsymbol{L}, t \in \boldsymbol{T} \quad (23)$$

The ANN model processes information in the same way that the human brain processes information. Specifically, an ANN model contains input, along with hidden and output layers, and each layer contains data processing components called neurons. These neurons are connected to each other and can form complex nonlinear models through activation functions. To have the best performance of the ANN model, we need to select the best configuration of the ANN model, such as how many hidden layers, how many neurons are in each layer, and what activation function transforms the information between every two layers. Generally, more hidden layers may increase the accuracy of the network but would result in overfitting. To avoid overfitting, the model is determined by using a cross-validation method with the evaluation of mean absolute error (MAE) and R^2. For more details about the model construction, please refer to our previous work [131, 137]. The structure of the best model has two hidden layers with 11 neurons in each layer, transformed with the sigmoid activation function.

4.2.2.4 System optimization model

Our system optimization model for deployment of the DWC lanes with the consideration of bus frequency setting is to minimize the social cost including total construction cost of DWC facilities, electric bus fleet purchase cost, passenger waiting cost, and cost for producing and transmitting electricity for charging facilities. Let c^{fix}, c^{coil}, c^{cons}, c^{wait}, c^{bus}, and c^{elec} be the fixed cost of one inverter, coil cost per unit, general construction cost per mile of the link, passenger waiting monetary cost per unit, bus purchase cost per unit, and electricity cost per unit. These costs are all uniform in the

amortized costs for one year. The developed system optimization model can be represented as follows:

$$\underset{(\boldsymbol{x},\boldsymbol{y},\boldsymbol{z},\boldsymbol{\theta},\boldsymbol{\pi},\boldsymbol{f},\boldsymbol{\tau},\boldsymbol{n^{bus}})}{\text{Min}} c^{fix}\left(\sum_w\left(\sum_i z_{iw} - \left(\sum_{(i,j)\in \boldsymbol{L}_{iw}} x_{ij} - \sum_i y_{iw}\right)\right) - \left(\sum_{i\in \boldsymbol{N}_+} \theta_i z_{iw} - \right.\right.$$

$$\left.\left.\left(\sum_{(i,j)\in \boldsymbol{L}_{i+}} \theta_i x_{ij} - \sum_{i\in \boldsymbol{N}_+} \theta_i y_{iw}\right)\right)\right) + \sum_{ij}(c^{coil}\pi_{ij} + c^{cons})x_{ij}d_{ij} + c^{wait}\sum_{r,t}\frac{sq_{r,t}}{2f_{r,t}} +$$

$$c^{bus}\sum_r n_r^{bus} + \frac{c^{elec}}{\varphi^s}\sum_{r,t} p^s \tau_{r,t} f_{r,t} + \frac{c^{elec}}{\varphi^l}\sum_{rij,t}\pi_{ij}x_{ij}f_{r,t}d_{ij}e\left(v_{ij,t}\right) \quad (25)$$

Subject to:

The DWC deployment constraints (1)-(8),

Bus frequency setting constraints (9)-(13),

Energy constraints (14)-(21).

The total construction cost of DWC lanes consists of the fixed cost of the inverter and the variable cost of transmitter coils. Based on the obtained number of inverters stated in section 2.2.1, the total cost of the inverters are $c^{fix}\left(\sum_w\left(\sum_i z_{iw} - \left(\sum_{(i,j)\in \boldsymbol{L}_{iw}} x_{ij} - \sum_i y_{iw}\right)\right) - \left(\sum_{i\in \boldsymbol{N}_+} \theta_i z_{iw} - \left(\sum_{(i,j)\in \boldsymbol{L}_{i+}} \theta_i x_{ij} - \sum_{i\in \boldsymbol{N}_+} \theta_i y_{iw}\right)\right)\right)$. The total cost of the power transmitter coils depends on the length of the DWC lanes and how many coils are used in each covered link. It is the summation of construction cost and cost of coils of each individual DWC link, $\sum_{ij}(c^{coil}\pi_{ij} + c^{cons})x_{ij}d_{ij}$. The passenger waiting time considered in this study is the time spent form the passenger arriving at the bus stop to the passenger getting on the bus. We assume random passenger arrivals where the average waiting time of each passenger's arrival at time slot t on bus line r is equal to half of the headway of buses on that bus line. The electricity cost includes the electricity charged at the base station and the electricity transferred from DWC lanes. We consider

the different charging efficiency of the static charger at the base station and the dynamic charging lane on the line as φ^s and φ^l, respectively.

4.2.2.5 Model linearization

The proposed system model is a mixed integer nonlinear program with, binary, integer, and continuous variables. The nonlinear terms that existed in the objective function and constraints make it hard to solve the above model directly. This subsection is to linearize our proposed nonlinear model by employing appropriate linearization techniques.

For the bilinear terms $\theta_i z_{iw}$, $\theta_i y_{iw}$, $\theta_i x_{ij}$, and $\tau_{r,t} f_{r,t}$ in the objective function and constraints (19)-(20), we use McCormick envelopes to relax the nonlinearity. McCormick envelopes are a type of convex relaxation that has been widely used in solving bilinear programming problems [138].

We introduce four auxiliary variables θ_{iw}^z, θ_{iw}^y, and θ_{ij}^x, and $\mu_{r,t}$ to represent the bilinear terms $\theta_i z_{iw}$, $\theta_i y_{iw}$, $\theta_i x_{ij}$, and $\tau_{r,t} f_{r,t}$, respectively. The linearization relationships are shown below:

$$\theta_{iw}^z \leq \theta_i, \forall i \in \boldsymbol{N}_+, w \in \boldsymbol{W} \tag{26}$$

$$\theta_{iw}^z \leq z_{iw}, \forall i \in \boldsymbol{N}_+, w \in \boldsymbol{W} \tag{27}$$

$$\theta_{iw}^z \geq \theta_i + z_{iw} - 1, \forall i \in \boldsymbol{N}_+, w \in \boldsymbol{W} \tag{28}$$

$$\theta_{iw}^y \leq \theta_i, \forall i \in \boldsymbol{N}_+, w \in \boldsymbol{W} \tag{29}$$

$$\theta_{iw}^y \leq y_{iw}, \forall i \in \boldsymbol{N}_+, w \in \boldsymbol{W} \tag{30}$$

$$\theta_{iw}^y \geq \theta_i + y_{iw} - 1, \forall i \in \boldsymbol{N}_+, w \in \boldsymbol{W} \tag{31}$$

$$\theta_{ij}^x \leq \theta_i, \forall (i,j) \in \boldsymbol{L}_{i+} \tag{32}$$

$$\theta_{ij}^x \leq x_{ij}, \forall (i,j) \in \boldsymbol{L}_{i+} \tag{33}$$

$$\theta_{ij}^{x} \geq \theta_i + x_{ij} - 1, \forall (i,j) \in \boldsymbol{L}_{i+} \tag{34}$$

$$\mu_{r,t} \geq \tau_{up} f_{r,t} + \tau_{r,t} f_{up} - \tau_{up} f_{up}, \forall r \in \boldsymbol{R}, t \in \boldsymbol{T} \tag{35}$$

$$\mu_{r,t} \leq \tau_{up} f_{r,t}, \forall r \in \boldsymbol{R}, t \in \boldsymbol{T} \tag{36}$$

$$\mu_{r,t} \leq \tau_{r,t} f_{up}, \forall r \in \boldsymbol{R}, t \in \boldsymbol{T} \tag{37}$$

As for the nonlinear terms $\pi_{ij} x_{ij}$ and $\pi_{ij} x_{ij} f_{r,t}$ in the objective function and constraints (18)-(20). We define an auxiliary variable ξ_{ij} and a big enough constant M to linearize the mutual term $\pi_{ij} x_{ij}$ of the two terms. The linearization process is presented in equations (38)-(41). In this way, the term $\pi_{ij} x_{ij} f_{r,t}$ can be denoted as $\xi_{ij} f_{r,t}$. We then introduce another variable $\omega_{rij,t}$ to replace $\xi_{ij} f_{r,t}$ and use McCormick envelopes to linearize it. The corresponding relationships are shown in equations (42)-(45).

$$\xi_{ij} \leq x_{ij} M, \forall (i,j) \in \boldsymbol{L} \tag{38}$$

$$\xi_{ij} \leq \pi_{ij}, \forall (i,j) \in \boldsymbol{L} \tag{39}$$

$$\xi_{ij} \geq \pi_{ij} - \left(1 - x_{ij}\right) M, \forall (i,j) \in \boldsymbol{L} \tag{40}$$

$$\xi_{ij} \geq 0, \forall (i,j) \in \boldsymbol{L} \tag{41}$$

$$\omega_{rij,t} \geq \pi_{low} f_{r,t}, \forall r \in \boldsymbol{R}, (i,j) \in \boldsymbol{L_r}, t \in \boldsymbol{T} \tag{42}$$

$$\omega_{rij,t} \geq \pi_{up} f_{r,t} + \xi_{ij} f_{up} - \pi_{up} f_{up}, \forall r \in \boldsymbol{R}, (i,j) \in \boldsymbol{L_r}, t \in \boldsymbol{T} \tag{43}$$

$$\omega_{rij,t} \leq \pi_{up} f_{r,t}, \forall r \in \boldsymbol{R}, (i,j) \in \boldsymbol{L_r}, t \in \boldsymbol{T} \tag{44}$$

$$\omega_{rij,t} \leq \xi_{ij} f_{up} + \pi_{low} f_{r,t} - \pi_{low} f_{up}, \forall r \in \boldsymbol{R}, (i,j) \in \boldsymbol{L_r}, t \in \boldsymbol{T} \tag{45}$$

It is noted that $c^{wait} \sum_{r,t} \frac{sq_{r,t}}{2 f_{r,t}}$ in the objective function and $\frac{sn^c}{f_{r,t}}$ in constraint (11) are both nonlinear terms with a mutual part $\frac{1}{f_{r,t}}$. It is difficult to directly introduce one variable to substitute $\frac{1}{f_{r,t}}$, because $f_{r,t}$ also exists in our model. Therefore, we use the

piecewise linear method proposed in [139] to approximate the nonlinear term. The term $\frac{1}{f_{r,t}}$ can be linearly expressed as $L(f(x)) = \sum_{h=1}^{p} f(a_h)\delta_{r,t,h}$, where a_h denotes the breaking point. We set five break points as $(1,5,10,15,20)$. The linearization is expressed with the following equations:

$$f_{r,t} = \sum_{h=1}^{p} a_h \delta_{r,t,h}, \forall r \in \boldsymbol{R}, t \in \boldsymbol{T} \quad (46)$$

$$\begin{cases} \sum_{h=1}^{p} \delta_{r,t,h} = 1 \\ \delta_{r,t,1} + \delta_{r,t,2} \le \gamma_{r,t,1} \\ \delta_{r,t,3} \le \gamma_{r,t,2} \\ \delta_{r,t,4} + \delta_{r,t,5} \le 1 - \gamma_{r,t,1} \\ \delta_{r,t,1} + \delta_{r,t,5} \le 1 - \gamma_{r,t,2} \end{cases}, \forall r \in \boldsymbol{R}, t \in \boldsymbol{T} \quad (47)$$

$$\delta_{r,t,h} \ge 0, \gamma_{r,t,u} \in \{0,1\},, \forall r \in \boldsymbol{R}, t \in \boldsymbol{T}, h \in \{1,2,3,4,5\}, u \in \{1,2\} \quad (48)$$

Thus, $c^{wait} \sum_{r,t} \frac{sq_{r,t}}{2f_{r,t}}$ can be replaced as $2\, c^{wait} s \sum_{r,t} q_{r,t}(\delta_{r,t,1} + 0.2\delta_{r,t,2} + 0.1\delta_{r,t,3} + 0.0625\delta_{r,t,4} + 0.05\delta_{r,t,5})$, and $\frac{sn^c}{f_{r,t}}$ can be substituted as $sn^c(\delta_{r,t,1} + 0.2\delta_{r,t,2} + 0.1\delta_{r,t,3} + 0.0625\delta_{r,t,4} + 0.05\delta_{r,t,5})$.

Based on the above linearization, we transform our system model into a MILP model, which can be easily solved with commercial optimization solvers.

4.3 Case Study

To examine our linearized optimization model, we implement the model on a real-world transit network from Chattanooga Area Regional Transportation Authority (CARTA). Figure 4. 4 shows the CARTA system map and the network of selected routes where electric buses are in operation. The selected network contains 579 nodes, 809 links with an average length of 105 m, and 4 routes, “Route 1”, “Route 4”, “Route 10”, and “Route 21”, with a total length of 53.05 miles. Four routes share the base station as a terminal. The four routes share some nodes and links as shown in Figure 4. 5. The exact

configuration information of each route is presented in Table 4. 2. The passenger arrivals and loaded at each bus stop at each time slot are extracted from Automatic Passenger Counting (APC) data provided by CARTA. The operation time of a day ranges from 6:00–22:00. We split it into four time slots, morning peak hours (6:00-9:59), moderate peak hours (10:00-13:59), afternoon peak hours (14:00-17:59), and off-peak hours (18:00-22:00).

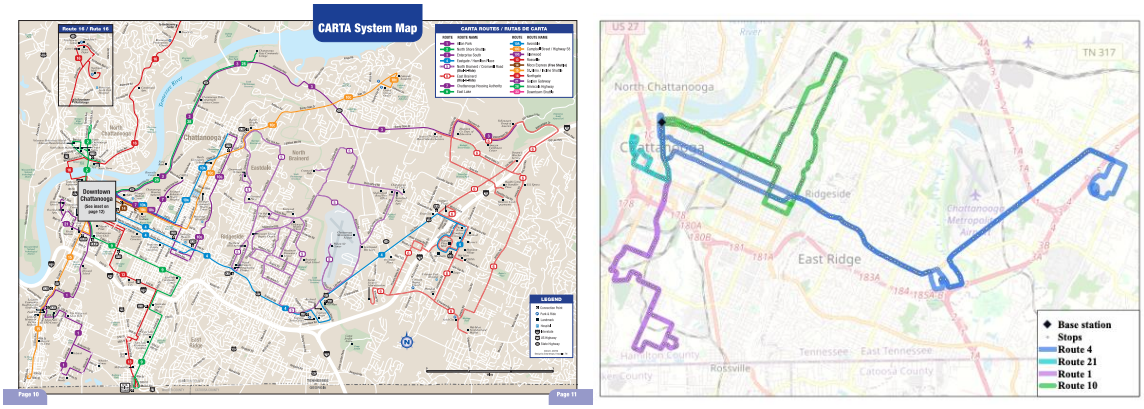

Figure 4.5 CARTA system map (left) and network of routes operated by electric buses (right).

Table 4.2 Route information.

Routes	Number of nodes	Number of links	Length (mile)
Route 1	115	198	13.65
Route 4	278	384	25.56
Route 10	175	199	12.43
Route 21	66	91	5.04

We assume the life of the constructed DWC lanes is 30 years, and the life of buses is 10 years. All the costs are amortized to one year. The default parameter settings for the case study are stated in Table 4.3. Most of the values are cited from literatures

[36-38, 125]. We assume the buses are bought for dynamic wireless charging specifically. These buses have power receiver equipment and a downsized battery. According to the study of life cycle assessment on electric cars [140], the onboard battery size would be reduced to one-third to one-fifth of the original battery throughout a day of bus operation. Battery downsizing enables significant energy savings owing to lighter vehicles, as well as financial savings on battery and use-phase electricity costs [141]. Many studies related to the optimization of deploying dynamic wireless charging technology have focused on the decision of the battery size. For example, [36] developed a model to simultaneously select the optimal location of the DWC facilities and find the optimal battery sizes of route-specific electric buses. The results reveal that the optimal battery capacity of buses for different routes ranges from 21.8 to 55.6 kWh. In a similar study [37], the optimal battery sizes are from 7.39 to 33.97 kWh for buses operating on different routes. They further show that the homogeneous buses carrying a uniform battery size of 18.1 kWh can serve all bus routes of 41 km. In our study, we assume the battery capacity of the buses is 30 kWh. The hourly monetary cost of the passenger waiting time is according to the average salary per hour in Chattanooga [142]. The charging efficiency of static charging and dynamic charging refers to the study [140]. The cost of a coil is about $1000 per mile [143]. We assume the diameter of the coil is 1.6 m which is the same as the coil topology used in [40]. Thus, the cost of each coil is $1600, and the upper limit number of coils for each line is 1000. We set the lower limit as 250 coils per mile to present the fewest energy supply. As derived in section 4.2.2.3, the term $\eta\pi_{ij}$ can be treated as the charging power rate. The value of η depends on the power level and the technology of DWC. We assume η is 0.08. It indicates the charging power rate will be

within the range of 20-80 kW, with the coil density ranges from 250 to 1000. This range is widely used in previous studies [36, 40, 125, 132].

Table 4.3 Parameter default values.

Parameters	Description	Value
c^{fix}	The fixed cost of one DWC facility	\$20,000/30
c^{coil}	Coil cost per unit	\$1,600/30
c^{cons}	Mill and Resurface cost of road per mile	\$200,000/30
c^{wait}	The hourly monetary cost of the passenger waiting time	\$17.35
c^{bus}	Cost of the electric bus per unit	\$360,438
c^{elec}	Electricity cost per unit	\$0.1031
φ^{s}	Charging efficiency of static charging	0.85
φ^{l}	Charging efficiency of dynamic charging	0.8
p^{s}	Charging power rate of static charging	100 kW
Q	Bus capacity	40
ρ	Bus occupancy rate	0.7
E	Battery capacity	30 kWh
s	Duration of time slots	4 hours
α	Lower battery level rate	0.2
β	Upper battery level rate	0.8
η	Coefficient of energy supply function of transmitter coils.	0.08
n^{c}	Number of chargers at the base station	1

f_{up}	The upper limit of bus frequency	20 vehicles/slot
τ_{up}	The upper limit of charging time at the base station	30 min
π_{low}	The lower limit of coils per mile	250 #/mile
π_{up}	The upper limit of coils per mile	1000 #/mile

4.3.1 Basic results

The commercial optimization solver Gurobi (V9.5.1) is used to solve the MILP using the branch and bound technique. Our model has 14961 variables (2713 integer variables) and 6992 constraints. It takes 5.46 minutes to solve the model with a 0.01% relative optimality gap. Table 4. 4 summarizes the basic optimal results. The overall social cost of the new charging system amortized for each year is $4,316,811, which consists of the deployment costs of DWC lanes ($138,491), buses cost ($432,526), passenger waiting cost ($3,711,725), and use-phase electricity cost ($34,069). The table reports that the deployment of DWC lanes needs 52 inverters and 1551 coils in total. The total length of the links covered by DWC lanes is 3.16 miles, which is 6% of the total route. The coverage of DWC lanes on Route 1 and Route 4 (7.5% and 7.1%) is larger than that on Route 10 and Route 21 (2% and 2.4%). This result is reasonable because buses traveling on Route 1 and Route 4 have higher speeds and need more energy to accomplish one service loop, compared with that on the other routes. Figure 4.6 depicts the specific location and coil density of each DWC link in the network. The gradient color from yellow to red shows the number of coils for each mile ranging from 250 to 1000. From Figure 4.6, we can observe that the locations of the DWC lanes do not have a significant relationship with the locations of stops. This result is different from that of

[36], reporting that DWC facilities are primarily located around bus stops. In our case, the deployment of DWC lanes is mainly involved with the extent of energy requirement.

Table 4.4 Summary of the basic results.

Description		Value
Total coils needed		1551
Number of inverters		52
Length of DWC lanes	Total length	3.16 miles (6.0%)
	DWC lanes on Route 1	1.02 mile (7.5%)
	DWC lanes on Route 4	1.81 mile (7.1%)
	DWC lanes on Route 10	0.25 mile (2.0%)
	DWC lanes on Route 21	0.12 mile (2.4%)
DWC deployment costs (1 year)	Total construction cost	$138,491
	Inverter cost	$34,667
	Costs of coils and road reconstruction	$103,824
Number of buses		12
	Buses fleet on Route 1	3
	Buses fleet on Route 4	6
	Buses fleet on Route 10	2
	Buses fleet on Route 21	1
The amortized cost of buses (1 year)		$432,526
Total waiting cost (1 year)		$3,711,725
Electricity cost (1 year)	Total electricity cost	$34,069
	Electricity cost at the base station	$19,052
	Electricity cost on DWC lanes	$15,017
Overall social cost (1 year)		$4,316,811

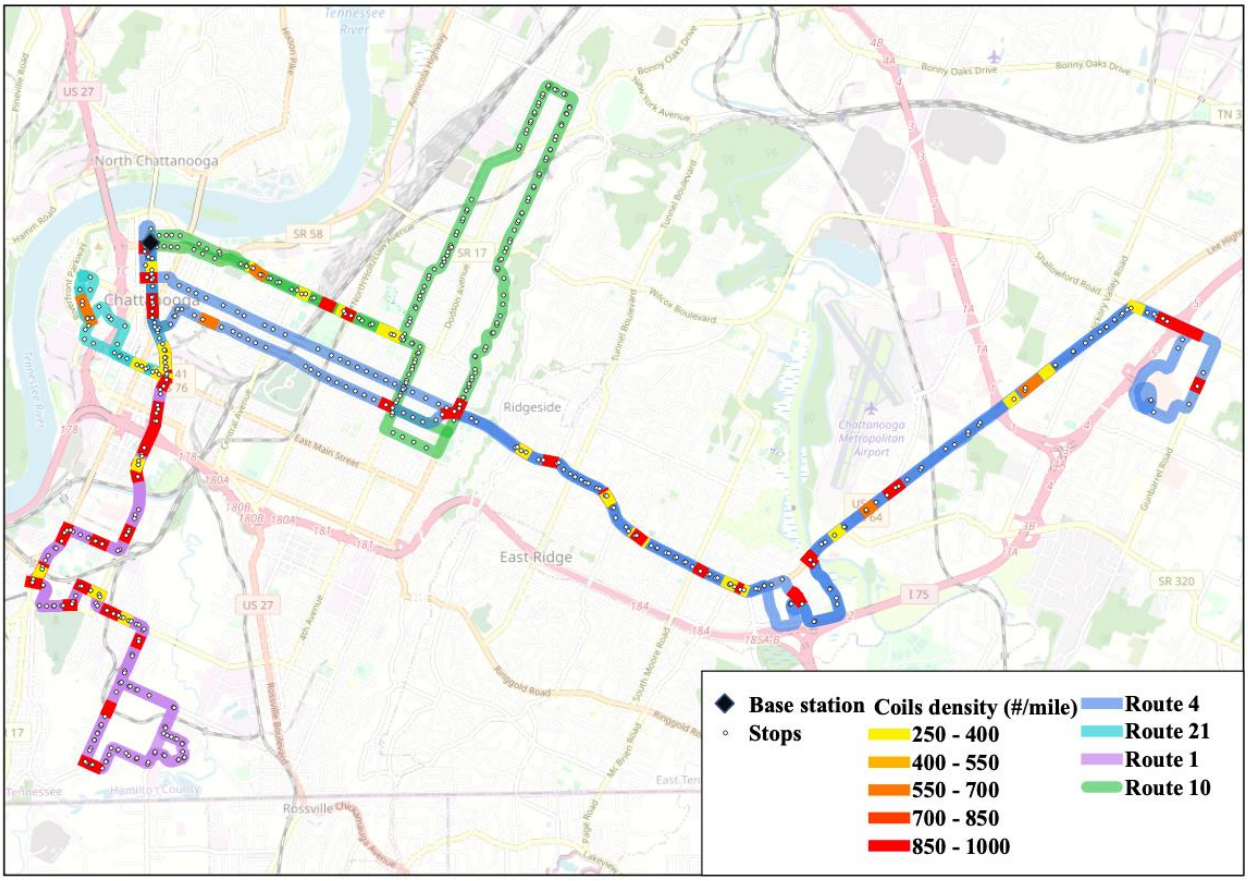

Figure 4.6 The optimal layout of DWC lanes with varied coil densities.

Our model ingrates the deployment of DWC lanes with the tactical bus frequency setting, considering the buses can have a partial charge at the base station. Figure 4.7 shows the bus frequency setting and charging time in minutes for the four routes at each time slot. It is observed in Figure 4.7 (left), the bus frequency of the four routes set for morning peak hours (6:00-9:59) is generally the largest, followed by that of the afternoon peak hours (14:00-17:59) and moderate peak hours (10:00-13:59), with the frequency for off-peak hours (18:00-22:00) is the smallest. We can also observe Route 4 has the most bus frequency, followed by Route 1, route 10, and Route 21. This result depends on the passenger demand, route distance, and the charging time at the base station.

Figure 4.7 (right) presents that the charging times of the four routes at the four time slots vary based on the available DWC facilities, bus frequency, and energy consumption on routes. According to the bus frequency and charging time at the base station, the optimal bus fleets for the four routes are obtained. As shown in Table 4.4, the agency needs to assign 3 buses for Route 1, 6 buses for Route 4, 2 buses for Route 10, and 1 bus for Route 21, 12 buses in total.

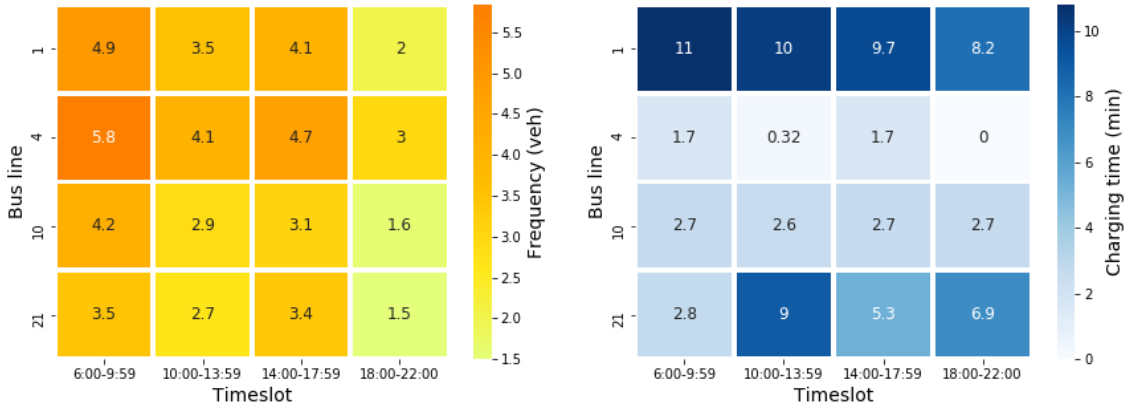

Figure 4.7 Result of bus frequency setting (left) and charging time at the base station (right).

4.3.2 Sensitivity analysis

In this section, we conduct a sensitivity analysis of our proposed model, to investigate the impact of fixed coil density and the impact of charging at the base station on the planning of the DWC system.

4.3.2.1 The impact of fixed coil density

To compare and analyze the effects of using different fixed coil densities on the deployment of DWC lanes, we conduct four scenarios under which the uniform coil density for DWC lanes is 250, 500, 750, and 1000, respectively. As mentioned before, coil density has a positive correlation with the charging power rate. As the coil density

ranges from 250 to 1000, the equivalent charging power rate of the DWC lanes will be within the range of 20-80 kW. Figure 4.8 shows the optimal location of the DWC lanes under the four scenarios. It is observed that the length of the DWC lanes increases as the coil density decreases. That is to say, the lower the charging power rate is, the more DWC lanes are required. Table 4.5 reports the optimal results for the four scenarios and compares them with the basic result. It is observed that the number of coils, the number of inverters, and the cost of DWC lanes all increase as the coil density decreases. Among the four scenarios, the scenario with the coil density fixed as 750 has the lowest overall social costs and lowest cost of electricity. The scenario with the coil density fixed as 1000 requires the lowest cost of DWC construction, but the highest electricity cost. The high electricity costs are mainly from the electricity transferred from the DWC lanes. The high coil density of 1000 might result in more unnecessary energy transferred from the DWC lanes. It is noted that the basic result with varied coil density remains the minimal social cost, compared with the four scenarios with fixed coil density.

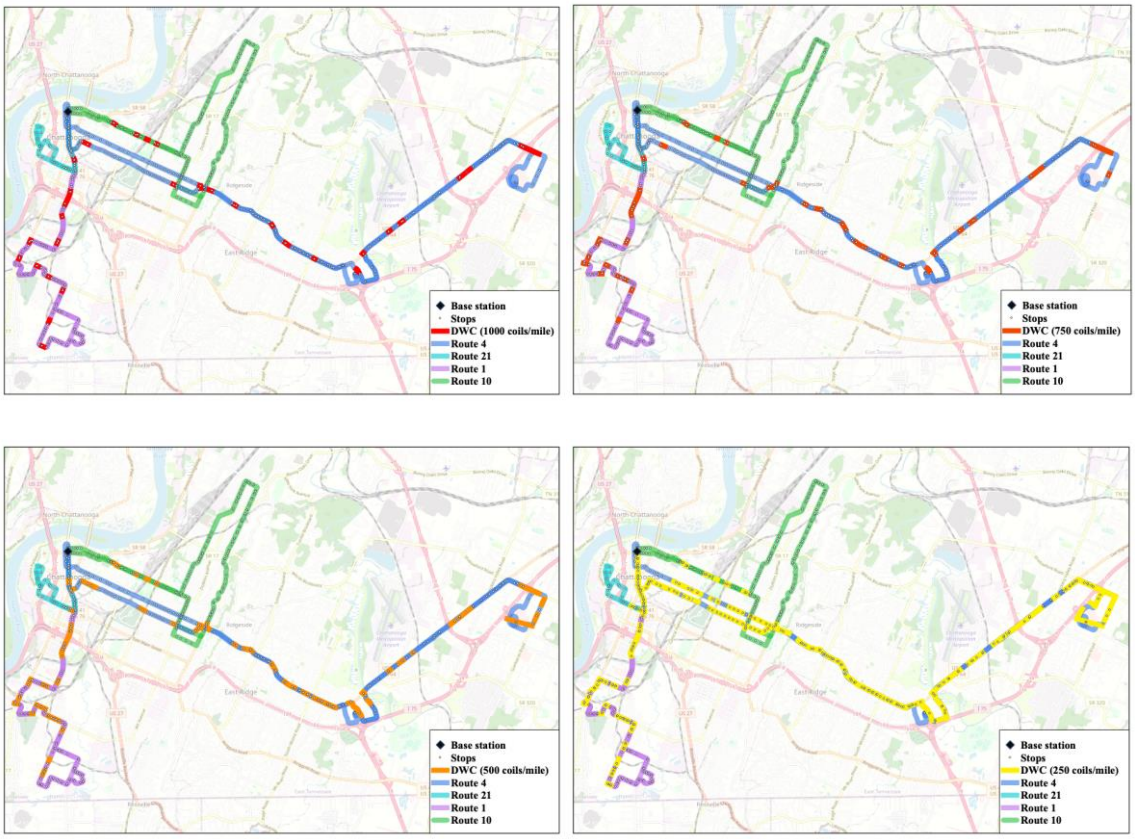

Figure 4.8 The optimal layout of DWC lanes of four scenarios with different fixed coil densities.

Table 4.5 The optimal results for different scenarios on coil density.

Description	Various coil density	Fixed coil density (#/mile)			
		1000	750	500	250
Total coils needed	1551	1718	1817	2169	5084
Number of inverters	52	37	41	51	56
DWC deployment costs	$138,491	$127,739	$140,369	$178,607	$444,119
Electricity cost	$34,069	$51,388	$29,006	$36,134	$50,547
Overall social cost	$4,316,811	$4,371,179	$4,337,669	$4,369,464	$4,571,594

4.3.2.2 The impact of fixed coil density

As illustrated before, we assume that the electric buses can have partial charge between services at the base station. The tradeoff between charging at the base station and charging in motion on the DWC lanes will impact the deployment of the DWC system. To investigate the influence of partial charging on the charging system, we vary the charging rate of the charger at the base station from 0 kW to 100 kW. Figure 4.9 reports the DWC facilities costs and the electricity costs with a different charging rate of the static charger. From Figure 4.9 (left), we can observe that the costs of inverters, coils and road reconstruction decreases as the charging rate increases. The reason is that as the charging rate increases, buses will get more energy from the partial charging at the base station. Therefore, the energy required from the length of the DWC lanes is reduced. We can also observe that the cost of inverters does not reduce significantly with the rising charging rate. This is likely because neighbor links can share one inverter. The number of inverters will not go up a lot even when there are increasing coils needed for energy transfer. It is also observed that the reduction of the number of coils tends to be flat as the charging rate is larger than 80 kW. It indicates that when the static charging rate is more than 80 kW, the benefit of static charge at the base station does not overweight the requirement of dynamic charge on the DWC lanes. This finding is also reflected in Figure 4.9 (right), where the electricity usage on the dynamic charging is reduced as the static charging rate goes up but remains flat when the rate is larger than 80 kW. Figure 4.9 (right) shows a clear tradeoff between the static charge at the base station and the dynamic charge on the DWC lanes. As the growing of static charging rate, the electricity gained at the base station is increased while the electricity transferred from the DWC lanes is reduced. The result also indicates that when the charging rate is 100 kW at the

base station, it can save about 40% of the construction cost for DWC facilities, compared with no stationary charging at the base station.

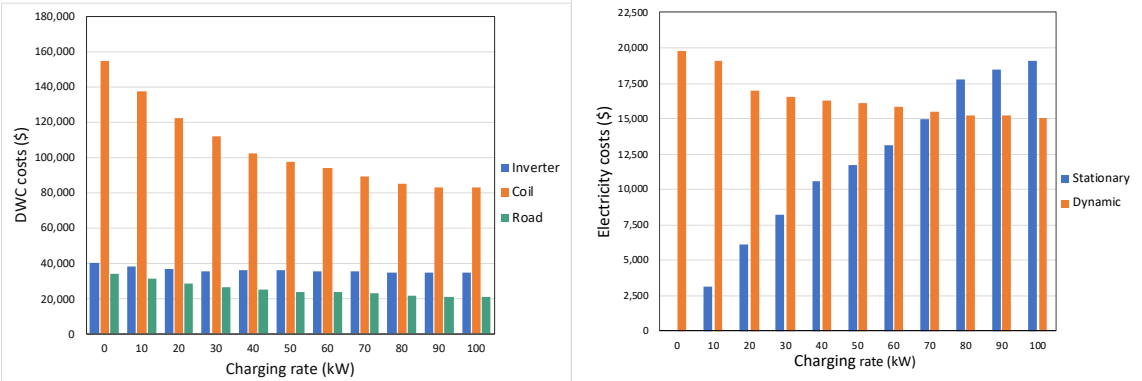

Figure 4.9 The DWC facilities costs (left) and the electricity costs (right) with different charging rates at the base station.

4.3.2.3 Comparison with existing models

As shown in the literature, the studies involving DWC system planning mainly focus on electric cars, and limited studies investigate the deployment of DWC facilities for transit buses. Our work is considered an extension of the existing works [36, 38]. In contrast to the previous studies, our optimization model addresses a number of issues that others have not. Table 4.6 summarizes the comparison of our model with the existing models. The primary distinctions of our model are the consideration of varied coil density, the integration of bus frequency setting, the treatment of bidirectional route, and the modeling of energy consumption. For intense, the decision of coil density can flexibly satisfy energy sustaining during the bus operation since the coil density can vary with the extent of energy requirement. It also can provide a cost-effective solution for the planning of the DWC system in practice. Our model considers the combination of DWC deployment with the tactical bus frequency setting to support the transit planning of the new charging system for the agencies. The integration of the bus frequency setting

produces nonlinearity in the model which is one of the difficulties we faced. However, we are able to resolve this difficulty by linearizing the model. Instead of treating the bidirectional route as two non-bidirectional routes, our model treats it as it is by introducing an additional index to identify the two directions of routes and cancel out the redundant inverters installed in both directions of the lanes with DWC. The existing studies applied predefined energy consumption or physical-based model to estimate the energy consumption of buses. However, they neglect the effects of regenerative braking and auxiliary electric devices for the estimation of energy consumption. We employ machine learning technology to capture the effect of these factors on energy estimation by training tremendous historical driving data under various driving conditions. Furthermore, we consider the changes in bus speed and passenger demand during different periods of one-day operation. These considerations bring robustness for the location of the DWC lanes and dynamic updates for bus frequency during daily operation, which makes our model more useful for realistic implementation. In addition, our model also considers the electricity cost, road reconstruction cost, flexible charge at the base station, and decision on bus fleet size.

Table 4.6 Comparison with existing models.

Description	Model in [129]	Model in [36]	Model in [38]	Our model
Considering variable coil density	×	×	×	✓
Bus frequency setting	×	×	×	✓
Bidirectional route	×	×	×	✓
Energy consumption model	Predefined	Physical-based	Physical-based	Machine learning
Speed of buses	Certain	Uncertain	Certain	Changing over time
Passenger demand	×	×	×	Changing over time
Electricity cost	×	×	×	✓
Cost of road reconstruction	×	×	×	✓
Flexible charge at the base station	×	×	✓	✓
Decision on bus fleet size	×	×	✓	✓

4.4 Conclusions

In this study, we develop a nonconvex mixed integer optimization model to address the allocation problem of DWC lanes on bidirectional multiple routes, considering the bus frequency setting for the new charging system. Our goal is to find an optimal DWC system design for electric buses that minimize the social costs relating to the bus operation on the new charging system, including the total construction cost of DWC facilities, electric bus fleet purchase cost, passenger waiting cost, and cost for producing and transmitting electricity for charging facilities. We consider three groups of constraints, including the DWC deployment constraints, bus frequency setting constraints, and energy constraints. The DWC deployment constraints are to make sure the neighbor

links (i.e., adjacent links and bidirectional parallel links) can share the fixed cost of the DWC construction. The constraints of bus frequency setting are formulated with the explicit consideration of the limited charging time at the base station and the coverage of passengers at different periods during the day. The energy constraints ensure the optimal allocation of the DWC lanes can satisfy the energy requirement for normal operations of electric buses in the transit system. Since our model contains many nonlinear terms, we employ several linearization approaches to linearize our model into a MILP model. We conduct a case study to verify the efficiency of our model. The results demonstrate that our model can effectively solve the planning problem of the DWC lanes in a complex bus transit system with bidirectional multiple bus lines in CARTA. Our sensitivity analysis with the changes in coil density and charging rate at the base station also provides insight into the planning of the DWC system.

We acknowledge there are limitations of the current research that could motivate future research directions. Our study considers uniform electric buses with the same size of battery and seat capacity. Various electric bus types with different sizes and mixed bus fleets (i.e., hybrid buses, diesel buses, electric buses) can be included in the planning of the DWC system. Another interesting area is the investigation of the relationship between the allocation of the DWC infrastructure and the power load in the grid. We also recommend exploring the prospect of installing DWC for public transit and private car in one charging system and analyzing the effect of installed DWC lanes on the traffic.

Chapter 5

Conclusions

This chapter highlights original contributions to achieving sustainability in urban transit and high occupancy vehicle systems and recommends potential research plans in the future.

5.1 Conclusions

Road transportation emissions can be minimized in the manner of reducing total VMT and lowering vehicle emission rate. Many strategies have been proven viable for achieving transportation sustainability. For example, the total VMT can be reduced by switching low-occupancy transportation modes (i.e., private cars) to high-occupancy transportation modes (i.e., public transit, ridesharing). The development of alternative-fuel vehicles (i.e., hybrid vehicles and electric vehicles) provides the capability of minimizing vehicle emission rates or achieving net zero emissions. This dissertation focuses on achieving transportation sustainability in urban transit and high-occupancy vehicle systems. It links to some main components of the above strategies, including transit buses, ridesharing, and hybrid and electric vehicles. Specifically, three studies were done to achieve the primary goal: (1) hybrid bus energy prediction, (2) ridesharing operations and assessment, and (3) electric transit system charging infrastructure design. This dissertation is capable of supporting transportation planning, decision-making, and policy design of transportation practitioners referring to achieving sustainability in urban transit and high-occupancy vehicle systems, taking efforts on various research technologies, such as artificial intelligence, simulation, and operations.

In chapter 2, the study of predicting the energy consumption of hybrid buses was investigated. It refers to using public transit to reduce VMT and leverage hybrid buses to lower vehicle emission rates. This study proposed ANN microscopic and mesoscopic

models to estimate the fuel consumption of hybrid diesel buses based on long-term transit bus monitoring data collected from Chattanooga Area Regional Transportation Authority (CARTA). The microscopic model predicted instantaneous fuel consumption rates based on driving, grade, and environment variables at the same frequency. The ANN-based microscopic model results showed 1–2% of cumulative absolute error when aggregating second-level results to 5 to 60-minute trips. The results showed that ANN models can achieve lower error, compared to linear regression models, using the same input variables. The mesoscopic model predicted average fuel rates for 5 to 60-minute trip durations based on traffic factors for the same period. Our results show that the absolute prediction error for mesoscopic models ranged between 5 and 9%. This range is higher than that of the microscopic model; however, the independent variables of the mesoscopic model, e.g., average traffic speed, congestion level, etc., are typically monitored by the local transportation authority. The experimental data contained 1 Hz data of hybrid and diesel buses that have similar driving conditions in terms of speed, engine demand, and road grade. Our investigation of fuel rates showed that hybrid buses have the largest fuel savings during low-speed driving with high acceleration and have none or increased fuel consumption during highway driving. The electric motor of hybrid buses normally engages to supplement or replace a portion of propulsion provided by the diesel engine at low-speed driving with high acceleration, which can help achieve better fuel efficiency. This study can provide transportation agencies with accurate and practical information on hybrid bus energy consumption for a better understanding of the performance of hybrid transit buses during transit operations and planning.

In chapter 3, the study of ridesharing operations and assessment referring to reducing total VMT was conducted. We investigate the efficiency and environmental benefits of ridesharing in a mid-size city (Chattanooga, Tennessee) using an agent-based simulation framework. The simulation and result analysis demonstrate that ridesharing services have the potential to reduce traffic volume and relieve congestion without significant impacts on travelers' schedules. Specifically, when ridesharing ratios are 5% to 75% (trips fulfilled by ridesharing services) in Chattanooga, many (65%–75%) of ridesharing travelers will experience a delay of up to 15 minutes. Longer delays, 30 minutes or more, are mainly due to ridesharing travelers in isolated areas because it takes time to match vehicles to pick them up. Ridesharing services can result in external outcomes that can be beneficial to other travelers and society. This analysis shows that 60%–80% of drive-alone travelers will arrive earlier compared with the baseline no-ridesharing scenario. The average early arrival time is 5.6 minutes for all drive-alone travelers. The results show ridesharing services can achieve a 2%–35% reduction in vehicle-related emissions and energy consumption with various ridesharing ratios. This is significant considering most vehicle emissions are generated in urban regions with high population density. The reduction in vehicle emissions has the potential to improve air quality and mitigate adverse impacts on the health of residents. The framework and results of this study can be helpful to transportation practitioners to evaluate the travel efficiency effects and environmental benefits with a systematic and comprehensive perspective when implementing ridesharing services on a city scale.

In chapter 4, the study of designing electric transit system charging infrastructure was completed. It is relevant to utilize urban transit to reduce VMT and employ battery

electric buses to minimize vehicle emission rates. This study developed a mixed integer programming model to address the allocation problem of DWC lanes on bidirectional multiple routes, considering the bus frequency setting for the new charging system. The goal is to find an optimal DWC system design for electric buses that minimize the social costs relating to the bus operation on the new charging system, including the total construction cost of DWC facilities, electric bus fleet purchase cost, passenger waiting cost, and cost for producing and transmitting electricity for charging facilities. The model considers three groups of constraints, including the DWC deployment constraints, bus frequency setting constraints, and energy constraints. The DWC deployment constraints are to make sure the neighbor links (i.e., adjacent links and bidirectional parallel links) can share the fixed cost of the DWC construction. The constraints of bus frequency are formulated with the explicit consideration of the limited charging time at the base station and the coverage of passengers at different periods during the day. The energy constraints ensure the optimal allocation of the DWC lanes can satisfy the energy requirement for normal operations of electric buses in the transit system. Since the proposed model contains many nonlinear terms, we employ several linearization approaches to linearize the initial model into a MILP model. A case study was conducted to verify the efficiency of our model. The results demonstrate that the proposed model can effectively solve the planning problem of the DWC lanes in a complex bus transit system with bidirectional multiple bus lines in CARTA. A sensitivity analysis with the changes in coil density and charging rate at the base station also provides insight into the planning of the DWC system.

The aforementioned conclusions were reached in light of the results of the initial research. There are expected to be more studies on this topic.

5.2 Future work

The primary goal of this dissertation is to support transportation planning, decision-making, and policy design of transportation practitioners to achieve sustainability in urban transit and high-occupancy vehicle systems, through intelligent modeling, simulation, and operations. Some challenges were addressed in this dissertation; however, more research should be conducted in the field of developing sustainability in urban transit and high-occupancy vehicle systems.

For the study of predicting hybrid bus energy consumption, the experiment did not collect operational data for electric motors within the hybrid bus. Therefore, we could not fully understand the energy management system mechanism within the hybrid bus. One future research direction may be to collect and leverage electric motor operation data from hybrid buses to better understand their fuel-saving mechanism. Another future research direction may be to collect passenger load information on buses and assess the impacts of passenger load on the fuel consumption of hybrid buses under real-world driving conditions.

The vehicles applied in the ridesharing operation and assessment framework were internal combustion vehicles. Electric vehicles are emerging fast and play an important role in reducing energy consumption and cutting emissions. It would be interesting for future research to consider a diversified vehicle fleet for ridesharing services and associated infrastructure planning. Second, it will be more realistic to establish an online ridesharing algorithm that can dynamically fill the empty-seat with the consideration of

spatial mismatch between supply and demand based on the real-world data. Third, researchers can include other travel modes, such as public transit, shared bike, or micro-mobility, with ridesharing to model multimodal travel implementation and estimate associated impacts. This requires more complex planning algorithms to search for optimal mode combinations to reach minimum monetary, time, or environmental impacts.

The study for designing dynamic wireless charging facilities considers uniform electric buses with the same size of battery and seat capacity. Various electric bus types with different sizes and mixed bus fleets (i.e., hybrid buses, diesel buses, electric buses) can be included in the planning of the DWC system. Another interesting area is the investigation of the relationship between the allocation of the DWC infrastructure and the power load in the grid. This dissertation also recommends exploring the prospect of installing DWC for public transit and private car in one charging system and analyzing the effect of installed DWC lanes on traffic.

References

[1] J. Blunden and D. Arndt, "A look at 2018: Takeaway points from the State of the Climate supplement," *Bulletin of the American Meteorological Society*, vol. 100, pp. 1625-1636, 2019.

[2] P. C. Change, "Global warming of 1.5° C," *World Meteorological Organization: Geneva, Switzerland*, 2018.

[3] V. Masson-Delmotte, P. Zhai, A. Pirani, S. L. Connors, C. Péan, S. Berger, *et al.*, "Climate change 2021: the physical science basis," *Contribution of working group I to the sixth assessment report of the intergovernmental panel on climate change*, p. 2, 2021.

[4] EPA. (2022, Oct 5. 2022). *Fast Facts: U.S. Transportation Sector GHG Emissions (EPA-420-F-22-018, May 2022)* Available: https://www.epa.gov/greenvehicles/fast-facts-transportation-greenhouse-gas-emissions

[5] R. W. Johnny Wood, "6 things you should know about air pollution and your health.," 2021.

[6] U. UNEP, "Emissions gap report 2020," *UN environment programme*, 2020.

[7] X. Wu and D. MacKenzie, "Assessing the VMT effect of ridesourcing services in the US," *Transportation Research Part D: Transport and Environment*, vol. 94, p. 102816, 2021.

[8] R. G. Boundy, "Transportation Energy Data Book: Edition 37," Oak Ridge National Lab.(ORNL), Oak Ridge, TN (United States)2019.

[9] B. Leard, J. Linn, and C. Munnings, "Explaining the evolution of passenger vehicle miles traveled in the United States," *The Energy Journal,* vol. 40, 2019.

[10] V. Schaper and P. Patterson, "Factors that Affect VMT Growth," 1998.

[11] R. Ewing, S. Hamidi, F. Gallivan, A. C. Nelson, and J. B. Grace, "Structural equation models of VMT growth in US urbanised areas," *Urban Studies,* vol. 51, pp. 3079-3096, 2014.

[12] C. Rodier, F. Alemi, and D. Smith, "Dynamic ridesharing: Exploration of potential for reduction in vehicle miles traveled," *Transportation Research Record,* vol. 2542, pp. 120-126, 2016.

[13] D. N. Anderson, "“Not just a taxi”? For-profit ridesharing, driver strategies, and VMT," *Transportation,* vol. 41, pp. 1099-1117, 2014.

[14] J. E. Moore, "The birth of topological insulators," *Nature,* vol. 464, pp. 194-198, 2010.

[15] H. Cheng, S. Madanat, and A. Horvath, "Planning hierarchical urban transit systems for reductions in greenhouse gas emissions," *Transportation Research Part D: Transport and Environment,* vol. 49, pp. 44-58, 2016.

[16] T. Ercan and O. Tatari, "A hybrid life cycle assessment of public transportation buses with alternative fuel options," *The International Journal of Life Cycle Assessment,* vol. 20, pp. 1213-1231, 2015.

[17] FTA. (2020). *National Transit Summaries and Trends.* Available: https://www.transit.dot.gov/sites/fta.dot.gov/files/2021-11/2020%20National%20Transit%20Summaries%20and%20Trends.pdf

[18] A. Lajunen, "Energy consumption and cost-benefit analysis of hybrid and electric city buses," *Transportation Research Part C: Emerging Technologies,* vol. 38, pp. 1-15, 2014.

[19] L. P. Anna Stokes, " Electric Drive Buses Report.," 2016.

[20] P. Delhomme and A. Gheorghiu, "Comparing French carpoolers and non-carpoolers: Which factors contribute the most to carpooling?," *Transportation Research Part D: Transport and Environment,* vol. 42, pp. 1-15, 2016.

[21] R. a. Market, "Ride Sharing Market by Type (E-hailing, Station-Based, Car Sharing & Rental), Car Sharing (P2P, Corporate), Service (Navigation, Payment, Information), Micro-Mobility (Bicycle, Scooter), Vehicle Type, and Region - Global Forecast to 2026," 2021.

[22] U. S. C. Bureau, "U.S. Census Bureau, 2019. Means of Transportation to Work, 2019 American Community Survey 5-year Estimates," 2019.

[23] S. Zhang, Y. Wu, H. Liu, R. Huang, L. Yang, Z. Li, *et al.*, "Real-world fuel consumption and CO2 emissions of urban public buses in Beijing," *Applied Energy,* vol. 113, pp. 1645-1655, 2014.

[24] H.-W. Choi and H. C. Frey, "Method for in-use measurement and evaluation of the activity, fuel use, electricity use, and emissions of a plug-in hybrid diesel-electric school bus," *Environmental science & technology,* vol. 44, pp. 3601-3607, 2010.

[25] X. Wu, S. Zhang, Y. Wu, Z. Li, Y. Zhou, L. Fu, *et al.*, "Real-world emissions and fuel consumption of diesel buses and trucks in Macao: From on-road

measurement to policy implications," *Atmospheric Environment,* vol. 120, pp. 393-403, 2015.

[26] B. A. Holmén and K. M. Sentoff, "Hybrid-electric passenger car carbon dioxide and fuel consumption benefits based on real-world driving," *Environmental science & technology*, vol. 49, pp. 10199-10208, 2015.

[27] T. Xiru, Z. Yueyan, and X. Liping, "The Analysis of Space-time Characteristics of Bus Operation and Energy Consumption based on ArcGIS," *Energy Procedia*, vol. 104, pp. 456-461, 2016.

[28] J. M. López-Martínez, F. Jiménez, F. J. Páez-Ayuso, M. N. Flores-Holgado, A. N. Arenas, B. Arenas-Ramirez, *et al.*, "Modelling the fuel consumption and pollutant emissions of the urban bus fleet of the city of Madrid," *Transportation Research Part D: Transport and Environment,* vol. 52, pp. 112-127, 2017.

[29] W. Zeng, T. Miwa, and T. Morikawa, "Exploring trip fuel consumption by machine learning from GPS and CAN bus data," *Journal of the Eastern Asia Society for Transportation Studies,* vol. 11, pp. 906-921, 2015.

[30] C. Wang, Z. Ye, Y. Yu, and W. Gong, "Estimation of bus emission models for different fuel types of buses under real conditions," *Science of the Total Environment*, vol. 640, pp. 965-972, 2018.

[31] B. Yu, Y. Ma, M. Xue, B. Tang, B. Wang, J. Yan, *et al.*, "Environmental benefits from ridesharing: A case of Beijing," *Applied energy*, vol. 191, pp. 141-152, 2017.

[32] R. Arteaga-Sánchez, M. Belda-Ruiz, A. Ros-Galvez, and A. Rosa-Garcia, "Why continue sharing: Determinants of behavior in ridesharing services," *International Journal of Market Research*, vol. 62, pp. 725-742, 2020.

[33] V. Cirimele, M. Diana, F. Freschi, and M. Mitolo, "Inductive power transfer for automotive applications: State-of-the-art and future trends," *IEEE Transactions on Industry Applications,* vol. 54, pp. 4069-4079, 2018.

[34] A. Brecher and D. Arthur, "Review and evaluation of wireless power transfer (WPT) for electric transit applications," 2014.

[35] S. Jeong, Y. J. Jang, and D. Kum, "Economic analysis of the dynamic charging electric vehicle," *IEEE Transactions on Power Electronics,* vol. 30, pp. 6368-6377, 2015.

[36] Z. Liu and Z. Song, "Robust planning of dynamic wireless charging infrastructure for battery electric buses," *Transportation Research Part C: Emerging Technologies,* vol. 83, pp. 77-103, 2017.

[37] Y. Alwesabi, Y. Wang, R. Avalos, and Z. Liu, "Electric bus scheduling under single depot dynamic wireless charging infrastructure planning," *Energy*, vol. 213, p. 118855, 2020.

[38] Y. Alwesabi, Z. Liu, S. Kwon, and Y. Wang, "A novel integration of scheduling and dynamic wireless charging planning models of battery electric buses," *Energy,* vol. 230, p. 120806, 2021.

[39] C. Möller, "Carbon neutral road transportation: an assessment of the potential of electrified road systems," ed, 2017.

[40] A. Foote, B. Ozpineci, M. Chinthavali, and J.-M. Li, "Sizing dynamic wireless charging for light-duty electric vehicles in roadway applications," in *2016 IEEE PELS Workshop on Emerging Technologies: Wireless Power Transfer (WoW)*, 2016, pp. 224-230.

[41] H. C. Frey, "Trends in onroad transportation energy and emissions," *Journal of the Air & Waste Management Association,* vol. 68, pp. 514-563, 2018.

[42] P. White, *Public transport: its planning, management and operation*: Routledge, 2016.

[43] Y. Shen, H. Zhang, and J. Zhao, "Integrating shared autonomous vehicle in public transportation system: A supply-side simulation of the first-mile service in Singapore," *Transportation Research Part A: Policy and Practice,* vol. 113, pp. 125-136, 2018.

[44] S. Brumbaugh, T. Firestine, K. Notis, and S. Randrianarivelo, "Transportation Economic Trends 2018," 2018.

[45] N. N. Clark, "Assessment of hybrid-electric transit bus technology," 2009.

[46] I. Taymaz and M. Benli, "Emissions and fuel economy for a hybrid vehicle," *Fuel*, vol. 115, pp. 812-817, 2014.

[47] J. Wang and H. A. Rakha, "Convex fuel consumption model for diesel and hybrid buses," *Transportation Research Record,* vol. 2647, pp. 50-60, 2017.

[48] J. L. Jimenez-Palacios, "Understanding and quantifying motor vehicle emissions with vehicle specific power and TILDAS remote sensing," *Massachusetts Institute of Technology,* 1998.

[49] Y. Chen, L. Zhu, J. Gonder, S. Young, and K. Walkowicz, "Data-driven fuel consumption estimation: A multivariate adaptive regression spline approach," *Transportation Research Part C: Emerging Technologies,* vol. 83, pp. 134-145, 2017.

[50] H. C. Frey, N. M. Rouphail, H. Zhai, T. L. Farias, and G. A. Gonçalves, "Comparing real-world fuel consumption for diesel-and hydrogen-fueled transit buses and implication for emissions," *Transportation Research Part D: Transport and Environment*, vol. 12, pp. 281-291, 2007.

[51] J. Wang and H. A. Rakha, "Fuel consumption model for conventional diesel buses," *Applied energy*, vol. 170, pp. 394-402, 2016.

[52] R. Zhang and E. Yao, "Electric vehicles' energy consumption estimation with real driving condition data," *Transportation Research Part D: Transport and Environment*, vol. 41, pp. 177-187, 2015.

[53] W. S. Wayne, N. N. Clark, R. D. Nine, and D. Elefante, "A comparison of emissions and fuel economy from hybrid-electric and conventional-drive transit buses," *Energy & fuels*, vol. 18, pp. 257-270, 2004.

[54] G. Wu, K. Boriboonsomsin, and M. J. Barth, "Development and evaluation of an intelligent energy-management strategy for plug-in hybrid electric vehicles," *IEEE Transactions on Intelligent Transportation Systems*, vol. 15, pp. 1091-1100, 2014.

[55] U. Epa, "Motor Vehicle Emission Simulator (MOVES) User Guide," *US Environmental Protection Agency*, 2010.

[56] L. Liu, A. Kotz, A. Salapaka, E. Miller, and W. F. Northrop, "Impact of time-varying passenger loading on conventional and electrified transit bus energy consumption," *Transportation Research Record*, vol. 2673, pp. 632-640, 2019.

[57] M. H. Hassoun, *Fundamentals of artificial neural networks*: MIT press, 1995.

[58] S. Karsoliya, "Approximating number of hidden layer neurons in multiple hidden layer BPNN architecture," *International Journal of Engineering Trends and Technology*, vol. 3, pp. 714-717, 2012.

[59] H. R. Maier and G. C. Dandy, "Neural network based modelling of environmental variables: a systematic approach," *Mathematical and Computer Modelling*, vol. 33, pp. 669-682, 2001.

[60] L. Ai, V. Soltangharaei, M. Bayat, M. van Tooren, and P. Ziehl, "Detection of impact on aircraft composite structure using machine learning techniques," *Measurement Science and Technology*, vol. 32, p. 084013, 2021.

[61] L. Ai, V. Soltangharaei, M. Bayat, B. Greer, and P. Ziehl, "Source localization on large-scale canisters for used nuclear fuel storage using optimal number of acoustic emission sensors," *Nuclear Engineering and Design*, vol. 375, p. 111097, 2021.

[62] L. L. Rogers and F. U. Dowla, "Optimization of groundwater remediation using artificial neural networks with parallel solute transport modeling," *Water Resources Research*, vol. 30, pp. 457-481, 1994.

[63] B. J. Taylor, *Methods and procedures for the verification and validation of artificial neural networks*: Springer Science & Business Media, 2006.

[64] M. Hughes-Cromwick, "2019 Public Transportation Fact Book," 2019.

[65] B. Boriboonsomsin and M. Barth, "Real-World CO 2 Impacts of Traffic Congestion," *Transportation Research Record*, pp. 1-23, 2008.

[66] M. U. Cuma and T. Koroglu, "A comprehensive review on estimation strategies used in hybrid and battery electric vehicles," *Renewable and Sustainable Energy Reviews,* vol. 42, pp. 517-531, 2015.

[67] Z. Sun, P. Hao, X. J. Ban, and D. Yang, "Trajectory-based vehicle energy/emissions estimation for signalized arterials using mobile sensing data," *Transportation Research Part D: Transport and Environment,* vol. 34, pp. 27-40, 2015.

[68] O. F. Delgado, N. N. Clark, and G. J. Thompson, "Modeling transit bus fuel consumption on the basis of cycle properties," *Journal of the Air & Waste Management Association,* vol. 61, pp. 443-452, 2011.

[69] W.-T. Hung, H.-Y. Tong, and C.-S. Cheung, "A modal approach to vehicular emissions and fuel consumption model development," *Journal of the Air & Waste Management Association,* vol. 55, pp. 1431-1440, 2005.

[70] S. C. Davis and R. G. Boundy, "Transportation energy data book: Edition 39," Oak Ridge National Lab.(ORNL), Oak Ridge, TN (United States)2021.

[71] E. C. D.-G. f. Energy and S. O. o. t. E. Communities, *EU Transport in Figures: Statistical Pocket Book*: Office for Official Publications of the European Communities, 2014.

[72] S. Shaheen, A. Cohen, and I. Zohdy, "Shared mobility: current practices and guiding principles," United States. Federal Highway Administration2016.

[73] R. Jalali, S. Koohi-Fayegh, K. El-Khatib, D. Hoornweg, and H. Li, "Investigating the potential of ridesharing to reduce vehicle emissions," *Urban Planning,* vol. 2, pp. 26-40, 2017.

[74] R. Dai, C. Ding, J. Gao, X. Wu, and B. Yu, "Optimization and evaluation for autonomous taxi ride-sharing schedule and depot location from the perspective of energy consumption," *Applied Energy*, vol. 308, p. 118388, 2022.

[75] G. Correia and J. M. Viegas, "Carpooling and carpool clubs: Clarifying concepts and assessing value enhancement possibilities through a Stated Preference web survey in Lisbon, Portugal," *Transportation Research Part A: Policy and Practice*, vol. 45, pp. 81-90, 2011.

[76] M. V. Ciasullo, G. Maione, C. Torre, and O. Troisi, "The growth of carpooling: Insights from a social media investigation," in *Proceedings of the 20th Excellence in Services International Conference*, 2017, pp. 183-195.

[77] W. Abrahamse and M. Keall, "Effectiveness of a web-based intervention to encourage carpooling to work: A case study of Wellington, New Zealand," *Transport policy*, vol. 21, pp. 45-51, 2012.

[78] S. A. Shaheen, N. D. Chan, and T. Gaynor, "Casual carpooling in the San Francisco Bay Area: Understanding user characteristics, behaviors, and motivations," *Transport Policy*, vol. 51, pp. 165-173, 2016.

[79] M. A. Javid, T. Mehmood, H. M. Asif, A. U. Vaince, and M. Raza, "Travelers' attitudes toward carpooling in Lahore: motives and constraints," *Journal of Modern Transportation*, vol. 25, pp. 268-278, 2017.

[80] J. A. Molina, J. I. Giménez-Nadal, and J. Velilla, "Sustainable commuting: Results from a social approach and international evidence on carpooling," *Sustainability*, vol. 12, p. 9587, 2020.

[81] Y. Guo, G. Goncalves, and T. Hsu, "RETRACTED ARTICLE: A Multi-agent Based Self-adaptive Genetic Algorithm for the Long-term Car Pooling Problem," *Journal of Mathematical Modelling and Algorithms in Operations Research,* vol. 12, pp. 45-66, 2013.

[82] Y. Guo, G. Goncalves, and T. Hsu, "A multi-destination daily carpooling problem and an ant colony based resolution method," *RAIRO-Operations Research,* vol. 47, pp. 399-428, 2013.

[83] C. Huang, D. Zhang, Y.-W. Si, and S. C. Leung, "Tabu search for the real-world carpooling problem," *Journal of Combinatorial Optimization,* vol. 32, pp. 492-512, 2016.

[84] M. Tamannaei and I. Irandoost, "Carpooling problem: A new mathematical model, branch-and-bound, and heuristic beam search algorithm," *Journal of Intelligent Transportation Systems,* vol. 23, pp. 203-215, 2019.

[85] S. Yan, C.-Y. Chen, and S.-C. Chang, "A car pooling model and solution method with stochastic vehicle travel times," *IEEE transactions on intelligent transportation systems,* vol. 15, pp. 47-61, 2013.

[86] O. Bahat and S. Bekhor, "Incorporating ridesharing in the static traffic assignment model," *Networks and Spatial Economics,* vol. 16, pp. 1125-1149, 2016.

[87] K. M. Gurumurthy, K. M. Kockelman, and M. D. Simoni, "Benefits and costs of ride-sharing in shared automated vehicles across Austin, Texas: Opportunities for congestion pricing," *Transportation Research Record,* vol. 2673, pp. 548-556, 2019.

[88] Z. Li, Y. Hong, and Z. Zhang, "Do ride-sharing services affect traffic congestion? An empirical study of uber entry," *Social Science Research Network*, vol. 2002, pp. 1-29, 2016.

[89] N. J. Vickers, "Animal communication: when i'm calling you, will you answer too?," *Current biology*, vol. 27, pp. R713-R715, 2017.

[90] B. Caulfield, "Estimating the environmental benefits of ride-sharing: A case study of Dublin," *Transportation Research Part D: Transport and Environment*, vol. 14, pp. 527-531, 2009.

[91] P. Minett and J. Pearce, "Estimating the energy consumption impact of casual carpooling," *Energies*, vol. 4, pp. 126-139, 2011.

[92] I. Tikoudis, L. Martinez, K. Farrow, C. G. Bouyssou, O. Petrik, and W. Oueslati, "Ridesharing services and urban transport CO2 emissions: Simulation-based evidence from 247 cities," *Transportation Research Part D: Transport and Environment*, vol. 97, p. 102923, 2021.

[93] E. Bonabeau, "Agent-based modeling: Methods and techniques for simulating human systems," *Proceedings of the national academy of sciences*, vol. 99, pp. 7280-7287, 2002.

[94] H. Becker, M. Balac, F. Ciari, and K. W. Axhausen, "Assessing the welfare impacts of Shared Mobility and Mobility as a Service (MaaS)," *Transportation Research Part A: Policy and Practice*, vol. 131, pp. 228-243, 2020.

[95] F. Ciari, M. Balac, and M. Balmer, "Modelling the effect of different pricing schemes on free-floating carsharing travel demand: a test case for Zurich, Switzerland," *Transportation*, vol. 42, pp. 413-433, 2015.

[96] M. Balac, H. Becker, F. Ciari, and K. W. Axhausen, "Modeling competing free-floating carsharing operators–A case study for Zurich, Switzerland," *Transportation Research Part C: Emerging Technologies,* vol. 98, pp. 101-117, 2019.

[97] G. Leich and J. Bischoff, "Should autonomous shared taxis replace buses? A simulation study," *Transportation Research Procedia,* vol. 41, pp. 450-460, 2019.

[98] Y. Huang, K. M. Kockelman, V. Garikapati, L. Zhu, and S. Young, "Use of shared automated vehicles for first-mile last-mile service: micro-simulation of rail-transit connections in Austin, Texas," *Transportation research record,* vol. 2675, pp. 135-149, 2021.

[99] D. Krajzewicz, G. Hertkorn, C. Rössel, and P. Wagner, "SUMO (Simulation of Urban MObility)-an open-source traffic simulation," in *Proceedings of the 4th middle East Symposium on Simulation and Modelling (MESM20002)*, 2002, pp. 183-187.

[100] A. Wegener, M. Piórkowski, M. Raya, H. Hellbrück, S. Fischer, and J.-P. Hubaux, "TraCI: an interface for coupling road traffic and network simulators," in *Proceedings of the 11th communications and networking simulation symposium*, 2008, pp. 155-163.

[101] P. A. Lopez, M. Behrisch, L. Bieker-Walz, J. Erdmann, Y.-P. Flötteröd, R. Hilbrich, *et al.*, "Microscopic traffic simulation using sumo," in *2018 21st international conference on intelligent transportation systems (ITSC)*, 2018, pp. 2575-2582.

[102] İ. G. Erdağı, M. A. Silgu, and H. B. Çelikoğlu, "Emission effects of cooperative adaptive cruise control: a simulation case using SUMO," *EPiC series in computing*, vol. 62, pp. 92-100, 2019.

[103] A. Validi, N. Polasek, L. Alabi, M. Leitner, and C. Olaverri-Monreal, "Environmental impact of bundling transport deliveries using sumo: Analysis of a cooperative approach in austria," in *2020 15th Iberian Conference on Information Systems and Technologies (CISTI)*, 2020, pp. 1-5.

[104] A. Gounni, N. Rais, and M. A. Idrissi, "New solutions to reduce the environmental impact of road traffic emissions, using sumo," in *Proceedings of the 2nd International Conference on Networking, Information Systems & Security*, 2019, pp. 1-7.

[105] TNDOT. (2016, Oct 6, 2022). *Statewide Transportation Demand Management Plan for Tennessee Nonattanment and Maintenance Areas, Commuter Survey Report*. Available: https://www.tn.gov/content/dam/tn/tdot/long-range-planning/TDOT%20Employee%20Survey%20Report%202016.pdf.

[106] U. S. C. Bureau. (2020, Oct 6, 2022). *American Community Survey 5-year estimates. Retrieved from Census Reporter Profile page for Chattanooga*. Available: https://censusreporter.org/profiles/16000US4714000-chattanooga-tn/

[107] U. S. C. Bureau. (2019, Oct 6, 2022). *Means of Transportation to Work, 2019 American Community Survey 5-year Estimates*. Available: https://data.census.gov/cedsci/table?q=B08&d=ACS%201-Year%20Estimates%20Detailed%20Tables&tid=ACSDT1Y2019.B08301.

[108] D. J. Fagnant and K. M. Kockelman, "The travel and environmental implications of shared autonomous vehicles, using agent-based model scenarios," *Transportation Research Part C: Emerging Technologies,* vol. 40, pp. 1-13, 2014.

[109] M. Barth and K. Boriboonsomsin, "Energy and emissions impacts of a freeway-based dynamic eco-driving system," *Transportation Research Part D: Transport and Environment,* vol. 14, pp. 400-410, 2009.

[110] S. H. Jacobson and D. M. King, "Fuel saving and ridesharing in the US: Motivations, limitations, and opportunities," *Transportation Research Part D: Transport and Environment,* vol. 14, pp. 14-21, 2009.

[111] J. Shi, Y. Gao, W. Wang, N. Yu, and P. A. Ioannou, "Operating electric vehicle fleet for ride-hailing services with reinforcement learning," *IEEE Transactions on Intelligent Transportation Systems,* vol. 21, pp. 4822-4834, 2019.

[112] W. Tu, P. Santi, T. Zhao, X. He, Q. Li, L. Dong, *et al.,* "Acceptability, energy consumption, and costs of electric vehicle for ride-hailing drivers in Beijing," *Applied Energy,* vol. 250, pp. 147-160, 2019.

[113] L. He, H.-Y. Mak, Y. Rong, and Z.-J. M. Shen, "Service region design for urban electric vehicle sharing systems," *Manufacturing & Service Operations Management,* vol. 19, pp. 309-327, 2017.

[114] N. Kang, F. M. Feinberg, and P. Y. Papalambros, "Autonomous electric vehicle sharing system design," *Journal of Mechanical Design,* vol. 139, p. 011402, 2017.

[115] X. Di, H. X. Liu, X. Ban, and H. Yang, "Ridesharing user equilibrium and its implications for high-occupancy toll lane pricing," *Transportation Research Record,* vol. 2667, pp. 39-50, 2017.

[116] H. Y. Ong, D. Freund, and D. Crapis, "Driver Positioning and Incentive Budgeting with an Escrow Mechanism for Ride-Sharing Platforms," *INFORMS Journal on Applied Analytics*, vol. 51, pp. 373-390, 2021.

[117] C. Song, J. Monteil, J.-L. Ygnace, and D. Rey, "Incentives for ridesharing: A case study of welfare and traffic congestion," *Journal of Advanced Transportation*, vol. 2021, 2021.

[118] EPA, "Fast Facts: U.S. Transportation Sector GHG Emissions (EPA-420-F-22-018, May 2022)," 2022.

[119] M. Anfinsen, V. A. Lagesen, and M. Ryghaug, "Green and gendered? Cultural perspectives on the road towards electric vehicles in Norway," *Transportation research part D: transport and environment*, vol. 71, pp. 37-46, 2019.

[120] A. Amditis, T. Theodoropoulos, G. Brusaglino, R. Rizzo, L. Di Noia, G. Rodella, *et al.*, "Energy management optimization within the Electric Mobility system," in *2017 6th International Conference on Clean Electrical Power (ICCEP)*, 2017, pp. 110-116.

[121] C. T. Rim and C. Mi, *Wireless power transfer for electric vehicles and mobile devices*: John Wiley & Sons, 2017.

[122] O. C. Onar, S. L. Campbell, L. E. Seiber, C. P. White, M. S. Chinthavali, L. Tang, *et al.*, "Oak Ridge National Laboratory Wireless Charging of Electric Vehicles-CRADA Report," Oak Ridge National Lab.(ORNL), Oak Ridge, TN (United States). National …2016.

[123] A. Van Driessche, D. G. Aggelis, and E. Tsangouri, "Complex fracture on thin-wall textile reinforced cement (TRC) shells monitored by acoustic emission," *Thin-Walled Structures,* vol. 167, p. 108216, 2021.

[124] A. C. Mpalaskas, T. E. Matikas, D. G. Aggelis, and N. Alver, "Acoustic Emission for Evaluating the Reinforcement Effectiveness in Steel Fiber Reinforced Concrete," *Applied Sciences,* vol. 11, p. 3850, 2021.

[125] Z. Chen, Y. Yin, and Z. Song, "A cost-competitiveness analysis of charging infrastructure for electric bus operations," *Transportation Research Part C: Emerging Technologies,* vol. 93, pp. 351-366, 2018.

[126] Y. D. Ko and Y. J. Jang, "The optimal system design of the online electric vehicle utilizing wireless power transmission technology," *IEEE Transactions on intelligent transportation systems,* vol. 14, pp. 1255-1265, 2013.

[127] NDS. (2018). *The 2018 National Design Specification (NDS) for Wood Construction*. Available: https://awc.org/publications/2018-nds/

[128] M. K. ElBatanouny, P. H. Ziehl, A. Larosche, J. Mangual, F. Matta, and A. Nanni, "Acoustic emission monitoring for assessment of prestressed concrete beams," *Construction and building materials,* vol. 58, pp. 46-53, 2014.

[129] I. Hwang, Y. J. Jang, Y. D. Ko, and M. S. Lee, "System optimization for dynamic wireless charging electric vehicles operating in a multiple-route environment," *IEEE Transactions on Intelligent Transportation Systems,* vol. 19, pp. 1709-1726, 2017.

[130] C. A. García-Vázquez, F. Llorens-Iborra, L. M. Fernández-Ramírez, H. Sánchez-Sainz, and F. Jurado, "Comparative study of dynamic wireless charging of electric

vehicles in motorway, highway and urban stretches," *Energy,* vol. 137, pp. 42-57, 2017.

[131] R. Sun, Y. Chen, A. Dubey, and P. Pugliese, "Hybrid electric buses fuel consumption prediction based on real-world driving data," *Transportation Research Part D: Transport and Environment,* vol. 91, p. 102637, 2021.

[132] Z. Chen, F. He, and Y. Yin, "Optimal deployment of charging lanes for electric vehicles in transportation networks," *Transportation Research Part B: Methodological,* vol. 91, pp. 344-365, 2016.

[133] A. Ceder, *Public transit planning and operation: Modeling, practice and behavior*: CRC press, 2016.

[134] N. Mohamed, F. Aymen, M. Ben Hamed, and S. Lassaad, "Analysis of battery‐EV state of charge for a dynamic wireless charging system," *Energy Storage,* vol. 2, p. e117, 2020.

[135] R. Anay, A. Lane, D. V. Jáuregui, B. D. Weldon, V. Soltangharaei, and P. Ziehl, "On-site acoustic-emission monitoring for a prestressed concrete BT-54 AASHTO girder bridge," *Journal of Performance of Constructed Facilities,* vol. 34, p. 04020034, 2020.

[136] M. K. ElBatanouny, J. Mangual, P. H. Ziehl, and F. Matta, "Early corrosion detection in prestressed concrete girders using acoustic emission," *J. Mater. Civ. Eng,* vol. 26, pp. 504-511, 2014.

[137] Y. Chen, Y. Zhang, and R. Sun, "Data-driven estimation of energy consumption for electric bus under real-world driving conditions," *Transportation Research Part D: Transport and Environment,* vol. 98, p. 102969, 2021.

[138] P. M. Castro, "Tightening piecewise McCormick relaxations for bilinear problems," *Computers & Chemical Engineering*, vol. 72, pp. 300-311, 2015.

[139] J.-F. Tsai and M.-H. Lin, "An efficient global approach for posynomial geometric programming problems," *INFORMS Journal on Computing*, vol. 23, pp. 483-492, 2011.

[140] Z. Bi, G. A. Keoleian, Z. Lin, M. R. Moore, K. Chen, L. Song, *et al.*, "Life cycle assessment and tempo-spatial optimization of deploying dynamic wireless charging technology for electric cars," *Transportation Research Part C: Emerging Technologies*, vol. 100, pp. 53-67, 2019.

[141] Z. Bi, T. Kan, C. C. Mi, Y. Zhang, Z. Zhao, and G. A. Keoleian, "A review of wireless power transfer for electric vehicles: Prospects to enhance sustainable mobility," *Applied Energy*, vol. 179, pp. 413-425, 2016.

[142] Payscale. (2022). *Average Hourly Rate in Chattanooga, Tennessee*. Available: https://www.payscale.com/research/US/Location=Chattanooga-TN/Salary

[143] R. Tavakoli, E. M. Dede, C. Chou, and Z. Pantic, "Cost-efficiency optimization of ground assemblies for dynamic wireless charging of electric vehicles," *IEEE Transactions on Transportation Electrification*, vol. 8, pp. 734-751, 2021.

Appendix A

Copyright Permission

The paper entitled “Hybrid electric buses fuel consumption prediction based on real-world driving data”:

Please note that, as the author of this Elsevier article, you retain the right to include it in a thesis or dissertation, provided it is not published commercially. Permission is not required, but please ensure that you reference the journal as the original source.

The paper entitled “Assessing the impacts of ridesharing services: An agent-based simulation approach”:

Please note that, as the author of this Elsevier article, you retain the right to include it in a thesis or dissertation, provided it is not published commercially. Permission is not required, but please ensure that you reference the journal as the original source.